MECHANICAL PROPERTIES OF CANCELLOUS BONE OF THE TIBIA

QUANTIFYING THE REGIONAL VARIATIONS IN THE

MECHANICAL PROPERTIES OF CANCELLOUS BONE OF THE TIBIA

USING INDENTATION TESTING AND CT IMAGING

By VIVEGA VIJAYAKUMAR, B.H.Sc.

A Thesis Submitted to the School of Graduate Studies in Partial Fulfillment of the
Requirements for the Degree Master of Applied Science

MASTER OF APPLIED SCIENCE (2013)   McMaster University
(School of Biomedical Engineering)   Hamilton, Ontario

TITLE: QUANTIFYING THE REGIONAL VARIATIONS IN THE MECHANICAL
       PROPERTIES OF CANCELLOUS BONE OF THE TIBIA USING
       INDENTATION TESTING AND CT IMAGING

AUTHOR: Vivega Vijayakumar, B.H.Sc. (University of Western Ontario)

SUPERVISOR: Cheryl E. Quenneville, Ph.D., P.Eng.

NUMBER OF PAGES: xiv, 132

ABSTRACT

Finite element (FE) models are a fast and cost-effective way to evaluate stress behavior in bone under various loading conditions. However, accurate material property assignment is required when developing the model. Bone is an inhomogeneous material as there is much variation in the distribution of its mechanical properties. However, there has been limited investigation into the extent of regional variations in the cancellous bone of the proximal tibia. Dynamic FE models simplify bone as a homogeneous material, which may affect their accuracy. However, density-modulus relationships have been successful in assigning accurate material properties in the development of static FE models. There are many such equations in the literature and the most appropriate density-modulus relationship for cancellous bone of the proximal tibia has yet to be determined.

In the first study of this thesis, indentation testing was performed on four slices, each consisting of nine regions, from five cadaveric tibiae. The modulus and yield strength were found to vary regionally, where the bone closest to the joint and in the medial condyle were strongest, and the intercondylar region the weakest. These areas of strength can serve as improved sites of attachment to ensure the long-term success of orthopaedic devices. It also suggests that regional variations in cancellous bone need to be considered in the development of subject-specific FE models.

In the second study, density-modulus relationships developed for cancellous bone of the tibia were evaluated for their ability to predict mechanical properties. Computed tomography (CT) was used to determine bone density, which was used in three equations from the literature to compare predicted modulus to experimental elastic modulus. It was

found that all three relationships consistently overestimated modulus. This inaccuracy should be accounted for through an improved density-modulus relationship for cancellous bone of the tibia.

ACKNOWLEDGEMENTS

whether by keeping me company through long hours of testing, offering to help with number-crunching and proof-reading, or consoling me when I was near emotional breakdown. I share my achievements with you, as you have all contributed to my success. I will be forever grateful.

TABLE OF CONTENTS

LIST OF FIGURES

LIST OF TABLES

LIST OF ABBREVIATIONS AND SYMBOLS

%	Percent
"	Inch
°	Degree
°C	Degree Celsius
δ	Deformation or displacement
θ	Angle
ε	Strain (mm/mm)
σ	Stress (MPa)
ν	Poisson's ratio
ρ	Density
α	Significance level
cm	Centimeter
A	Anterior
AC	Anterior central
AL	Anterior lateral
AM	Anterior medial
ANOVA	Analysis of variance
app	Apparent
C	Central
CC	Central central
CL	Central lateral

cm	Centimeter
CM	Central medial
CT	Computed tomography
d	Diameter
E	Elastic modulus
F	Applied load/force
FE	Finite element
g	Gram
GPa	Gigapascal
L	Lateral
L	Length
lb	Pound
HA	Hydroxyapatite
HU	Hounsfield Unit
Hz	Hertz
kg	Kilogram
kV	Kilovolt
m	Metre
mAs	Milli-ampere second
mg	Milligram
min	Minute
m	Metre

mm	Millimeter
MPa	Megapascal
N	Newton
P	Posterior
PC	Posterior central
PL	Posterior lateral
PM	Posterior medial
R^2	Variation error
s	Second
S	Stiffness
SB3	Epoxy resin (cortical bone insert) (Gammex-RMI)
SD	Standard deviation
STL+	Stereolithography (file format)
x	By

Chapter 1: Introduction

OVERVIEW: This introductory chapter provides insight towards the goal of quantifying the mechanical properties of the tibia to identify the extent of regional variations in cancellous bone. This chapter covers background on the tibia and bone structures, mechanical properties, and density-modulus relationships used in finite element models. It concludes with the rationale and purpose of the thesis.

1.1. Anatomy

1.1.1 The Tibia

The tibia is the major weight-bearing long bone of the lower leg, located medially to the fibula (Figure 1.1) (Appendix A). Long bones consist of a shaft, called the diaphysis, which is capped on either end by an epiphysis. Cortical bone is a strong, dense structure found in the diaphysis and covering the epiphyses. Cancellous bone is a 3D matrix of trabeculae enclosed within the epiphyses (see 1.1.2). The tibia is prismoid in shape, being large at the proximal end and narrow through the center until it widens slightly at the distal end. The tibia articulates proximally with the femur at the tibiofemoral joint of the knee, where the meniscus covers the superior articular surface. The tibia also articulates with the fibula at the superior and inferior tibiofibular joints. The tibia and fibula articulate together distally with the talus bone at the ankle joint (Gray, 1918).
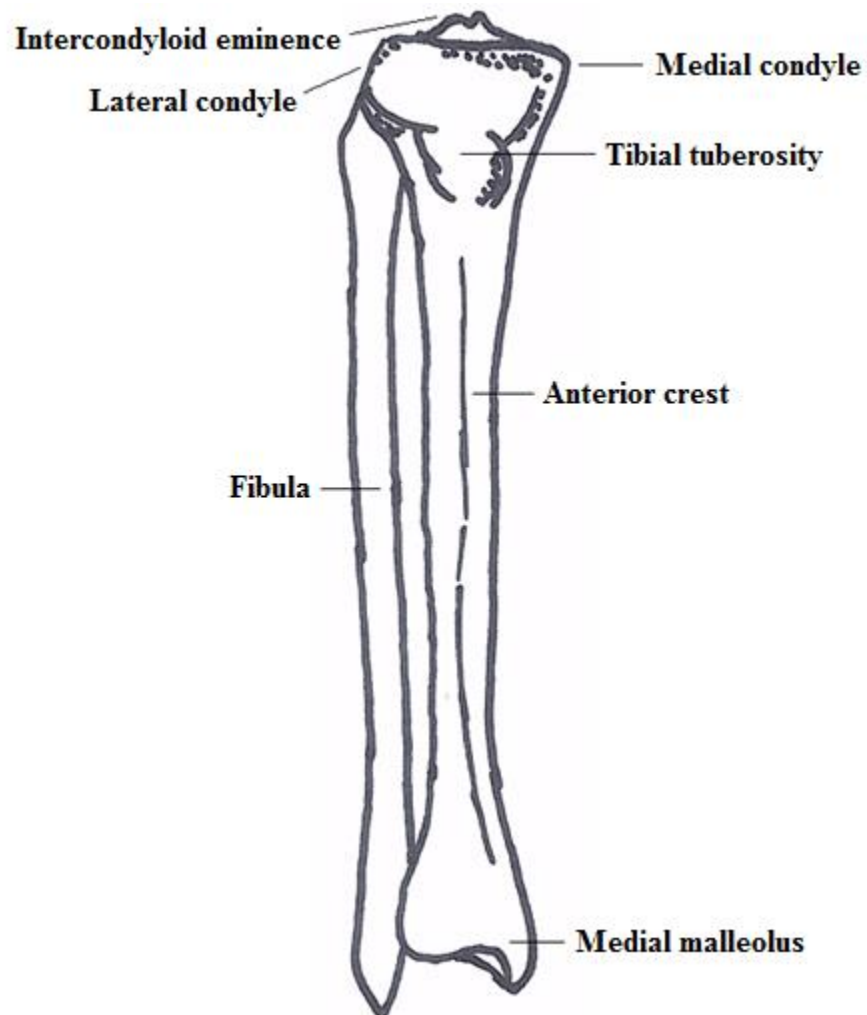
Figure 1.1   Anatomical Landmarks of the Tibia.
The tibia articulates with the fibula, femur, and talus. Anatomical landmarks of the tibia include: the medial and lateral condyles, intercondyloid eminence, tibial tuberosity, anterior crest, and medial malleolus.

There are numerous anatomical structures forming landmarks on the tibia. The medial and lateral condyles are separated by the intercondyloid eminence to form the tibial plateau at the proximal epiphysis. The intercondyloid eminence extends from the tibial tuberosity to the posterior intercondyloid fossa. The anterior crest runs over the anterior surface of the tibia, forming the prominent ridge of the shin. The tibia has a roughly circular cross-section, which varies in diameter through its length. The medial malleolus is a prominence located on the distal epiphysis, which serves as an attachment site for ligaments (Gray, 1918). Subchondral bone layers are located directly below the cortical shell at both ends of the tibia.

1.1.2 Bone Structure

Bone consists of two types of structures. Cortical bone is the hard, exterior shell that extends through the diaphysis and covers the epiphyses. It is dense and has a porosity of 5-30% (Carter and Spengler, 1978). The basic functional unit of cortical bone is the osteon, consisting of concentric lamellae surrounding the Haversian canal (Figure 1.2) (van Oers et al., 2008). Osteons are oriented along the long axis of the bone in the direction of maximum principal stress (Hert et al., 1994). The primary function of cortical bone is to bear load and protect the body (Johnson et al., 2010).

Cancellous bone is continuous with the cortical layer and is enclosed within the epiphyses of long bones. It is a three-dimensional matrix of trabeculae that are organized as columns and plates and filled with marrow (Figure 1.3) (Goldstein et al., 1983). Cancellous bone has a lower mineral content and higher turnover rate than cortical bone, and has a porosity of 30-90% (Currey, 2012). Wolff's Law states that the trabeculae are
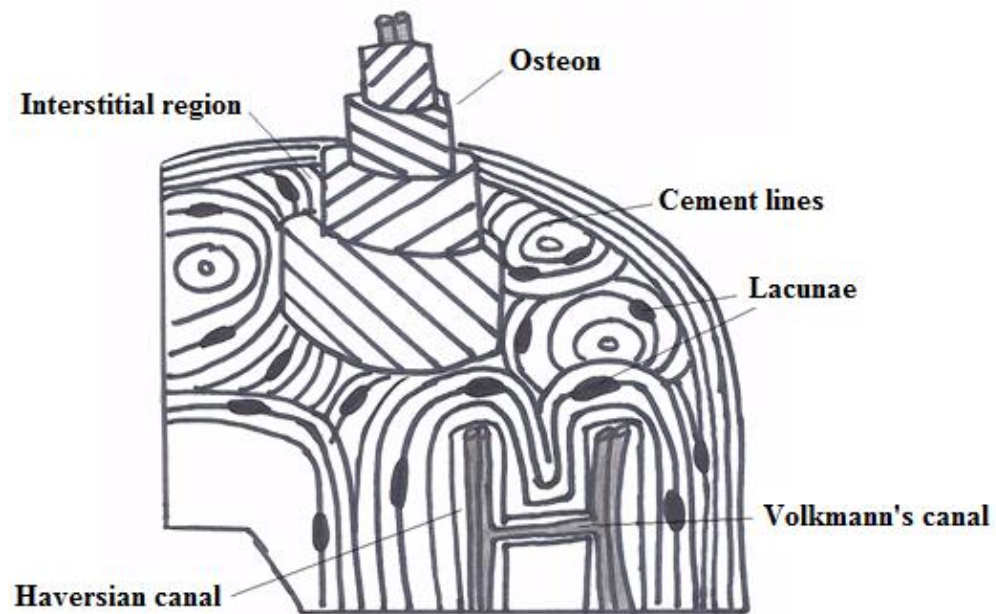
Figure 1.2 **Structure of Cortical Bone.**
Cortical bone is the dense shell surrounding long bones. It consists of osteons, interstitial regions, cement lines, Haversian and Volkmann's canals, and lacunae.

Figure 1.3 **Structure of Cancellous Bone.**
Cancellous bone is the porous, spongy bone found within the epiphyses of long bone. It is a 3D matrix of columns and plates, where the pores are filled with marrow.

oriented along the lines of principal stress (Hvid and Hansen, 1985). The trabeculae transmit load away from the joint to the cortical bone in the diaphysis. The trabeculae within the first 3 cm of the proximal tibia are oriented to be primarily vertical (Aitken et al., 1985; Currey, 2012). For the purpose of this thesis, cancellous bone will be the focus of attention.

1.2 Properties of Bone

Bone is a complex material. It is viscoelastic in that its stress-strain relationship is time-dependent. Under a given load, bone experiences elastic followed by plastic deformation until the point of failure (Gibson, 1985). Elastic deformation allows the material to return to its original shape whereas plastic deformation is permanent. Bone is inhomogeneous in terms of the distribution of its mechanical properties, and is highly anisotropic where its properties differ according to direction (Currey, 2012). The mechanical properties of bone can be influenced by age, gender, strain rate, hydration level, anatomic location, geometry of the specimen, microstructure, and mineral content as described below.

1.2.1 Mechanical Properties

Mechanical properties describe the behavior of a deformable material under a given load. A material's mechanical properties are derived from the measured response during experimental deformations under a known stress. Compression tests are the most common method of determining the mechanical properties of cancellous bone (Figure 1.4). Modulus of elasticity and ultimate compressive strength are two of the most commonly measured parameters to describe the mechanical response of bone
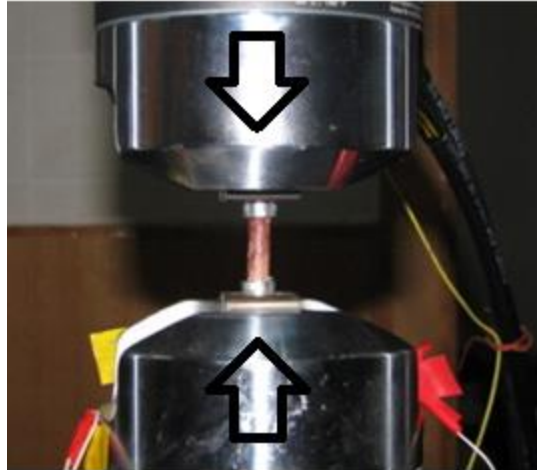
Figure 1.4   Uniaxial compression test for bone cylinder.
Mechanical properties of a material are quantified through experiments such as compression tests. A load is applied to deform the material, and the response is measured. *(From Wu et al., 2008).*

(Harada et al., 1988). As load is applied to the specimen, displacement occurs. These data can be converted to stress and strain values by dividing load by area (F/A) and displacement by the original thickness (ΔL/L), respectively. The stress-strain curve of cancellous bone has three distinct regions of behavior (Figure 1.5). The first region describes the trabeculae undergoing non-permanent deformation, which behaves in a linear elastic manner. Elastic modulus describes its elastic response and is equal to the slope of the linear portion of the stress-strain curve. At higher loads, the trabeculae begin to buckle. Yield strength is the point where the material begins to behave plastically, in that its deformation is permanent. A 0.2% offset of the strain is used to determine yield strength when yield is not clearly defined. The trabeculae continue to collapse at a near-constant load until resistance to load increases due to material accumulation, giving rise to the steep final portion of the stress-strain curve.

The mechanical properties of bone vary between individuals, anatomic sites, regions within a site, orientation, and over time (Helgason et al., 2008). These properties depend on the density, porosity, architecture, and mineral content of the bone (Rho et al., 1995). As bone is remodeled to meet the body's functional needs, density and mechanical properties change accordingly. The variation in the mechanical properties of cancellous bone is greater than that found in cortical bone. The mechanical properties of cancellous bone can vary by a factor of two to five between anatomical locations (Rho et al., 1995). Although cancellous bone has greater mineral content than cortical bone, trabecular bone tissue (single trabeculae) has a lower elastic modulus (Choi and Goldstein, 1992). The
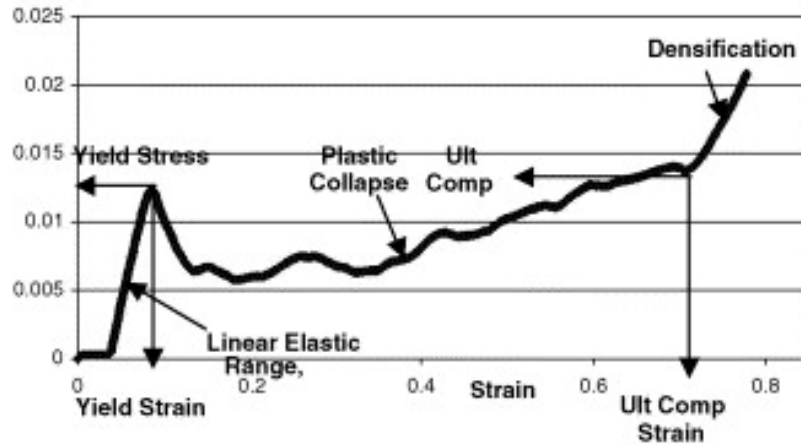
Figure 1.5   **Standard Stress-Strain Curve for Compression of Cancellous Bone.** Mechanical tests record load versus displacement data, which can be converted into a stress-strain curve. The slope of the curve in the elastic region gives the elastic modulus. As bone begins to deform plastically, yield strength can be defined at a 0.2% offset. *(From Teo et al., 2006).*

mechanical properties of the cancellous bone of the tibia are associated with the organization of the trabeculae, where the highest compressive resistance is observed at the areas of greatest radiodensity in radiographs (Aitken et al., 1985). In the distal tibia, lower elastic modulus and maximum strength correspond to the thinner trabeculae found in regions proximal to the distal subchondral bone plate (Aitken et al, 1985). Healthy adult bone has an average elastic modulus of 400 MPa, whereas the bone of older individuals has an average elastic modulus of 300 MPa (Sumner et al., 1994). This can vary widely though, with values from 4.2 MPa to 1250 MPa being noted (Sumner et al., 1994; Goldstein et al., 1983).

1.2.2 Material Properties

1.2.2.1 Anisotropy

Cancellous bone is highly anisotropic, meaning its mechanical properties differ according to direction of loading (Reilly and Burstein, 1974). Keyak et al. (1994) found that the elastic modulus and strength were greatest in the superior-inferior direction compared to the anterior-posterior and medial-lateral directions. Specimens loaded in the superior-inferior direction have been shown to be over twice as strong as those loaded in the lateral-medial direction (Carter and Hayes, 1977). Keyak et al. (1994) speculated that high axial strength was a result of the trabeculae being organized in axially oriented columns transmitting the loads applied normal to the joint surface. The effect of isotropic simplification was investigated by Peng et al. (2006) who found that there were minimal differences with isotropic and orthotropic material property assignment in the stresses computed by a finite element model of the femur. Therefore, axial strength is greater than

the strength in other directions, so it would most likely be the most important parameter to measure.

Bone can fail by being loaded in any direction, with the failure mechanism differing under tensile and compressive loading (Currey, 2012). Bone is typically under compressive stress in the body. However, for ease of testing, bone is often tested in bending or tension. The modulus of elasticity of bone is equal in tension and compression; however, yield occurs at lower stresses in tension compared to compression (Ebacher et al., 2007).

1.2.2.2 Viscoelasticity

The bones of the human body can be exposed to a wide range of strain rates during daily activities. Walking applies a strain rate on the order of 0.004/s, while sprinting and downhill running applies a strain rate closer to 0.05/s (Hansen et al., 2008). Traumatic events, such as motor vehicle accidents, can apply strain rates of up to 25/s (Hansen et al., 2008).

The mechanical properties of bone are usually studied at low strain rates; however, strain rate influences the material properties of bone (Hansen et al., 2008; McElhaney, 1966; Ural et al., 2011). This characteristic defines bone as a viscoelastic material (Adharapurapu et al., 2006; Reilly and Burstein, 1974). The strength of bone is increases with increasing magnitude, duration, and frequency of applied stress (Behrens et al., 1974).

The compressive strength and modulus of bone are proportional to strain rate raised to the 0.06 power (Carter and Hayes, 1977). As strain rate increases, the yield and

post-yield properties of bone accordingly increase (Currey, 2012; Hansen et al., 2008; McElhaney, 1966; Ural et al., 2011). Compared to specimens loaded at 0.01 cm/min, those loaded at a rate of 0.1 cm/min were found to be approximately 30% stronger (Carter and Hayes, 1977). Bone marrow increases the measured strength and modulus at strain rates above 10/s, which may serve to absorb energy in traumatic accidents (Carter and Hayes, 1977).

1.2.2.3 Inhomogeneity

Bone is inhomogeneous in terms of the distribution of its material properties. The orientation and density of the trabeculae affect the mechanical properties of the bone (Carter and Hayes, 1977). Regions of high trabecular density have been found in load-bearing areas, which also corresponded with regions of maximum strength (Harada et al., 1988). The mechanical properties of cancellous bone tend to exhibit regional variations. These can vary by up to two orders of magnitudes between sites within a single bone (Goldstein et al., 1983). Moreover, there are significant variations among individuals (Rho et al., 1995). Baca et al. (2008) found that orthotropic material property assignment was not essential for finite element models of long bones if inhomogeneous properties were applied.

1.3   Cancellous Testing Methods

1.3.1 Isolated Sections

Uniaxial compression testing of specimens between two parallel platens is the most widely used method for defining mechanical properties of cancellous bone as it is

simple and typically gives elastic modulus values within the range found by previous studies (Linde et al., 1992). This method has been used in several studies of the proximal tibia. Goldstein et al. (1983) machined 400 cancellous 7 mm x 10 mm cylindrical plugs from the first 40 mm of the tibia, which were subjected to uniaxial compression tests. They found that the greatest elastic modulus and ultimate strength at the contact regions beneath the femoral condyles and the cortical shell of the metaphysis. The elastic modulus ranged from 4.2 to 430 MPa in a single slice from one of their subjects. The medial region was found to be stronger than the lateral region, with the central region having the lowest strength. The greater strength on the medial side was attributed to the greater stress that is experienced in that region from daily dynamic activities such as walking (Sumner et al., 1994).

However, several problems arise when performing these tests. Uniaxial compression tests on machined specimens are affected by the structural end phenomenon. When cancellous specimens are extracted, the vertical trabeculae at the surface become unstable and bend as they lose the support of the horizontal struts. As a result, stiffness may be underestimated (Linde et al., 1992). The geometry of the machined specimen also influences its mechanical property. The modulus of 5 mm cubes has been shown to be 36% greater than cylindrical cancellous specimens with a diameter of 5 mm and length of 10 mm (Keyak et al., 1994; Linde et al., 1992). Machine compliance also can affect strain measurements, as small deformations in the load cell and trabeculae lead to an underestimation of stiffness (Linde et al., 1992). Finally, friction at the bone-platen

interface causes stress inhomogeneity at the surface of the specimen, which can lead to an overestimation of stiffness (Linde et al., 1992).

1.3.2 Indentation Testing

In an indentation test, an indentor with a known cross-sectional area is pressed into a site on the specimen with a known force so the trabeculae fail by buckling or bending (Carter and Hayes, 1977; Rincon-Kohli and Zysset, 2009). This generates a load versus displacement stiffness curve. The load-displacement data directly correlate with the specimen's stress-strain response (Wright and Hayes, 1976). Force is divided by the cross-sectional area of the indentor to determine the applied stress. The change in thickness divided by the original thickness of the specimen characterizes the resulting strain. Indentation modulus is the slope of the linear region of the stress-strain curve in an indentation test and the yield point occurs at 0.2% of the strain (Figure 1.5) (Reilly, 1974).

Although indentation testing does not completely account for all of the mechanical properties of bone, it is a simple and accurate way to measure the regional variation of *in situ* properties of cortical bone, cancellous bone, and cartilage (Hvid and Hansen, 1985; Harada et al., 1988). Testing bone *in situ* is more representative of the bone's physiologic response to loading. The bone matrix introduces boundary support around the indentation site to give a better approximation of bone strength. Higher stresses are encountered along the outer edges of the indentor during penetration tests; however, it was shown in a previous study that plastic deformation did not occur beyond

0.5 mm from its periphery (Finlay et al., 1989). Therefore, penetration in one test site does not alter the behavior of the material in adjacent sites (Finlay et al., 1989).

Hvid and Hansen (1985) examined the strength of cancellous bone in the proximal tibia. A 2.5 mm conical osteopenetrometer was used to penetrate into 2 cm thick slices of bone, which took measurements at 2 mm intervals at 1 mm/s. They found that the central and anterior regions of the medial condyle and the posterior region of the lateral condyle were the strongest. The lowest strength was found in the central, intercondylar region. These findings were in agreement with Finlay et al. (1989) who reported that the medial side was approximately two times stronger than the lateral side in a healthy knee. Moreover, the anterior region of the medial side was 50% stiffer and the posterior region was 25% stiffer than the same regions on the lateral side (Finlay et al., 1989). Hvid and Hansen (1985) also found that bone strength decreased towards the outer edges of the condyles. The areas of maximum strength corresponded with load transmission from cancellous bone to the cortical diaphysis of the tibia. This corresponded with the contact pressures experimentally measured in the knee under physiological loads (Hvid and Hansen, 1985). The high strength posterior area arises from the flexion of the knee resulting from being loaded in walking. The lateral center of contact moves over the posterior surface as the tibia internally rotates when the knee flexes (Hvid and Hansen, 1985).

Hvid and Hansen (1985) determined that bone strength was greatest in the proximal slice and decreased moving away from the joint surface. Areas with the greatest strength at the surface experienced the greatest decrease in strength through the depth of

the tibia. They concluded that there were central islands of strong cancellous bone beneath the subchondral bone layer, which serve to distribute loads over the joint. Limitations of the study include the fact that the conversion of penetration strength to compressive strength introduced error due to the shape of the needle, friction, and cross-sectional area. Furthermore, only 15 test sites were selected to study the variation of strength with depth.

Harada et al. (1988) performed indentation tests at a rate of 2 mm/min on exposed surfaces of the proximal tibia, and also found that the medial condyle was stronger than the lateral condyle. This trend continued through a depth of 25 mm in the proximal tibia. Strength decreased away from the proximal surface, especially over the first 5 mm. The regions of greatest strength in the medial and lateral condyles varied with depth. They found that the region of maximum strength moved from the central contact regions at the surface towards the periphery of the tibia through the depth. Regional variation in the mechanical properties of bone over the transverse plane of the tibia parallels the trabecular integrity and load distribution over load-bearing contact surfaces (Harada et al., 1988). Having only 19 to 39 test sites per slice, this study was limited in the number of test sites used to quantify the variation of mechanical properties. Furthermore, five unequal regions representing regions of contact were used to group test sites at varying levels in the proximal tibia.

Behrens et al. (1974) extracted 1 cm cubic specimens from the knee joint at contact areas at 0°, 45°, and 90° flexion. Indentation tests were run at 10 cm/min on embedded slices of cancellous bone. They found that the strength was highest in the

medial region, intermediate in the lateral region, and lowest in the central region. The central area of the medial region and the posterior area of the lateral region were reported to be the strongest overall (Behrens et al., 1974). The medial and lateral condyles function to bear load; however, higher forces are transmitted over the greater contact area of the medial condyle, which corresponds with increased bone strength (Behrens et al., 1974). Limitations of the study include that only two specimens were extracted from the lateral condyle and three from the medial condyle, which were not spatially aligned. Furthermore, Behrens et al. (1974) included normal and arthritic specimens within the investigation.

The strongest cancellous bone is typically found near the subchondral bone layer where elastic modulus was found to be between 300-450 MPa in the distal tibia (Aitken et al., 1985). Similar trends have been found in the distal humerus and the glenoid, where the strongest regions were closest to the subchondral bone layer (Anglin et al., 1999; Dunham et al., 2005). Transverse variations in properties were also noted in these studies. Interestingly, regional variation in yield strength but not elastic modulus was found in the radial head (Gordon et al., 2003).

The indentation modulus calculated from an indentation test can be converted to the conventional elastic modulus of a material through the Timoshenko-Goodier equation (Timoshenko and Goodier, 1970). The Timoshenko-Goodier theory of elasticity describes the stress distribution of an indentor applying a force on a linear, isotropic material with restricted boundaries. Elastic modulus (MPa) is calculated as:

$$E = S(1-v^2)/d \hspace{3cm} \textbf{Equation 1.1}$$

where S is indentation stiffness (N/mm), v is Poisson's ratio, and d is the diameter of the indentor (mm). This equation is limited in application to materials that are isotropic and homogenous. Moreover, the specimen surface must be semi-infinite, whereby it must be greater than six times the indentor diameter and greater than six times the depth at which maximum shear stress occurs (Sumner, 1994). Finlay et al. (1989) indicated that the equation does not account for the anisotropic nature of trabeculae.

1.4   Applications of Properties

1.4.1 Orthopaedic Devices

An understanding of the mechanical properties of bone is useful in the design of orthopaedic devices. The success of these devices, such as joint replacements and fracture plates, relies on achieving adequate fixation to the host bone. Orthopaedic devices, such as total knee replacements, require proper fixation in host bone (Figure 1.6). Proper fixation reduces the amount of stress experienced at the bone-device interface. This prevents the device from becoming loose and failing (Bourne and Finlay, 1986; Stern et al., 1997). The loosening of the tibial component through the soft central canal of the proximal tibia is the major cause of failure in total knee replacements (Bourne and Finlay, 1986; Stern et al., 1997). Therefore, the strongest regions of bone should be taken advantage of as sites of attachment to ensure device stability and be preserved to reduce the need for revision surgeries.

1.4.2 Finite Element Analysis
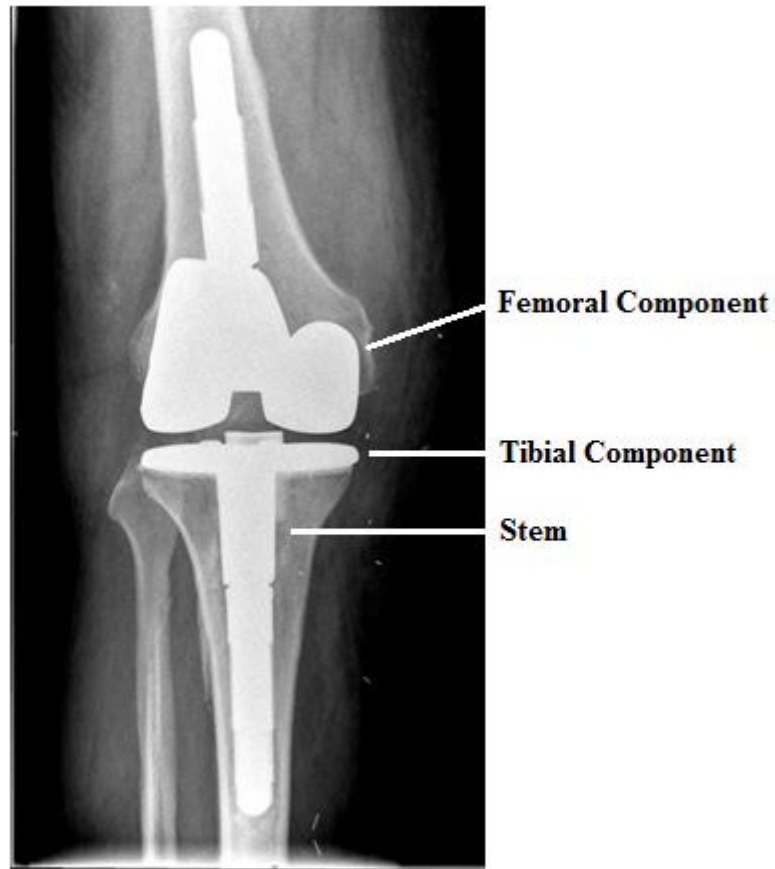
Figure 1.6 **Total Knee Replacement Device Components.**
Examples of orthopaedic devices include total knee replacements, which rely on achieving proper fixation in the host bone for long-term success. Loosening of the tibial component may be attributed to its attachment to the soft intramedullary canal of the tibia. *(From http://kneesurgeryclinic.co.uk).*
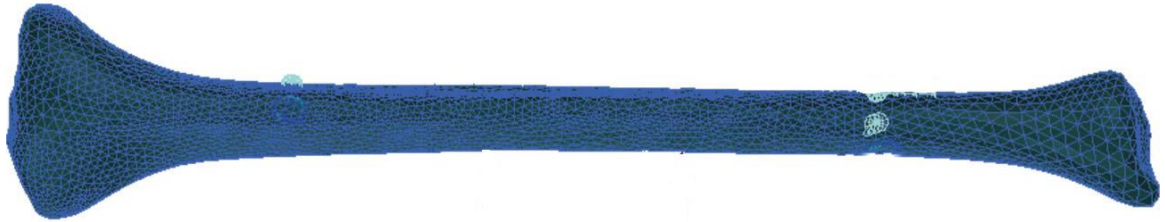
Figure 1.7 **Finite Element Model of the Tibia.**
FE models of bone require defining geometry, meshing, material properties, and boundary conditions. These models can then be used to simulate loading scenarios to observe the corresponding response. FE models can be used to predict the risk of injury to the bone and optimize orthopaedic device design. *(From Gray et al., 2008).*

Finite element (FE) models are used to simulate loading conditions to analyze the mechanical response of bone (Figure 1.7) (Carter and Hayes, 1977; Quenneville et al., 2011). FE analyses model the stress and strain experienced by a structure (Currey, 2012). They can thus be used to non-invasively predict the risk of injury under a variety of conditions specific to the subject (Schileo et al., 2007; Currey, 2012; Quenneville et al., 2011). FE models can also be used to optimize fixation as they allow for the determination of stresses and strains arising at the bone-device interface (Gray et al., 2008). Furthermore, improved prosthetic designs can be tested through FE modeling prior to manufacturing a prototype, thus reducing development costs.

FE modeling of bone involves geometry extraction, meshing, material property assignment, and applying boundary conditions and loads (Austman et al., 2008). Many studies use static FE models where bone is modeled as an inhomogeneous material using density-modulus relationships. Dynamic FE models are more computationally intensive, and therefore tend to apply bulk, rather than subject-specific, properties (Quenneville et al., 2011). These simplifications may affect the accuracy of the model, as stresses that develop in the bone depend on the defined material properties. The mechanical properties that characterize bone in modeling are often arbitrarily chosen by researchers, and have been shown to affect the results of the stress analysis (Hvid and Hansen, 1985). Furthermore, there has been a lack of emphasis on the convergence and validation of FE models through experimental testing to ensure that they are accurate (Currey, 2012; Quenneville et al., 2011; Gray et al., 2008).

The material properties of bone need to be precisely mapped during model construction (Quenneville et al., 2011). Most FE models use an average elastic modulus for cortical bone and less than six average elastic moduli to represent the variations in cancellous bone (Rho et al., 1995). Inhomogeneous material properties can be assigned to subject-specific FE models of bone by using computed tomography (CT)-derived density information. Density data can be applied to a density-modulus relationship to determine the corresponding modulus. The use of an appropriate density-modulus relationship can increase the accuracy of a model (Schileo et al., 2007; Helgason et al., 2008).

1.4.3 Computed Tomography

Computed tomography (CT) is a non-invasive method to evaluate the properties of bone (Figure 1.8). X-ray beams pass through a specimen and the attenuation data from discrete locations are recorded (Snyder and Schneider, 1991). The CT data are processed by a computer and reconstructed into slices of cross-sectional images (Arnold, 1994). Raw CT data are in the form of attenuation coefficients. The values relate the linear attenuation coefficient of bone to the linear attenuation coefficient of water. CT data are expressed as dimensionless Hounsfield Units (HU) (Table 1.1) (Snyder and Schneider, 1991). CT numbers linearly relate to the ash density of bone, which can be converted to apparent density for use in density-modulus equations (Schileo et al., 2007). CT has been found to give an accurate estimation of the mechanical properties of cancellous bone (Rho et al., 1995). However, there is uncertainty in the ability of CT to predict the mechanical properties of cortical bone due to differences in imaging methods and higher densities (Snyder and Schneider, 1991; Rho et al., 1995; Bentzen et al., 1987).

(a)
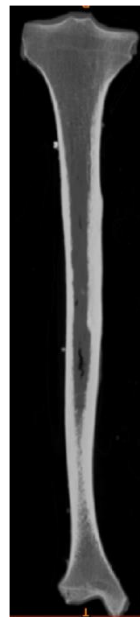
(b)

Figure 1.8   CT Scan of the Tibia.
The tibia is placed in (a) a CT scanner where X-rays pass through the bone and the image is re-constructed so density information, in the form of HU, can be extracted from (b) the CT scan. Cortical bone, cancellous bone and air appear as white, gray, and black, respectively, in a CT scan. *(From Toshiba America Medical Systems, http://medical.toshiba.com).*

22

Table 1.1   **Hounsfield Unit (HU) Scale.**
CT data is expressed in Hounsfield Units, which can be converted to density. Air, water, and bone correspond to -1000, 0, and +1000 HU, respectively. *(Adapted from Murphy, 2005).*

Tissue	HU
Air	-1000
Fat	-200 to -50
Water	0
Muscle	+25 to +40
Cancellous Bone	+100 to +200
Cortical Bone	+500 to +1000

Scanning energy influences the attenuation coefficient of fat which affects the measured CT number (Keyak et al., 1994). Although scanning energy can be held constant, calibrations will vary according to the dimension of the specimen (Keyak et al., 1994). The content of the image, the placement of the specimen within the field of view, and the alterations in structure all account for the differences in measured density (Keyak et al., 1994). Comparing CT numbers is difficult when different scanners are used and scanner drift is introduced. Specific CT scanners and extensive analysis would be needed to accurately collect density information (Snyder and Schneider, 1991). Therefore, a calibration phantom containing varying concentrations of potassium phosphate (K_2HPO_4) is often scanned simultaneously with a bone specimen to normalize mineralized skeletal tissue across CT scans (Nazarian et al., 2008; Snyder and Schneider, 1991; Keyak et al., 1994). The calibration phantom is used to quantify bone mineral density from CT images by reporting values in terms of mg/cm^3 K_2HPO_4 equivalent mineral density (Keyak et al., 1994). The calibration phantom corrects for variations in the x-ray beams and beam hardening effects (Arnold, 1994). CT values from different scanners can thereby be compared, as the phantom does not depend on the scanner model (Keyak et al., 1994).

The CT numbers of the calibration phantom are correlated with the CT numbers of bone to accurately calculate density (Figure 1.9). Epoxy resin corresponds to +1500 HU, water is 0 HU, and air is -1000 HU (Table 1.1). Cortical bone is typically around +1000 HU and cancellous bone is +200 HU. An accurate density value can thus be obtained. Density, however, does not account for the structural or anisotropic properties of bone (Linde et al., 1992). CT numbers thus reflect the degree of porosity rather than

The figure shows a plot of Ash Density (g/cm³) on the y-axis (0 to 1.2) versus Hounsfied Unit on the x-axis (0 to 1600). A line labeled with the equation $y = 0.0007x + 0.02$ passes from "Water" at the origin to "Epoxy Resin" at approximately 1500. Labels "Scaled" and "Measured" indicate projections at an x-value of about 800.
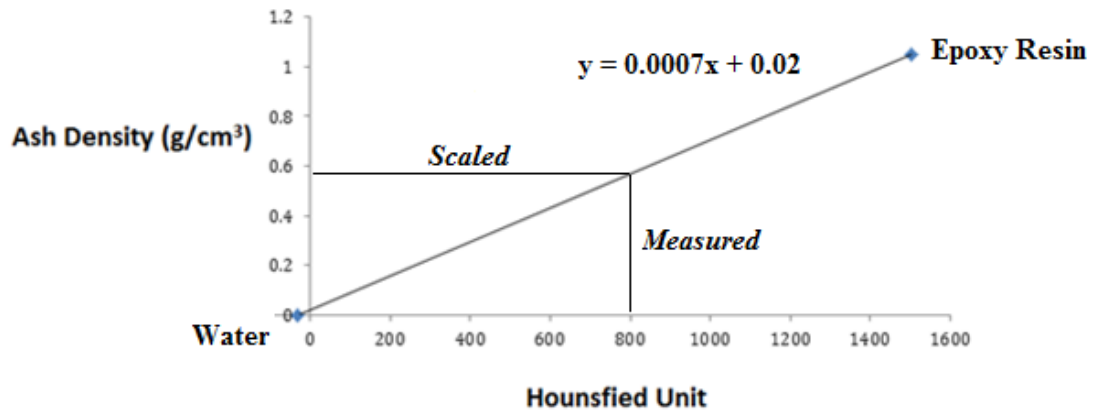
Figure 1.9   Correlation between Bone and Calibration Phantom CT Numbers.
A calibration phantom is used to convert CT numbers of bone to ash density. An equation of a line is generated between two points that define the CT number and ash density of water and the epoxy resin. The CT number of bone is input as the variable, x, to calculate the corresponding value, y.

the mineral content of bone (Rho et al., 1995). Therefore, the use of CT number and calculated density may not fully encompass the wide variations in elastic modulus found in cancellous bone (Rho et al., 1995).

1.4.4 Density-Modulus Relationships

Accurate FE models require proper material property assignment. Density-modulus relationships allow the assignment of inhomogeneous material properties to bone to develop the most representative FE model (Austman et al., 2008). Density-modulus relationships typically take the form:

$$\text{elastic modulus} = (a)(\text{density})^b \qquad\qquad \textbf{Equation 1.2}$$

where a and b are constants and the densitometric measure can be either apparent density or ash density (Carter and Hayes, 1977). Apparent density is the ratio of dry material to its volume, or its "waterless" density, and ash density is the ash weight per total tissue volume. Porosity, ash density, and apparent density all give accurate estimations of the volume of mineralized tissue (Carter and Hayes, 1977). However, ash density is the more easily reproduced measure, which facilitates comparison among studies (Keyak et al., 1994).

It has been shown that there is a positive power relationship between both ash and apparent density and modulus for cancellous bone (Duchemin et al., 2008; Rho et al., 1995; Keyak et al., 1994). A simple power relation forces the regression curve through the origin. This would mean that when CT density is zero, the modulus and strength of the bone is zero. However, CT density can in fact be less than zero for a bone with low ash density and fat content. This bone would still have an appreciable elastic modulus and

strength. CT data must be transformed by correlating it to ash density so that there can be a negative intercept and modulus can then be extracted from the regression analysis (Keyak et al., 1994).

There are many density-modulus relationships in the literature, with the most appropriate density-modulus relationship for all long bones yet to be determined (Figure 1.10). Furthermore, there is a lack of specific relationships for cortical versus cancellous bone and different directions within a single bone (Rho et al., 1995). These relationships are commonly developed for pooled specimens and are applied in studies without consideration of their applicability. Architectural differences between bone types gives rise to density-modulus relationships that are specific to the anatomic location (Morgan et al., 2003). Exponents in the density-modulus relationships (*i.e.* 'b' in equation 1.2) for cancellous bone have been proposed to fall in the range of 1.3 and 2.2, suggesting that trabeculae deform differently in bending across different types of bone (Morgan et al., 2003; Rho et al, 1995). The coefficients of the density-modulus equations (*i.e.* 'a' in equation 1.2) have greater variation in their possible values across bone sites. Differences in elastic modulus and structure may influence the coefficients to be more varied and site-specific (Morgan et al., 2003). In a previous study, elastic modulus values were found to vary by 49% between sites in the body (Morgan et al., 2003). As a result, a universal equation cannot be applied across bones (Morgan et al., 2003). The accuracy of FE models can be improved by using site-specific density-modulus relationships to predict material properties. However, the ability of these equations to predict modulus needs to be evaluated by making comparisons to the modulus derived through experimental tests.
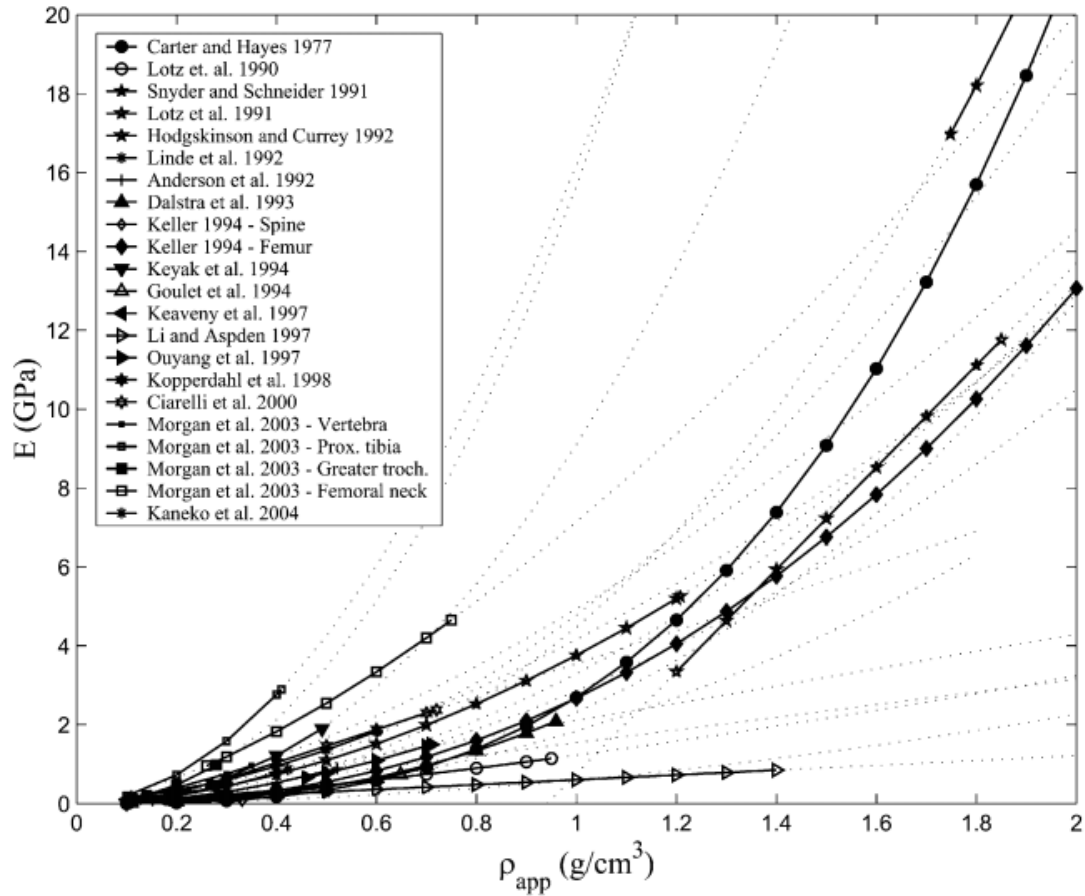
Figure 1.10   Density-modulus Relationships.
There are many density-modulus relationships in the literature. Selecting the most accurate relationship will increase the accuracy of a FE model. These relationships are site-specific; however, they are typically formed using pooled specimens under varying testing methods. *(From Helgason et al., 2008).*

1.5   Study Rationale

Accurate FE models can be used to improve the design of orthopaedic devices and predict the risk of injury to bone. The goal of this study is to quantify indentation modulus and yield strength from a large number of test sites through the proximal tibia to capture the inhomogeneous nature of cancellous bone. These findings will be useful in improving surgical outcomes where the identified regions of strength can be taken advantage of to ensure the long-term stability of orthopaedic devices. The second aim of this study is to investigate three site-specific density-modulus relationships from the literature to evaluate which one can most accurately predict material properties for cancellous bone from CT-derived density values, based on the aforementioned experimental testing. Selecting the best density-modulus relationship will assist in the assignment of inhomogeneous material properties to increase the accuracy of FE models of the tibia. This could dramatically decrease the need for costly and time-consuming experimental simulations, as improved models will better demonstrate how the tibia behaves under various loading conditions.

1.6   Objectives and Hypotheses

The objectives of this thesis were:

1. To determine the elastic modulus and yield strength of cancellous bone over transverse slices and through the depth of the proximal tibia using indentation tests, and

2. To compare the experimental data to CT-predicted modulus values to evaluate the applicability of three current density-modulus relationships to the tibia.

The corresponding hypotheses were:

1. Elastic modulus and yield strength of cancellous bone will vary through the depth and over the transverse slices of the proximal tibia. The area closest to the joint surface will be strongest and will decrease in strength where cancellous bone located furthest away will have the lowest modulus and yield strength. The medial condyle will be the stronger than the lateral condyle where the central medial, anterior medial, and posterior lateral regions will have the highest elastic modulus and yield strength. The intercondylar region will have the lowest elastic modulus and yield strength values.

2. Current density-modulus relationships will not reflect the regional variations of mechanical properties in the tibia. Therefore, a new equation will need to be developed that reflects regional variations in order to increase the accuracy of future finite element models.

1.7   Thesis Overview

This thesis provides insight into the mechanical properties of the tibia as determined through mechanical testing and CT analysis. Chapter 2 gives a thorough look into the regional variations of elastic modulus and yield strength of cancellous bone in the proximal tibia. Chapter 3 details the conversion of CT data into density values to calculate modulus from established density-modulus relationships, and a comparison to those values obtained through the mechanical testing. Chapter 4 concludes this work by summarizing the results and reflecting on their potential impact on orthopaedic device

design and FE analysis development, explaining the strengths and limitations of the study,

and presenting future steps in this area.

1.8 References

Adharapurapu, R., Jiang, F., Vecchio, K. S. (2006). Dynamic fracture of bovine bone. *Materials Science and Engineering*, *26*(8), 1325–1332.

Aitken, G.K., Bourne, M.D., Finay, J.B., Rorabeck, C.H., Andreae, P. R. (1985). Indentation Stiffness of the Cancellous Bone in the Distal Human Tibia. *Clinical Orthopaedics and Related Research*, (201), 264–271.

Anglin, C., Tolhurst, P., Wyss, U., Pichora, D. R. (1999). Glenoid Cancellous Bone Strength and Modulus. *Journal of biomechanics*, *32*, 1091–1097.

Arnold, B. A. (1994). Calibration phantom and improved method of quantifying calcium and bone. United States.

Askew, M.J., Lewis, J. L. (1981). Analysis of model variables and fixation post length effects on stresses around a prosthesis in the proximal tibia. *J Biomech Eng*, *103*(4), 239–245.

Austman, R. L., Milner, J.S., Holdsworth, D.W., and Dunning, C. E. (2008). The effect of the density-modulus relationship selected to apply material properties in a finite element model of long bone. *Journal of Biomechanics*, *41*, 3171–3176.

Baca, V., Horak, Z., Mikulenka, P., and Dzupa, V. (2008) Comparison of an inhomogeneous orthotropic and isotropic material models used for FE analyses. *Med Eng Phys 30(7)*, 924-930.

Behrens, J.C., Walker, P.S., Shoji, H. (1974). Variations in Strength and Structure of Cancellous Bone at the Knee. *Journal of biomechanics*, *7*, 201–207.

Bentzen, S. M., Hvid, I., and Johnson, J. (1987). Mechanical Strength of Tibial Trabecular Bone Evaluated by X-Ray Computed Tomography. *Journal of Biomechanics, 20(8),* 734-752.

Bourne, R.B. and Finlay, J. B. (1986). he influence of tibial component intramedullary stems and implant-cortex contact on the strain distribution of the proximal tibia following total knee arthroplasty: an in vivo study. *Clinical Orthopaedics and Related Research*, *208*, 95–99.

Carter, D.R. and Spengler, D. M. (1978). Mechanical Properties and Composition of Cortical Bone. *Clinical Orthopaedics and Related Research*, *135*, 192–217.

Carter, D.R., Hayes, W. C. (1977). The compressive behavior of bone as a two-phase porous structure. *J Bone Joint Surg Am*, *59*(7), 954–962.

Choi, K., Goldstein, S. A. (1992). A comparison of the fatigue behavior of human trabecular and cortical bone tissue. *J Biomech*, *25*(12), 1371–1381.

Crowninshield, R. D., & Pope, M. H. (1974). The response of compact bone in tension at various strain rates. *Annals of Biomedical Engineering*, *2*(2), 217–225.

Currey, J. D. (1974). The effect of strain rate, reconstruction and mineral content on some mechanical properties of bovine bone. *Journal of Biomechanics*, *Volume 8*(1), 81–86.

Currey, J.D. (2012). The structure and mechanics of bone. *J Mater Sci*, *47*, 41–54.

Currey, John D. (2004). Tensile yield in compact bone is determined by strain, post-yield behaviour by mineral content. *Journal of biomechanics*, *37*(4), 549–56.

Duchemin, L., Bousson, V., Raossanaly, C., Bergot, C., Laredo, J. D., Skalli, W., & Mitton, D. (2008). Prediction of mechanical properties of cortical bone by quantitative computed tomography. *Medical engineering & physics*, *30*(3), 321–8.

Dunham, C.E., Takaki, S.E., Johnson, J.A., Dunning, C. E. . (2005). Mechanical Properties of Cancellous Bone of the Distal Humerus. *Clinical Biomechanics*, *20*, 834–838.

Ebacher, V., Tang, C., McKay, H., Oxland, T.R., Guy, P., Wang, R. (2007). Strain redistribution and cracking behavior of human bone during bending. *Bone*, *40*(5), 1265–1275.

Finlay, J.B., Bourne, R.B., Kraemer, W.J., Moroz, T.K., Rorabeck, C. H. (1989). Stiffness of Bone Underlying Tibial Plateaus of Osteoarthritic and Normal Knees. *Clinical Orthopaedics and Related Research*, *247*, 193–201.

Gibson, L. J. (1985). The Mechanical Behaviour of Cancellous Bone. *J. Biomechanics*, *18*(5), 317–328.

Goldstein, S.A., Wilson, D.L., Sonstegard, D.A., Matthews, L. S. (1983). The Mechanical Properties of Human Tibial Trabeculae Bone as a Function of Metaphyseal Location. *Journal of biomechanics*, *16*(12), 965–969.

Gordon, K.D., Duck, T.R., Wing, G.J.W., Johnson, J. A. (2003). Mechanical Propertes of Subchondral Cancellous Bone of the Radial Head. *Journal of Orthopaedic Trauma*, *17*(4), 285–289.

Gray, H. (1918). *Anatomy of the Human Body*. (W. H. Lewis, Ed.) (20th ed.). Philadelphia: Lea & Febiger.

Gray, H.A., Taddei, F., Zavatsky, A.B., Cristofolini, L., and Gill, H. S. (2008). Experimental validation of a finite element model of a human cadaveric tibia. *Journal of Biomechanical Engineering*, *130*.

Hansen, U., Zioupos, P., Simpson, R., Currey, J. D., & Hynd, D. (2008). The effect of strain rate on the mechanical properties of human cortical bone. *Journal of biomechanical engineering*, *130*(1), 011011.

Harada, E., Wevers, H.W., Cooke, T. D. V. (1988). Distribution of Bone Strength in the Proximal Tibia. *The Journal of Arthroplasty*, *3*(2), 167–175.

Helgason, B., Perilli, E., Schileo, E., Taddei, F., Brynjolfsson, S., Viceconti, M. (2008). Mathematical relationships between bone density and mechanical properties: a literature review. *Clin Biomech*, *23*(2), 135–146.

Hert, J., Fiala, P., and Petrtyl, M. (1994). Osteon orientation of the diaphysis of the long bones in man. *Bone*, *15*(3), 269–277.

Hvid, I., Hansen, S. L. (1985). Trabeculae Bone Strength Patterns at the Proximal Tibial Epiphysis. *Journal of Orthopaedic Research*, *3*, 464–472.

Johnson, T. P. M., Socrate, S., & Boyce, M. C. (2010). A viscoelastic, viscoplastic model of cortical bone valid at low and high strain rates. *Acta biomaterialia*, *6*(10), 4073–80.

Keyak, J.H., Lee, I.Y., and Skinner, H. B. (1994). Correlations between orthogonal mechanical properties and density of trabeculae bone: use of different densitometric measures. *Journal of Biomedical Materials Research*, *28*, 1329–1336.

McElhaney, J. H. (1966). Dynamic response of bone and muscle tissue. *J Appl Physiol*, *21*(4), 1231–1236.

Morgan, E.F., Bayraktar, H.H., and Keaveny, T. M. (2003). Trabecule bone modulus-density relationships depend on anatomic site. *Journal of Biomechanics*, *36*, 897–904.

Nazarian, A., Snyder, B.D., Zurakowski, D., and Muller, R. (2008). Quantitative micro-computed tomography: a non-invasive method to assess equivalent bone mineral density. *Bone*, *43*(2), 302–311.

Peng, L., Bai, J., Zeng, X., and Zhou, Y. (2006) Comparison of isotropic and orthotropic material property assignments on femoral finite element models under two loading conditions. *Med Eng Phys 28(3),* 227-233.

Quenneville, C.E., McLachlin, S.D., Greeley, G.S., and Dunning, C. (2011). Injury tolerance criteria for short-duration axial impulse loading of the isolated tibia. *Journal of Trauma-Injury Infection and Critical Care*, *70*(1), 12–18.

Reilly, D. T., & Burstein, a H. (1974). Review article. The mechanical properties of cortical bone. *The Journal of bone and joint surgery. American volume*, *56*(5), 1001–22.

Rho, J.Y., Hobatho, M.C., Ashman, R. B. (1995). Relations of mechanical properties to density and CT numbers in human bone. *Med Eng Phys*, *17*(5), 347–355.

Rincon-Kohli, L. and Zysset, P. K. (2009). Multi-axial mechanical properties of human trabecular bone. *Biomechanics and Modeling in Mechanobiology*, *8*(3), 195–208.

Schileo, E., Taddei, F., Malandrino, A., Cristofolini, L., and Viceconti, M. (2007). Subject-specific finite element models can accurately predict strain levels in long bones. *Journal of Biomechanics*, *40*(13), 2982–2989.

Snyder, S. M. and Schneider, E. (1991). Estimation of mechanical properties of cortical bone by computed tomography. *Journal of Orthopaedic Research*, *9*(3), 422–431.

Stern, S., Wills, R.D., and Gilbert, J. L. (1997). The effect of tibial stem design on component micromotion in knee arthroplasty. *Clinical Orthopaedics and Related Research*, *345*(44-52).

Sumner, D.R., Berzins, W.A., Turner, T. M. (1994). Distribution of Young's Modulus in the Cancellous Bone of the Proximal Canine Tibia. *Journal of biomechanics*, *27*(8), 1095–1099.

Timoshenko, S. and Goodier, J. (1970). *Theory of Elasticity* (3rd ed.). New York: McGraw-Hill.

Ural, A., Zioupos, P., Buchanan, D., & Vashishth, D. (2011). The effect of strain rate on fracture toughness of human cortical bone: A finite element study. *Journal of the mechanical behavior of biomedical materials*, *4*(7), 1021–32.

Van Oers, R.F.M., Ruimerman, R., van Retbergen, B., Hilbers, P.A.J., and Huiskes, R. (2008). Relating osteon diameter to strain. *Bone*, *43*(3), 476–482.

Wolff, J. (1870). Ueber die innere architektur der knochen. *Virchow's Arch*, *50*(1), 389–453.

Wright, T. M., & Hayes, W. C. (1976). Tensile testing of bone over a wide range of strain rates: effects of strain rate, microstructure and density. *Medical & biological engineering*, *14*(6), 671–80.

Chapter 2: The Mechanical Properties of Cancellous Bone in the Proximal Tibia

OVERVIEW: This chapter explains the motivation behind the undertaking of a comprehensive study to investigate the mechanical properties of cancellous bone in the proximal epiphysis of the tibia. Elastic modulus and yield strength were evaluated using indentation testing on slices of bone. This chapter describes the extent of regional variations of bone properties observed through mechanical experimentation.

2.1   Introduction

Cancellous bone is found enclosed within the epiphyses of long bones, and consists of a network of interconnected trabeculae (Harada et al., 1988). The organization of trabeculae along the lines of principal stress gives bone its anisotropic and inhomogeneous behavior (Hvid and Hansen, 1985). However, dynamic finite element (FE) models tend to generalize bone as a homogenous and isotropic material (Taddei et al., 2006). This simplification in the material properties may affect the accuracy and the applicability of dynamic finite element analysis in the understanding of stress behavior in the tibia.

Quantification of the regional variations in the mechanical properties of the proximal tibia can also improve the success of orthopaedic devices, such as total knee replacements. Proper fixation of the orthopaedic device in the host bone reduces the amount of stress that is experienced at the bone-device interface, and ensures its long-term stability (Bourne and Finlay, 1986; Stern et al., 1997). Therefore, achieving

purchase in strong bone stock would help to prevent these devices from becoming loose, ultimately leading to their failure.

Regional variations in the mechanical properties of cancellous bone of the tibia have been well noted in the literature (Behrens et al., 1974; Goldstein et al., 1983; Harada et al., 1988; Hvid & Hansen, 1985). Previous studies have determined that the strength of cancellous bone decreases through the depth of the proximal tibia, especially over the first 5 mm distal to the subchondral bone surface as the trabeculae begin to thin (Harada et al., 1988; Hvid & Hansen, 1985; Aitken et al., 1985).

Multiple studies have also found that the mechanical properties vary over the transverse plane relative to load distributions in the tibia (Behrens et al., 1974; Goldstein et al., 1983; Harada et al., 1988; Hvid & Hansen, 1985). It has been well established that strength is greater in the weight-bearing medial condyle than the lateral condyle, and lowest in the intercondylar region (Behrens et al., 1974; Goldstein et al., 1983; Harada et al., 1988; Hvid, & Hansen, 1985). Within the condyles, the central region of the medial condyle and the posterior region of the lateral condyle have been identified as having the highest strength (Behrens et al., 1974; Hvid & Hansen, 1985). However, the area of maximum strength shifts toward the outer margins moving away from the subchondral bone layer in both condyles (Harada et al., 1988). Furthermore, the regions that had the highest strength at the proximal surface had the most pronounced decrease in strength moving down the tibia (Hvid & Hansen, 1985). These studies suggest that areas of highest strength extend from the metaphyseal cortices towards the central contact regions of the condyles, where bone strength decreases toward the margins of the slice.

Mechanical properties have also been noted at other locations in the body to vary with depth (Aitken et al., 1985; Anglin et al., 1999; Dunham et al., 2005; Sumner et al., 1994) and across the transverse section (Anglin et al., 1999; Dunham et al., 2005; Sumner et al., 1994). Although previous studies have sought to characterize the properties of cancellous bone of the proximal tibia, they are difficult to compare, as the mechanical response of bone is affected by the testing technique employed. Techniques used have included conical osteopenetrometer (Hvid and Hansen, 1985), removal of bone plugs (Goldstein et al., 1983), cubes (Behrens et al., 1984), and indentation testing (Harada et al., 1988). Tests requiring machining may have damaged trabeculae at the surface of the specimen, causing an underestimation of stiffness (Linde et al., 1992). Furthermore, previous studies have quantified mechanical properties from a limited number of test sites, which have been grouped into three to six regions (Goldstein et al., 1983; Hvid and Hansen, 1985; Behrens et al., 1974; Harada et al., 1988). Some studies have also included older and arthritic tibias in their evaluation of mechanical properties, which may have affected their results (Behrens et al., 1984; Harada et al., 1988). Although compressive strength is closely related to elastic modulus, past studies have not specifically quantified the elastic modulus of the cancellous bone of the proximal tibia (Hvid and Hansen, 1985). The purpose of this study was to therefore quantify the modulus and yield strength of cancellous bone over transverse slices and through the depth of the proximal tibia through indentation testing of a large number of test sites, in order to provide a comprehensive investigation of all regional variations.

2.2   Materials and Methods

2.2.1 Specimen Preparation

Five fresh-frozen cadaveric tibias (age range: 46-70 years; mean age: 55.4 (10.7) years) were obtained from Mount Sinai Allograft Technologies (Toronto, ON) (Table 2.1). All tibias were from male donors, with two tibias from left legs and three from right legs. There were no paired specimens. All donors were free of disease and no abnormalities were observed. All tibias were stripped of soft tissues with a scalpel and sandpaper and kept frozen at -20°C.

The length of each tibia was measured from the inferior articular surface to the base of the intercondyloid eminence (Table 2.1). Each tibia was scanned using a standard clinical CT scanner (GE Medical Systems LightSpeed VCT, Hamilton, Canada) with scan parameters 120 kV and 59.4 mAs and 0.625 mm slice thickness. A CT image of a representative specimen was opened with Mimics® (Materialise, Leuven, Belgium) to determine the length of the epiphyses relative to the whole bone. The length of one tibia was found to be 403.8 mm. Its proximal end was measured from the midpoint of the epiphyseal line to the intercondyloid eminence and found to be 64.6 mm. The distal epiphysis was measured from the midpoint of the distal epiphyseal line to the inferior articular surface, which was 40.1 mm. Therefore, cancellous bone was found to fill the proximal 16% and distal 10% of the tibia and assumed to be similar in the remaining tibiae. The locations of the cancellous bone slices were outlined by five marks drawn 5 mm apart from the proximal end over the anterior-medial surface (Figure 2.1).

Four consecutive, transverse slices were cut orthogonal to the long axis of each frozen tibia using a 5" x 0.3 mm thick diamond wafering blade (Cedarlane, Burlington,

Table 2.1. **Specimen information.**
Donor information was obtained from Mount Sinai Allograft Technologies. The length of each tibia was measured from the inferior articular surface to the base of the intercondyloid eminence.

ID Number	Side	Age	Gender	Length (cm)
1469-95341	Left	46	Male	40.4
1336-68687	Right	46	Male	37.9
1325-67581	Right	52	Male	41.0
1403-79389	Left	70	Male	36.6
1393-77645	Right	63	Male	38.5
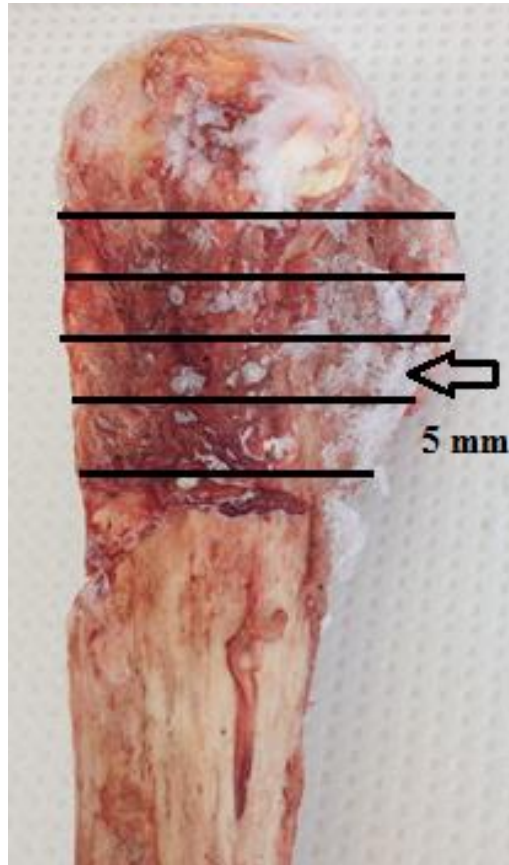
Figure 2.1   Cancellous slices were marked out on the proximal epiphyses.
Five cut sites were marked 5 mm apart on each tibia, distal to the subchondral bone layer (not to scale).

ON) mounted on an Isomet low speed saw (Buehler, Lake Bluff, Illinois, USA) (Figure 2.2a, b). The tibia was held in place, over the blade, by a custom-designed clamp attached to the arm of the saw (Figure 2.3; Appendix B). The tibia was horizontally oriented through the clamp so that it rested on its flattest surface to prevent it from slipping during a cut (Figure 2.4). Furthermore, the tibia was positioned to ensure the cut would go through the entire width of the epiphysis. The tibia was manually pressed into the blade rotating at medium speed through an ethanol bath to facilitate making precision cuts and slices were removed in a proximal to distal sequence. Following each cut, the tibia was slid through the clamp to make the subsequent transverse cut. The most proximal layer was cut to be the minimum thickness required to reveal a flat, smooth bone surface with no cortical bone present. Subsequent cuts were made relative to this surface, approximately 5 mm apart, and the slices were frozen at -20°C (Figure 2.5; Appendix C). Prior to performing mechanical testing, CT scans of the frozen slices were taken under the aforementioned parameters.

In order to standardize the generation of a grid, slices were oriented such that the posterior edges of the condyles were aligned along a straight surface and a parallel line was drawn across the widest point of each slice using a permanent marker and ruler. From this reference point, each slice was marked with a 5 x 5 mm grid on its superior surface to allow for a large number of test sites to be generated (Figure 2.6).

2.2.2 Indentation

(a)   (b)

**Figure 2.2   Tibias were cut with (a) a diamond wafering blade attached to (b) a
low speed saw.**
Precision cuts were made as each bone was pressed into the blade, which
rotated at medium speed through an ethanol bath.
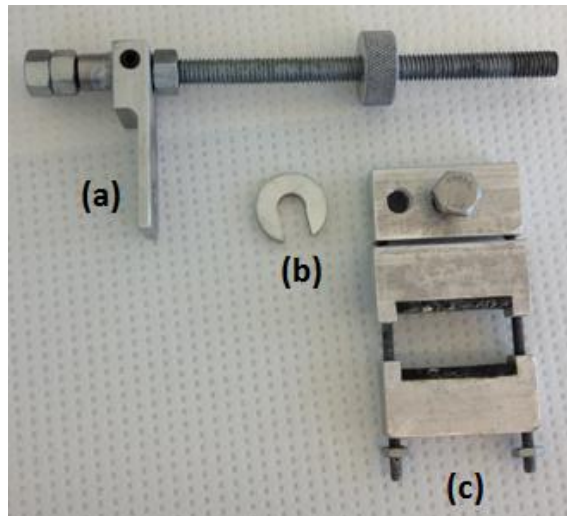
Figure 2.3   The custom-designed clamp to secure the tibias during cuts.
The clamp consisted of: (a) an arm that allowed the tibia to be held at its diaphysis; (b) 5 mm thick, removable spacers that helped maintain a consistent orientation; and (c) a rubber-lined clamp that prevented the tibia from slipping.
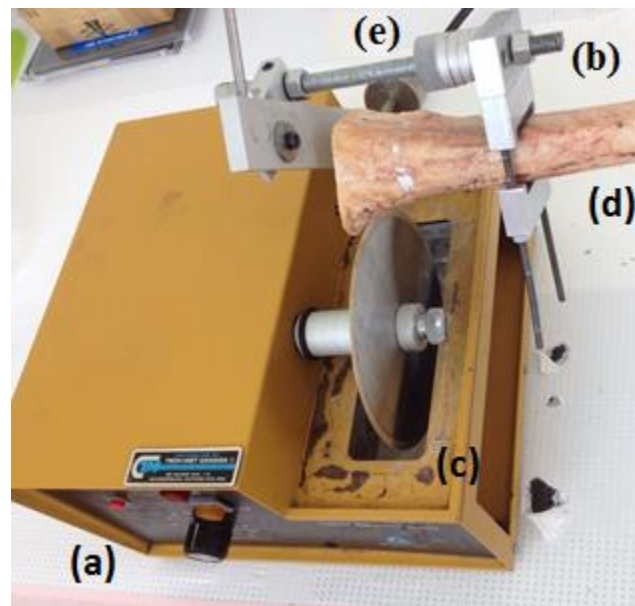
Figure 2.4   The experimental setup used for the extraction of cancellous slices.
(a) A low speed saw was equipped with (b) a clamp positioned over (c) the blade, which rotated as (d) the tibia was pressed into it to make the cut. (e) A spacer was removed after each cut, which moved the tibia to the left by 5 mm.
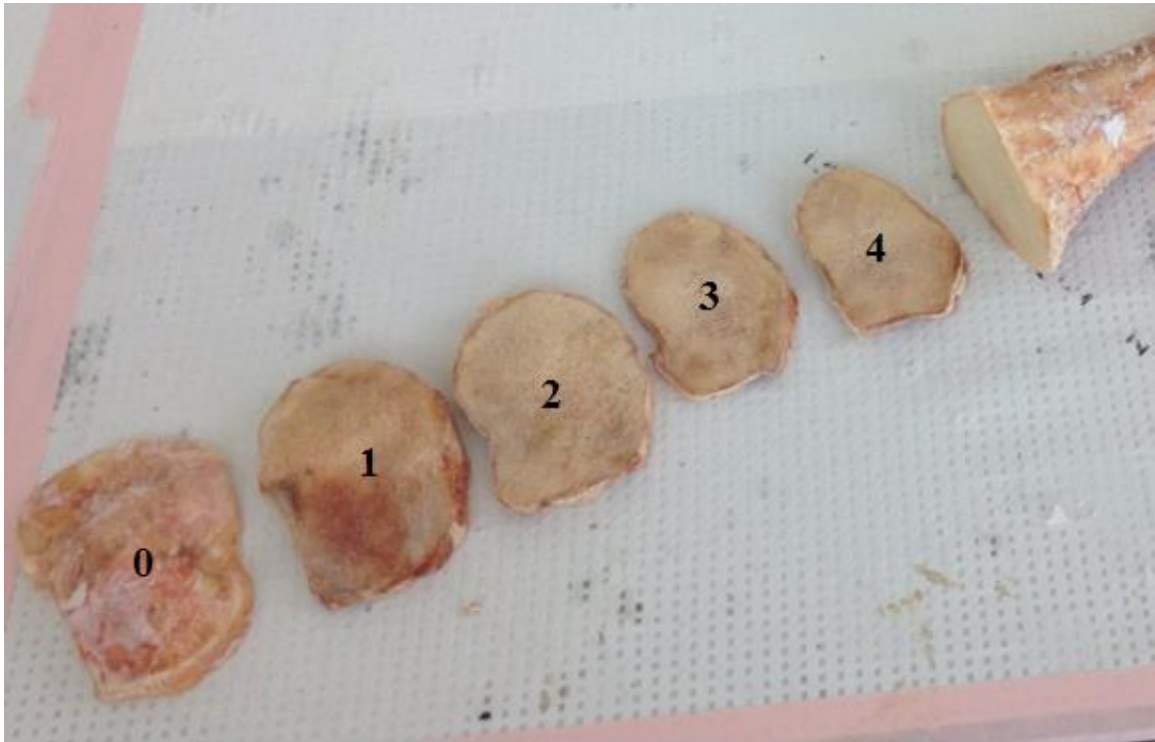
Figure 2.5 **Cancellous slices extracted from the proximal end of each tibia.**
The first layer (0) consisted of cortical bone and was discarded. The subsequent slices (1, 2, 3, 4) were each approximately 5 mm thick and used for mechanical testing.

Figure 2.6   **The 5 mm by 5 mm grid defining the test sites.**
This grid size allowed a large number of test sites to be available for indentation testing.

The slices were thawed for two hours prior to testing and kept moist with saline during testing. Indentation tests were conducted using a 1334 N (300 lb) load cell attached to a materials testing machine (ADMET, Norwood, MA). Each slice was placed on a flat metal plate and a 4 mm diameter stainless steel indentor was brought to contact the surface (Figure 2.7a). Subsequently it was pressed into the center of each test site from the superior to inferior direction to emulate the normal physiological loading direction, at a rate of 1 mm/min to a depth of 2 mm (Figure 2.7b). The order of testing of sites was randomized to minimize any testing effects from adjacent sites. Tests were terminated if tilt occurred whereby the specimen lifted off the metal plate. Any sites visually identified to contain cortical bone were excluded. Load-displacement data were collected at 64 Hz.

2.2.3 Analysis and Regional Pooling

The load-displacement data of each test site were converted into a stress-strain curve. Stress was calculated by dividing load by the area of the indentor, 12.6 mm^2. Displacement was converted to strain by dividing the displacement by the original, measured thickness of that particular slice. A custom-written Matlab® program (MathWorks, Nattick, MA, USA) was used to calculate yield strength and indentation modulus by applying a linear regression to the stress-strain data points (Appendix D). Indentation modulus was calculated as the slope of the line of best fit on the linear portion of the curve. Yield strength was the point on the curve at which there was a 0.2% deviation from the line of best fit.

(a)   (b)

Figure 2.7   Indentation testing setup.
Indentation testing was performed using (a) an indentor attached to (b) a
load cell on a materials testing machine.

The sites were pooled into nine equally spaced regions based on anatomical landmarks. Columns were grouped into approximately equal thirds in the medial to lateral direction, thus defining the medial, central, and lateral regions. From the anterior to posterior direction, columns were again divided into approximately equal thirds to create anterior, central, and posterior regions. This resulted in a grid of nine regions: anterior medial (AM), anterior central (AC), anterior lateral (AL), central medial (CM), central central (CC), central lateral (CL), posterior medial (PM), posterior central (PC), and posterior lateral (PL) (Figure 2.8). A two-way ANOVA ($\alpha=0.05$) was performed on the indentation modulus and yield strength data, with depth and region as the independent variables. Post-hoc Student-Neuman-Keuls tests were run for all analyses ($p<0.05$).

A sensitivity analysis was performed on three slices from two tibias to determine if the size of the region affected the average modulus. The nine regions were re-established by shifting the dividing boundaries by two test sites in the rows and columns in each of the medial, lateral, anterior, and posterior directions (Appendix E). The percent difference in indentation modulus was calculated between original (equally divided) region and the new region. Inter-specimen variability was calculated as the coefficient of variation (the ratio of standard deviation to mean).

As the modulus obtained herein represents indentation modulus, it was converted to true elastic modulus for comparison with other studies. True elastic modulus was calculated by utilizing the Timoshenko formula (Timoshenko and Goodier, 1970):

$$E = S(1-\upsilon^2)/d \qquad\qquad\qquad \text{Eq. 2.1}$$
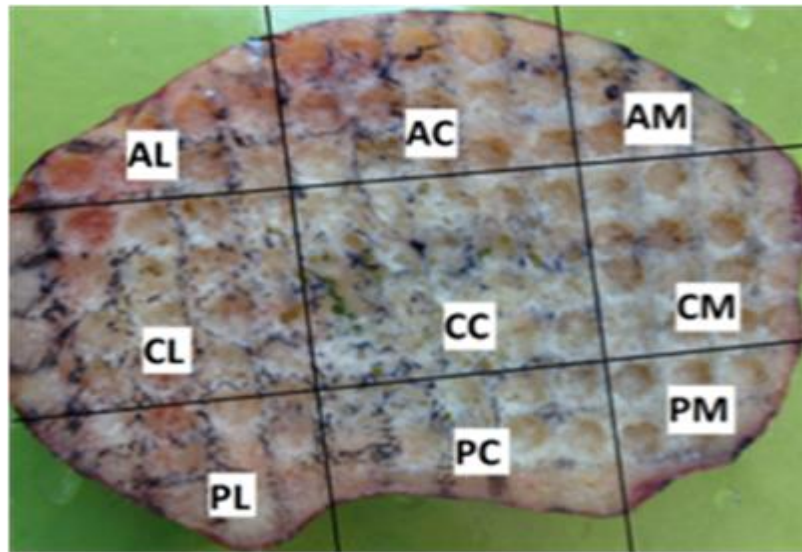
Figure 2.8   Definition of the nine transverse regions.
The test sites on each slice were divided into nine approximately equal regions: anterior medial (AM), anterior central (AC), anterior lateral (AL), central medial (CM), central central (CC), central lateral (CL), posterior medial (PM), posterior central (PC), and posterior lateral (PL) according to anatomical landmarks.

where S was the stiffness, or slope of the load-displacement curve, υ is Poisson's ratio, and d is the diameter. Stiffness was equal to the indentation modulus multiplied by the area of the indentor divided by the thickness of the specific slice (Appendix F). A Poisson's ratio (υ) of 0.3 was assumed (Helgason et al., 2008) and d was 4 mm, the diameter of the indentor. A two-way ANOVA was performed, using a significance level of $\alpha = 0.05$, on the elastic modulus data, with depth and region as the independent variables. Post hoc Student-Neuman-Keuls tests were run for all analyses ($p<0.05$) to look at slice by region interactions.

2.3   Results

Variations in the surface area of the slices created between 66 and 139 (mean = 113) test sites for indentation per slice. Values for each region of each bone slice were averaged prior to performing statistical analyses to prevent the number of test sites from affecting the outcome. A characteristic stress-strain curve was consistently observed, whereby a straight line followed a toe-in region to the point of yield, after which the bone softened and experienced near constant load (Figure 2.9). Approximately 30 yield strength data points, over all the specimens, were discarded due to lift-off that occurred when the superior surface had a larger diameter than the inferior surface within the same slice. The slices had a mean (SD) thickness of 6.3 (2.0) mm (Appendix C). The discarded slice ranged in thickness from 3.7 to 7.1 mm and was not tested.

Indentation modulus for pooled data from all regions ranged from 0.05 to 1223.1 MPa with a mean (SD) of 166.3 (39.3) MPa (Table 2.2; Figure 2.10a, b). Yield strength
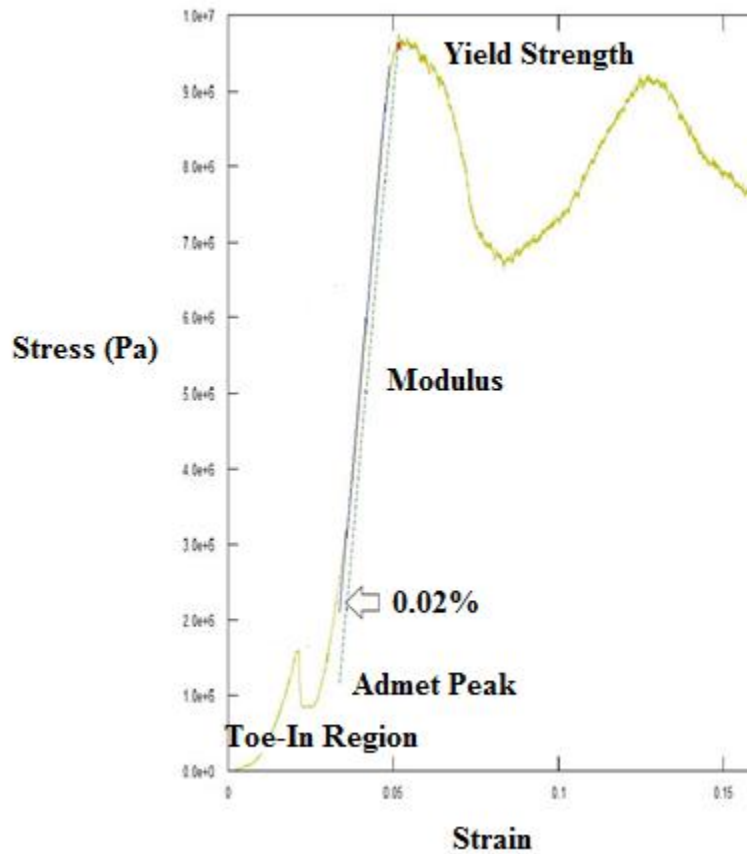
Figure 2.9   **Representative stress-strain curve.**
The load-displacement data were converted to a stress-strain curve using Matlab. The toe-in region and the Admet peak were not considered during analysis. Elastic modulus was calculated as the slope of the linear portion of the curve. A 0.02% offset was used to determine yield strength.

Table 2.2 **Indentation modulus and yield strength of specimens.**
The mean and standard deviation were calculated for each bone.

Bone	Age	Mean Modulus (MPa)	Standard Deviation (MPa)	Yield Strength (MPa)	Standard Deviation (MPa)
1325	52	202.9	63.4	11.8	6.6
1336	46	231.9	104.3	12.0	4.8
1393	63	143.5	51.7	8.1	3.7
1469	46	148.7	28.4	11.7	5.9
1403	70	134.6	32.3	6.7	3.9

a > 2, 3, 4

(a)

a > AC, CC, PC, AL, CL, PL

b > AC, CL

c < AM, CM, PM, AC, PC, AL, CL, PL

(b)
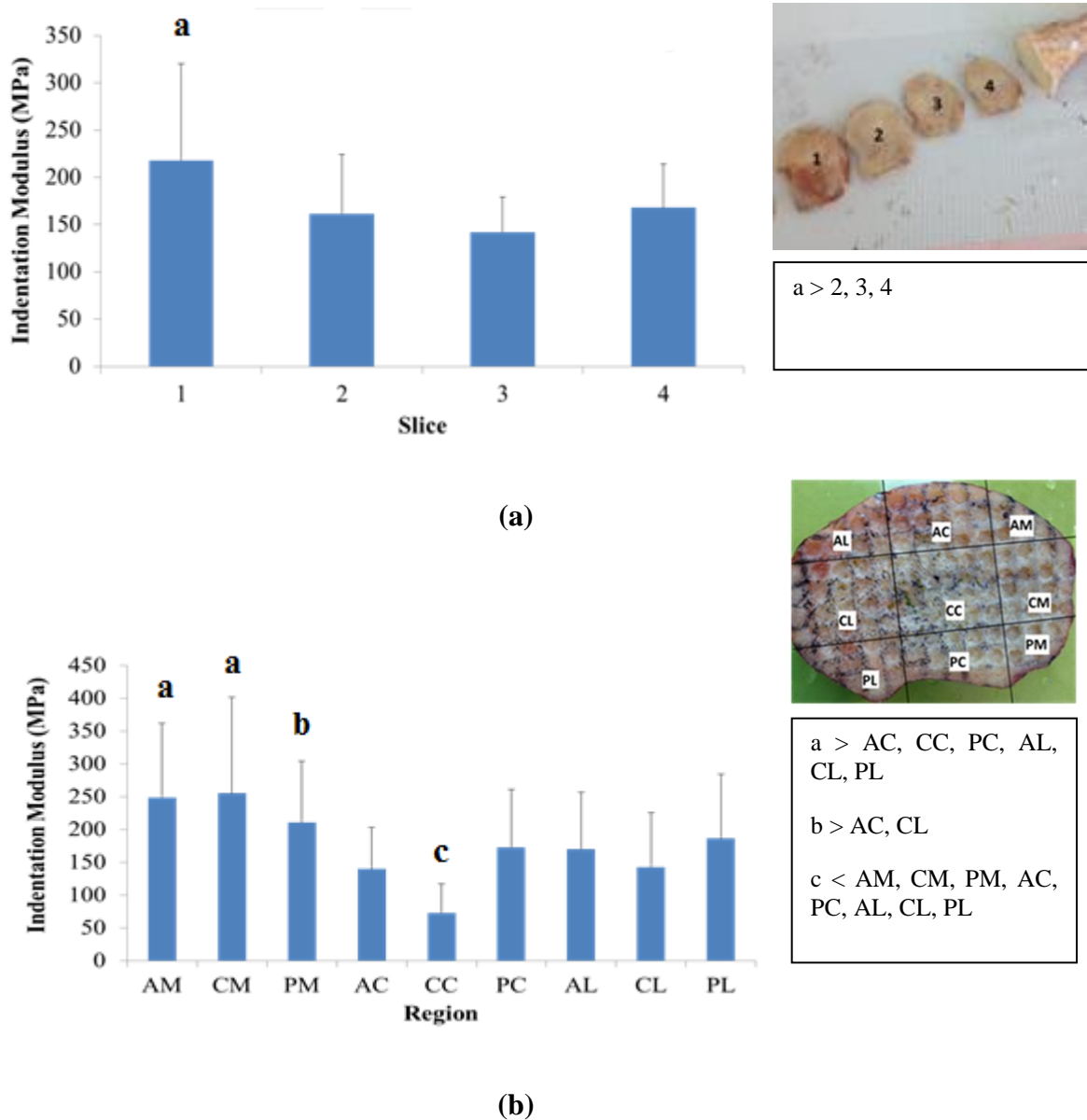
Figure 2.10   Indentation modulus of each (a) slice and (b) region.
Standard deviation is represented with error bars. A two-way ANOVA (p<0.05) was used to determine if there were significant differences, as indicated by the letters above the bars and explained in the legend.

ranged from 0.01 to 79.5 MPa with a mean of 10.1 (2.5) MPa (Figure 2.11a, b). The results from the two-way ANOVA test showed that yield strength and indentation modulus were significantly greater in the first, most proximal slice when compared to the second, third, and fourth slices ($p < 0.05$) (Figure 2.10a, 2.11a). The second slice also had a significantly greater yield strength than the third and fourth slices (Figure 2.11a). A positive, exponential correlation was found between yield strength and indentation modulus ($R^2 = 0.8$) (Figure 2.12).

The central central (CC) region had a significantly lower indentation modulus than all the surrounding regions (AM, AC, AL, CM, CL, PM, PC, PL) (Figure 2.10b). The indentation moduli of the anterior medial (AM) and central medial (CM) regions were significantly higher than all regions except for the posterior medial (PM) region. The PM region had a significantly higher indentation modulus than the anterior central (AC) and central lateral (CL) regions. The CC region also had a significantly lower yield strength than all the other regions, with the exception of AC (Figure 2.11b). Yield strength was significantly higher in the medial (AM, CM, PM) regions compared to all the other regions (AC, AL, CC, CL, PC, PL). AM and CM also had significantly greater yield strength than PM.

A pattern was observed over the transverse slices where the outer edges displayed moderate indentation modulus values, which increased towards the centers of each condyle and then decreased to the lowest values within the intercondylar region (Figure 2.13). The highest indentation modulus on the medial side was found in the central region (CM) of the most proximal slice. The highest indentation modulus on the lateral side was

(a)

(b)
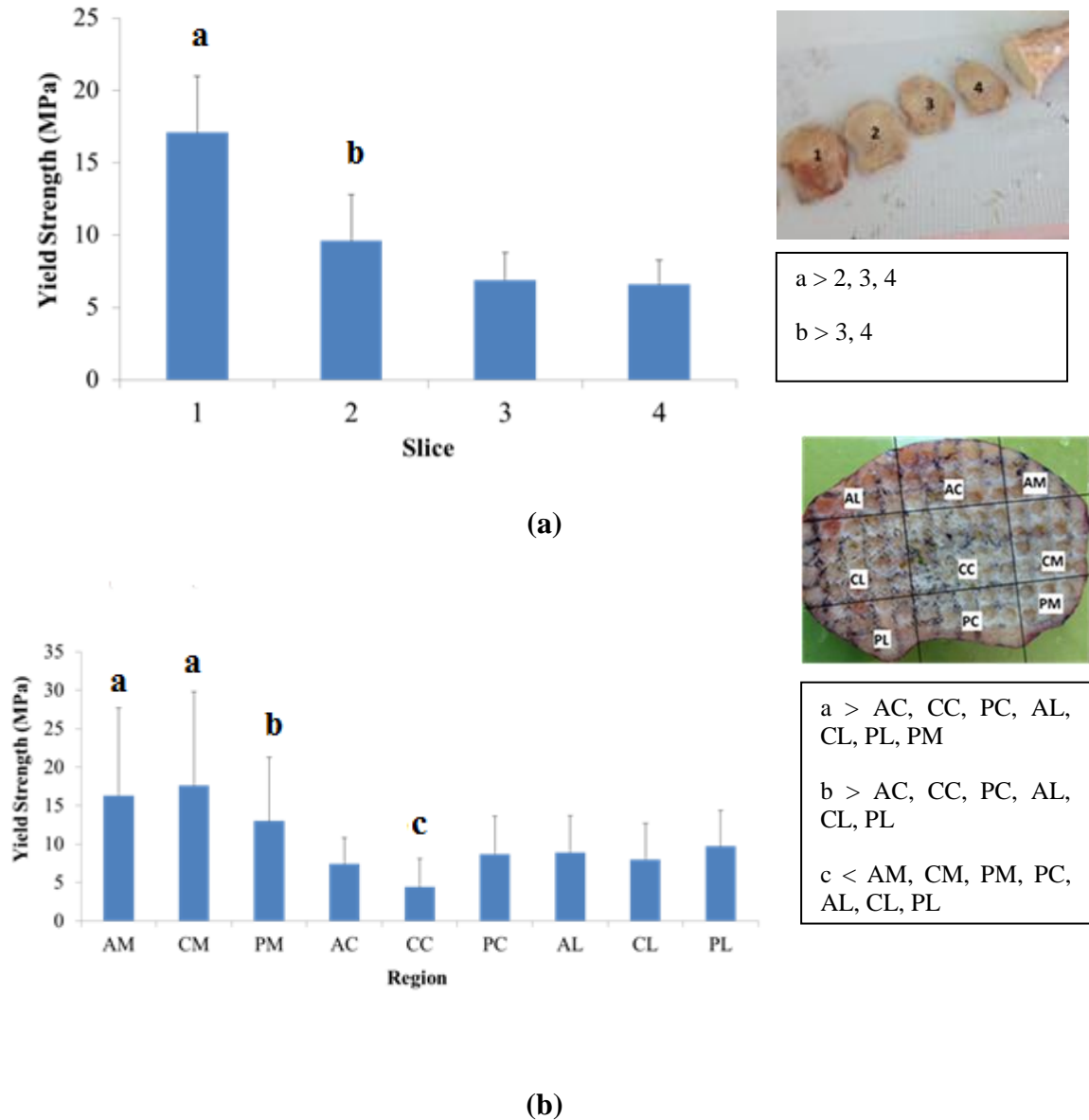
Figure 2.11   Yield strength of each (a) slice and (b) region.
Standard deviation is represented with error bars. A two-way ANOVA ($p<0.05$) was used to determine if there were significant differences, as indicated by the letters above the bars and explained in the legend.
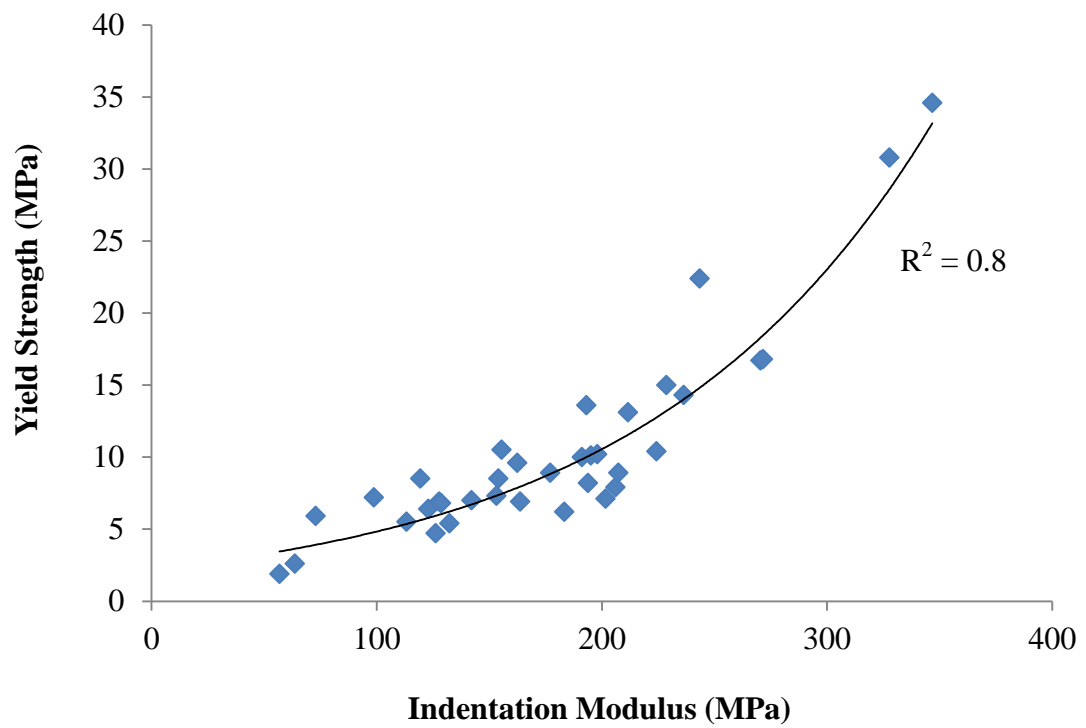
Figure 2.12   **The correlation between indentation modulus and yield strength.**
An exponential relationship was found between indentation modulus and yield strength ($R^2 = 0.8$).
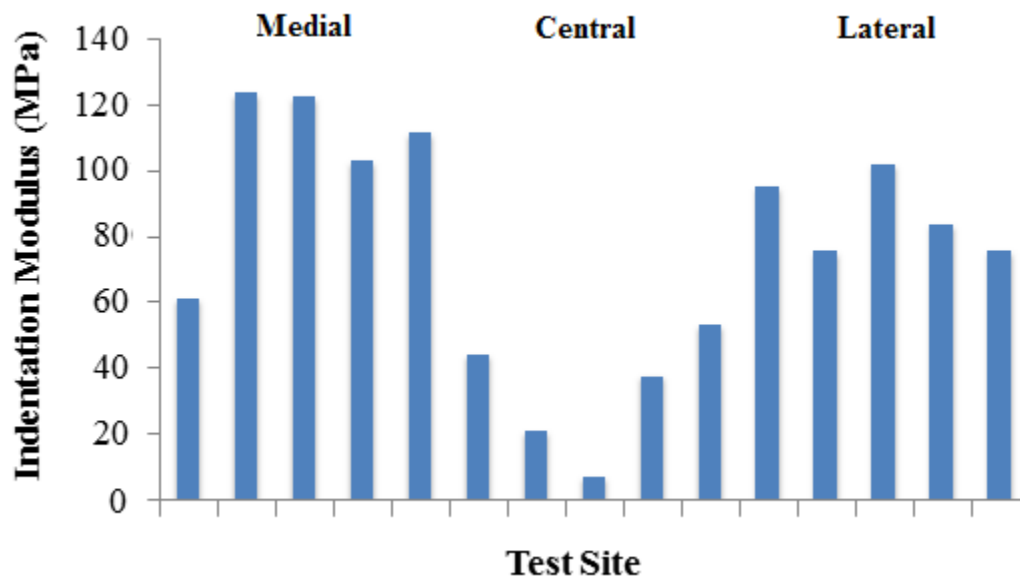
Figure 2.13 **The variation of modulus over a row of test sites on a representative slice.**
Each bar represents a test site that occurred along the widest point of the most proximal slice of one tibia. Modulus decreased around the margins of the slice, increased under the contact regions, and decreased to the lowest values in the central region.

found in the anterior region (AL), also on the first slice. Although there were no significant differences between regions in each condyle over one slice, the greatest elastic modulus values were observed in the posterior region in both the medial (PM) and lateral (PL) sides with increasing slice depth (Table 2.3).

The sensitivity analysis showed that average percent differences between test sites from the standard region and those included in the new region ranged from -29.6 to +27.0% with a mean of +0.7 (11.9)% (Appendix E). The coefficient of variation was 0.25.

Elastic modulus ranged from 0.05 to 494.4 MPa with a mean of 80.4 (19.9) MPa (Figure 2.14a, b). The elastic modulus of the first slice was significantly greater than slices two, three, and four. There were no significant differences in elastic modulus between the second, third, and fourth slices. The AM and CM regions were significantly greater in elastic modulus than all regions except for PM. Elastic modulus was significantly greater in the PM region than in the AC, AL, and CL regions. The CC region had the significantly lowest elastic modulus out of all the regions.

2.4   Discussion

Cancellous bone of the proximal tibia was tested by indentation to quantify the extent of regional variations in modulus and yield strength over four slices and nine transverse regions with a high number of test sites. The central medial (CM) region was found to have the highest mean indentation modulus of 255.1 MPa and yield strength of 17.7 MPa. In the present study the central central (CC) region had the lowest indentation modulus and yield strength at 73.0 MPa and 4.4 MPa, respectively.

Table 2.3 **Mean (SD) indentation modulus through the proximal end of the tibia.** The highest mean indentation modulus was found on the medial side through all the slices over all specimens. There were no significant differences between regions within each slice but the highest values were seen posteriorly in both condyles in the distal slices.

Medial Condyle (MPa)			
		AM	CM	PM
Slice Number	1	327.7 (162.6)	346.7 (245.6)	243.5 (111.5)
	2	270.5 (93.5)	271.6 (115.6)	177.1 (118.6)
	3	191.2 (52.5)	195.2 (54.6)	198.0 (50.4)
	4	206.1 (90.5)	207.4 (83.8)	224.2 (97.0)

Lateral Condyle (MPa)			
		AM	CM	PM
Slice Number	1	236.3 (133.5)	193.1 (130.5)	228.7 (163.1)
	2	122.9 (62.2)	119.4 (31.7)	162.4 (66.6)
	3	128.6 (27.6)	132.3 (86.4)	153.2 (50.5)
	4	193.9 (39.9)	126.2 (54.5)	201.7 (85.8)

a > 2, 3, 4

(a)

a > AC, CC, PC, AL, CL, PL

b > AC, AL, CL

c < AM, CM, PM, AC, PC, AL, CL, PL

(b)
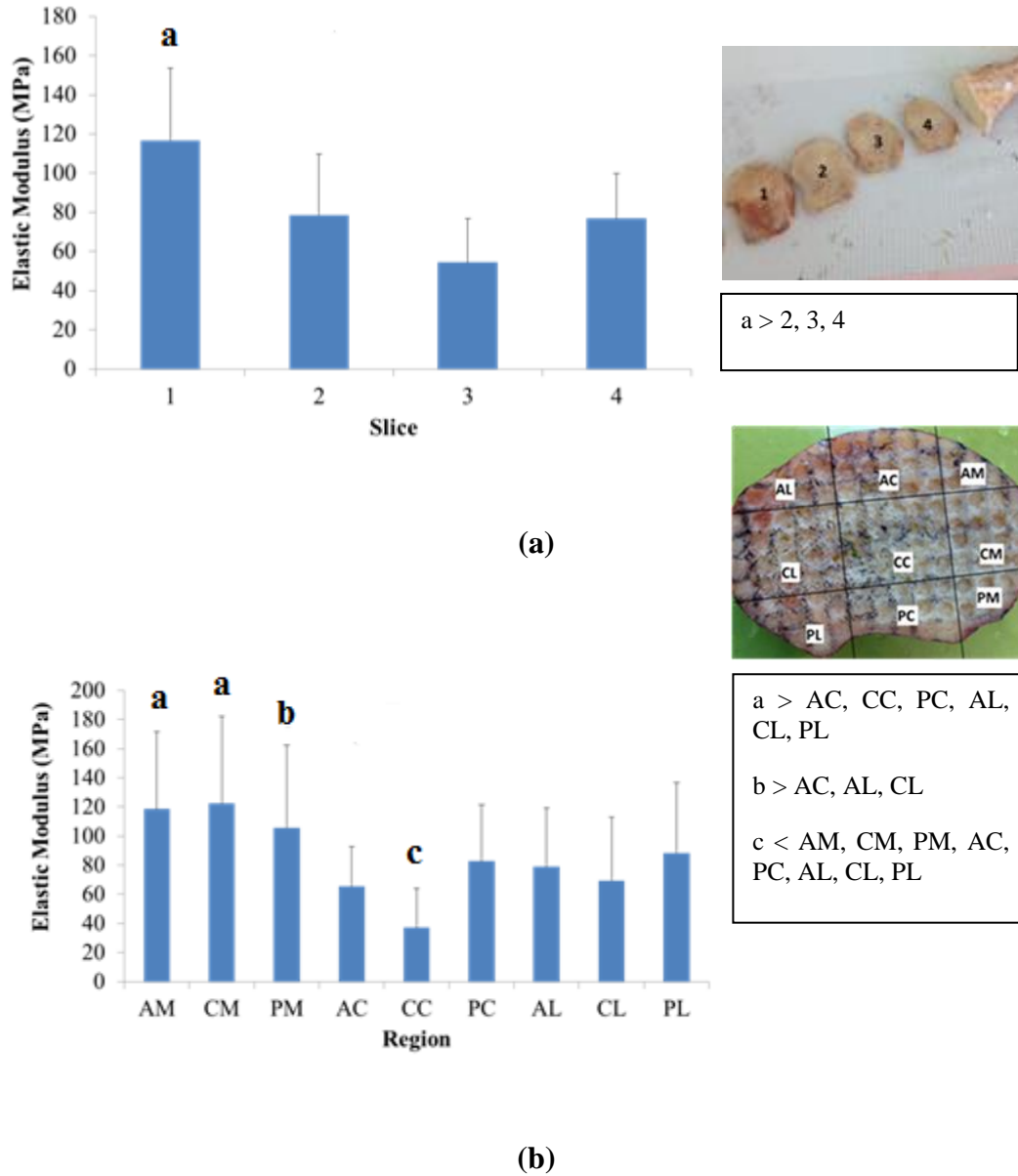
Figure 2.14 **Elastic modulus of each (a) slice and (b) region.**
Elastic modulus was calculated using the Timoshenko-Goodier formula. Standard deviation is represented with error bars. A two-way ANOVA ($p < 0.05$) was used to determine if there were significant differences, as indicated by the letters above the bars and explained in the legend.

The most proximal level was found to have the highest mean indentation modulus of 226.8 MPa and yield strength of 17.9 MPa. No significant differences were found beyond the first slice in indentation modulus and beyond the second slice in yield strength. The proximal slice is likely strongest because it is closest to the subchondral bone layer and has increased trabecular contiguity (Aitken et al., 1985). Decreasing bone strength with depth is consistent with past studies (Hvid and Hansen, 1985; Harada et al., 1988). Significant differences in indentation modulus may not have been seen past the first 5 mm due to micro-architectural differences that occur in the organization of trabeculae distal to the joint surface.

Indentation tests have fewer variables to control for compared to compression tests, as only the surface area of the indentor, applied load, and specimen deformation need to be known. Past axial compression tests have revealed that a decrease in strength only occurs through the lateral condyle (Hvid and Jensen, 1984). Indentation tests, however, have showed that strength decreased distally in both condyles (Hvid and Hansen, 1985). Indentation testing of cancellous slices also allows the trabecular matrix to remain intact and better mimic *in vivo* conditions (Harada et al., 1988). Therefore, the present study was able to quantify mechanical properties from cancellous specimens that were able to behave as they most naturally would. However, high standard deviations, as are common in the study of bone properties, result from the use of a small indentor (Anglin et al., 1999). Hvid and Hansen (1985) obtained measurements of compressive strength through the use of an osteopenetrometer, where the observed mechanical

properties reflected the design of the needle and the penetration speed. This makes it difficult to compare to the current study.

Although past studies have defined regions differently, it is generally agreed that the medial condyle possesses the greatest strength and the intercondylar region is the weakest (Hvid and Hansen, 1985; Harada et al., 1988; Behrens et al., 1974; Goldstein et al., 1983). The central and anterior regions of the medial condyle and the posterior region of the lateral condyle have been noted as the strongest areas (Hvid and Hansen, 1985; Behrens et al., 1974; Harada et al., 1988; Goldstein et al., 1983). The results of the present study agree with the medial results but no differences were noted in the lateral. This may have been the result of the sample size leading to a type two error. Goldstein et al. (1983) found elastic modulus to range from 430 MPa in the medial condyle to 4.2 MPa in the central region over a single slice. The present study found a very similar range in elastic modulus values (0.05 – 494.4 MPa). However, Goldstein et al. (1983) applied uniaxial compression tests on cylindrical bone plugs, which does not fully account for the variation of strength through the 1 cm bone plug. Furthermore, their machined specimens most likely lost the support of the surrounding trabeculae, which would lead to an underestimation of stiffness. The mean elastic modulus from the present study, of 80.4 MPa, was lower than their finding of 128.1 MPa (Goldstein et al., 1983).

The present study found that the medial regions had the highest indentation values through the depth of the proximal tibia, which agrees with the findings by Harada et al. (1988). The present study also found that the region with the highest indentation modulus values shifted from the center to the posterior in the medial side and from anterior to

posterior in the lateral side. The posterior regions are likely stronger because the contact areas move in this direction as the knee is loaded in flexion (Hvid and Hansen, 1985; Behrens et al., 1974). However, a posterior shift in strength may have been influenced by the fact that the nine regions were defined on a slice by slice basis. The posterior condyles are robust prominences at the proximal epiphysis of the tibia, which dramatically slope in the anterior direction and narrow distally. Therefore, the regions shift forward through the depth of the proximal tibia where the posterior region of the first slice is anatomically different from the posterior region of the fourth slice. This would explain why no significant differences were found between regions within the medial and lateral condyles over each slice. The present study found that modulus decreased from the contact regions towards the periphery through all the slices, but to a lesser extent in the distal slices. A decrease in the mechanical properties around the outside margins of the bone corresponds with the distribution of contact stresses experimentally measured in the intact knee near physiological levels (Hvid and Hansen, 1985). This agrees with past studies that found a concentration of strength beneath the condyles, which extended towards the cortical shell of the metaphysis (Goldstein et al., 1983; Hvid and Hansen, 1985; Harada et al., 1988).

Past studies have quantified bone properties using ultimate strength, compressive strength, and elastic modulus measures. To the author's knowledge, there has been no previous investigation into the regional variation of yield strength over a transverse slice of the tibia. Yield strength was found to be significantly higher, at 17.1 MPa, in the first slice compared to the other slices. The yield strength was 9.6 MPa in the second slice, which was significantly higher than the third and fourth slices (6.9 MPa and 6.6 MPa,

respectively). Over the transverse plane, the highest yield strength was found in the medial condyle (AM, CM, PM), and CC had the lowest yield strength. In the present study an exponential correlation was found between indentation modulus and yield strength. As a result, indentation modulus would be a good predictor of yield strength. Goldstein et al. (1983) had previously determined that there is a linear relationship between ultimate strength and elastic modulus in the cancellous bone of the tibia. Therefore, there may be some disagreement on the most appropriate conversion from modulus to strength.

Medial-lateral load splits have been reported to range from 55%-75% to 25%-45% during dynamic activities such as walking (Schipplein and Andriacchi, 1991; Shelburne et al., 2006; Taylor et al., 2011; Zhao et al., 2007). Since the medial condyle bears a greater share of the load, the underlying bone may have adapted to become stronger to meet its functional demands, as stipulated by Wolff's law (Behrens et al., 1974). The medial side has a larger average contact area of 1.8 cm^2 compared to the lateral side of 1.4 cm^2 (Walker and Hajek, 1972). Therefore, the medial side is approximately 30% larger than the lateral side. Since the present study shows that the medial side is stronger, this suggests that the force in this area is at least 30% greater than the force in the lateral side. The mechanical properties of cancellous bone vary depending on the location and function within the body (Figure 2.15). The strongest bone has been shown to be closest to the subchondral bone layer (Aitken et al., 1985; Sumner et al., 1994; Dunham et al., 2005; Anglin et al., 1999). Transverse variations in modulus were also noted in the cancellous bone of the distal humerus and glenoid (Dunham et al., 2005; Anglin et al.,
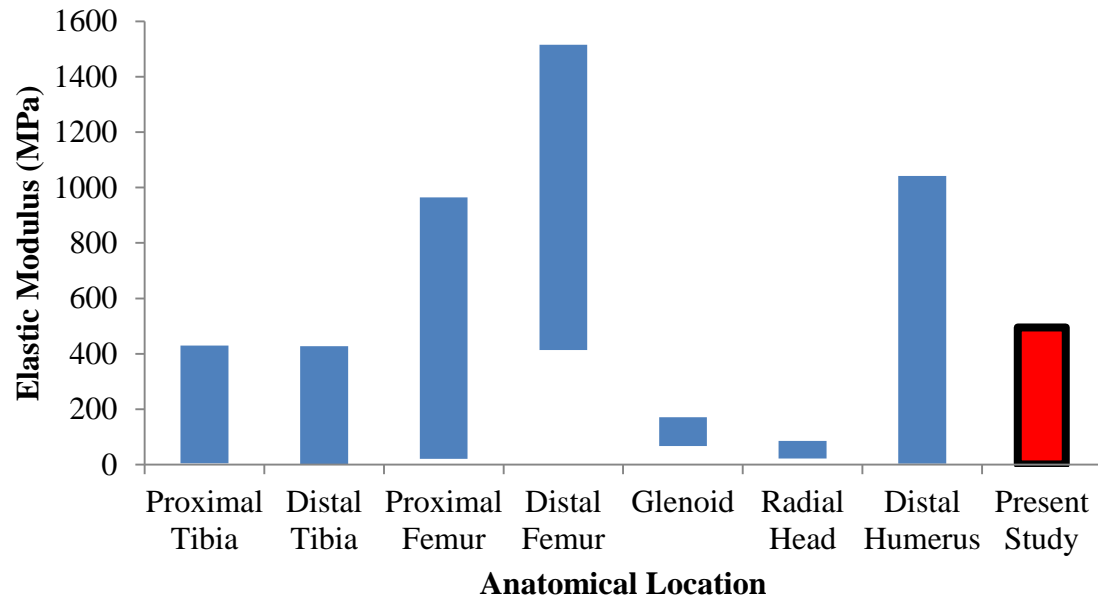
Figure 2.15   Elastic modulus at various anatomic locations.
Modulus values were reported in the following studies: proximal tibia, Goldstein et al. (1983); distal tibia, Aitken et al. (1985); proximal femur, Schoenfeld, et al. (1974); distal femur, Pugh et al. (1973); glenoid, Anglin et al. (1999); radial head, Gordon et al. (2003); and distal humerus, Dunham et al. (2005).

1999). However, regional variations in yield strength were found only in the subchondral cancellous bone of the radial head (Gordon et al., 2003).

True elastic modulus was calculated using the Timoshenko-Goodier formula for semi-infinite elastic solids. Indentation modulus was converted to elastic modulus by a factor between 0.3 and 1.0 (Appendix F). The scaling factor varied depending on the thickness of the slice. The Timoshenko-Goodier formula assumes material to be isotropic and homogenous, thereby disregarding the trabecular nature of cancellous bone. However, such an assumption is common when investigating the mechanical behavior of bone (Anglin et al., 1999). Sumner et al. (1994) found that elastic modulus calculated using the formula was highly correlated to the results from nondestructive tests of bone specimens. Although the trends observed in indentation modulus values were the same for elastic modulus, the values of elastic modulus were lower (mean of 80.4 MPa). The range of values in the present study was in general agreement with the results generated from isolated section tests (Goldstein et al., 1983).

A sensitivity analysis was performed to determine how the selection of region borders affected the indentation modulus (Appendix E). Inter-specimen variability, represented by the coefficient of variation, gives an indication of the extent of variability in the population. The average sensitivities for all regions except for CC were less than the coefficient of variation. As such, variations from individuals likely dominated any variations from boundary definitions. CC had a large sensitivity due to the overall small mean modulus, where any fluctuations resulted in a large percent difference.

There were some limitations to the present study, which should be noted. The trabecular nature of cancellous bone makes it a difficult material to characterize. Indentation tests give limited information on the mechanical properties of cancellous bone, as they do not provide information on the orientation of trabeculae. Furthermore, testing was only conducted in the superior to inferior direction, so the anisotropic properties of cancellous bone could not be quantified. However, the trabeculae in the proximal tibia are predominately vertically oriented (Williams and Lewis, 1982). As the primary direction of loading, mechanical properties observed in the axial direction are therefore the most important to quantify.

A constant penetration depth of 2 mm was employed, which was less than half the thickness of the slice to reach yield and thus fully characterize trabecular behavior. Making precision parallel cuts with the saw proved to be challenging, leading to a range in thickness of cancellous slices (2.9-10.3 mm) (Appendix G). There was minimal variation in thickness within each slice (1.2 (0.8) mm). Therefore, the total depth investigated in a given tibia varied from 19.2 mm to 27.3 mm, excluding the discarded slices. As such, the slices at each depth were not taken from precisely the same locations. The variations in thickness were taken into account when converting the load-displacement curve into a stress-strain curve. As slices were cut out of the proximal epiphysis of each tibia, the surface trabeculae may have been damaged, thus limiting their ability to bear load. Anatomically, the lateral condyle is positioned higher on the tibia than the medial condyle (2º tilt) (Figure 2.16) (Kulkarni, 2009; Yoshioka et al., 1989). This was confirmed by measuring the thickness of the discarded slices and noting that the
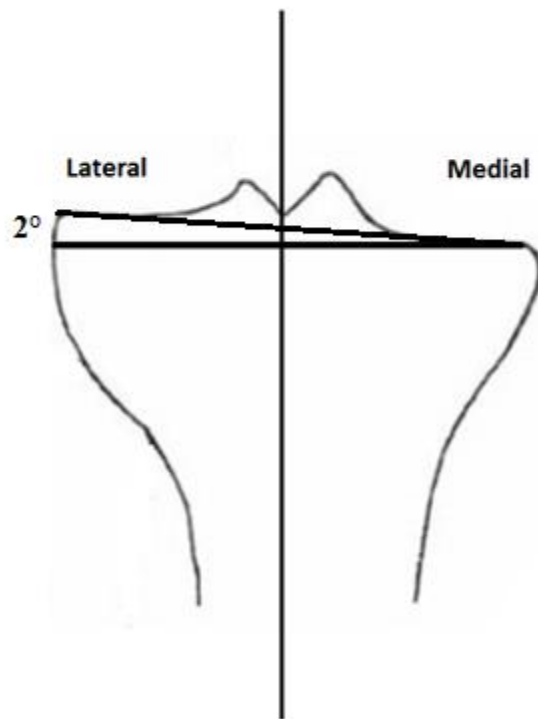
Figure 2.16   The anatomical features of the proximal tibia.
The lateral condyle is positioned slightly higher than the medial condyle (Kulkarni, 2009). Medial-lateral comparisons were made on transverse slices cut perpendicular to the line of the axis of the tibia. *(Adapted from http://www.orthoworlds.com).*

lateral side was thicker than the medial side (Appendix H). As a result, comparison of strength in the medial and lateral regions of a transverse slice may be slightly inaccurate, as the medial side may be better correlated to the lateral side of the preceding slice. This could result in a smaller difference in bone strength between the condyles when looking at depth effects, as the lateral side would be stronger closer to the subchondral bone layer. However, it was noted that the mean indentation modulus values in the medial regions (AM, CM, PM) of each slice was higher than the indentation modulus values observed in the lateral regions (AL, CL, PL) of the preceding slice, thus emphasizing that the medial condyle is stronger than the lateral condyle through the depth of the proximal tibia.

Each tibia was out of the freezer for 24-48 hours over the course of cutting and testing, but was kept moist with saline. Randomizing site order helped eliminate any drift from drying effects. The grid size and random test order also ensured that there were no edge effects. A 5 mm by 5 mm grid size and an indentor diameter of 4 mm ensured that 1 mm of space was maintained between adjacent test sites to contain damage. The materials testing machine introduced a consistently small, distinct peak early in the load-displacement curve, which was ignored when calculating elastic modulus and yield strength. Some graphs (approximately 5-10 per slice) did not display an obvious yield point, which occurred when indentation tests were performed on the specimen that was less than 3 mm thick or when cortical bone may have been present. This reduced the number of data points for yield strength, which may have slightly affected the results of this study. However, due to the large number of sites tested, this would most likely not have a large effect.

The loosening of total knee arthroplasties is a problem leading to failure and often requires intrusive revision surgery (Bourne and Finlay, 1986; Stern et al., 1997). The tibial component of this orthopaedic device has a central stem to promote stability. The quality of bone stock is known to be a contributing factor to its stability (Bourne and Finlay, 1986; Stern et al., 1997). Therefore, if the host bone is of higher quality, there is a greater chance of fixation. The results of the present study can be used to guide the design of orthopaedic devices whereby fixation in the strong anterior and central regions of the medial condyle and limited central fixation may promote long-term stability of the device. Furthermore, as the strongest bone is found near the subchondral bone layer, it should be preserved as much as possible during surgery to further maximize the stability of the device.

Dynamic finite element models of the tibia that use homogenous and isotropic properties do not account for the regional variations of mechanical properties noted herein. The inclusion of the results of the present study in finite element analysis would increase the accuracy of the behavior of bone; however, it is unknown how large of an effect this would be, or how detailed the variations need to be modeled. In the future it would be of great interest to further investigate how the mechanical properties of cancellous bone are affected by strain rate and anisotropy.

In conclusion, the mechanical properties of cancellous bone of the proximal tibia varied over the transverse plane and with depth. The highest elastic modulus and yield strength were found in the medial condyle, where dynamic joint forces are predominately transmitted. As well, the highest elastic modulus and yield strength were found in the

most proximal slice, which is closest to the hard subchondral bone layer. The clinical

implications of these results have the potential to increase the accuracy of finite element

models and improve the design and success of orthopaedic devices.

2.5   References

Aitken, G.K., Bourne, M.D., Finay, J.B., Rorabeck, C.H., Andreae, P. R. (1985). Indentation Stiffness of the Cancellous Bone in the Distal Human Tibia. *Clinical Orthopaedics and Related Research*, (201), 264–271.

Anglin, C., Tolhurst, P., Wyss, U., Pichora, D. R. (1999). Glenoid Cancellous Bone Strength and Modulus. *Journal of biomechanics*, *32*, 1091–1097.

Behrens, J.C., Walker, P.S., Shoji, H. (1974). Variations in Strength and Structure of Cancellous Bone at the Knee. *Journal of biomechanics*, *7*, 201–207

Bourne, R.B. and Finlay, J. B. (1986). The influence of tibial component intramedullary stems and implant-cortex contact on the strain distribution of the proximal tibia following total knee arthroplasty: an in vivo study. *Clinical Orthopaedics and Related Research*, *208*, 95–99.

Dunham, C.E., Takaki, S.E., Johnson, J.A., Dunning, C. E. . (2005). Mechanical Properties of Cancellous Bone of the Distal Humerus. *Clinical Biomechanics*, *20*, 834–838.

Goldstein, S.A., Wilson, D.L., Sonstegard, D.A., Matthews, L. S. (1983). The Mechanical Properties of Human Tibial Trabeculae Bone as a Function of Metaphyseal Location. *Journal of biomechanics*, *16*(12), 965–969.

Gordon, K.D., Duck, T.R., Wing, G.J.W., Johnson, J. A. (2003). Mechanical Propertes of Subchondral Cancellous Bone of the Radial Head. *Journal of Orthopaedic Trauma*, *17*(4), 285–289.

Harada, E., Wevers, H.W., Cooke, T. D. V. (1988). Distribution of Bone Strength in the Proximal Tibia. *The Journal of Arthroplasty*, *3*(2), 167–175.

Helgason, B., Perilli, E., Schileo, E., Taddei, F., Brynjolfsson, S., Viceconti, M. (2008). Mathematical relationships between bone density and mechanical properties: a literature review. *Clin Biomech*, *23*(2), 135–146.

Hvid, I. and Jensen, J. (1984). Cancellous bone strength at the proximal human tibia. *Eng Med*, *13*(1), 21–25.

Hvid, I., Hansen, S. L. (1985). Trabeculae Bone Strength Patterns at the Proximal Tibial Epiphysis. *Journal of Orthopaedic Research*, *3*, 464–472.

Keyak, J. H. (1990). Automated three-dimensional finite element modeling of bone : a new method, *12*, 389–397.

Kulkarni, G. S. (2009). Intra-articular fractures of the tibial plateau. In *Textbook of Orthopaedics and Trauma* (2nd ed.). New Delhi: Jaypee Brothers Publishers.

Pugh, J.W., Rose, R.M., and Radin, E. . (1973). Elastic and viscoelastic properties of trabecular bone: dependence on structure. *J Biomech*, *6*(5), 475–485.

Schipplein, O. D., & Andriacchi, T. P. (1991). Interaction between active and passive knee stabilizers during level walking. *Journal of orthopaedic research : official publication of the Orthopaedic Research Society*, *9*(1), 113–9.

Schoenfeld, C.M., Lautenschlager, E.P. and Meyer, P. R. (1974). Mechanical properties of human cancellous bone in the femoral head. *Med Biol Eng*, *12*(3), 313–317.

Shelburne, K. B., Torry, M. R., & Pandy, M. G. (2006). Contributions of Muscles , Ligaments , and the Ground-Reaction Force to Tibiofemoral Joint Loading During Normal Gait, (October), 1983–1990.

Stern, S., Wills, R.D., and Gilbert, J. L. (1997). The effect of tibial stem design on component micromotion in knee arthroplasty. *Clinical Orthopaedics and Related Research*, *345*(44-52).

Sumner, D.R., Berzins, W.A., Turner, T. M. (1994). Distribution of Young's Modulus in the Cancellous Bone of the Proximal Canine Tibia. *Journal of biomechanics*, *27*(8), 1095–1099.

Taylor, W. R., Poepplau, B. M., König, C., Ehrig, R. M., Zachow, S., Duda, G. N., & Heller, M. O. (2011). The medial-lateral force distribution in the ovine stifle joint during walking. *Journal of orthopaedic research : official publication of the Orthopaedic Research Society*, *29*(4), 567–71.

Timoshenko, S. and Goodier, J. (1970). *Theory of Elasticity* (3rd ed.). New York: McGraw-Hill.

Walker, P.S. and Hajek, J. V. (1972). The load-bearing area in the knee joint. *Journal of Biomechanics*, *5*(6), 581–584.

Williams, J. L. and L. J. L. (1982). Properties and an anisotropic model of cancellous bone from the proximal tibial epiphysis. *J Biomech Eng*, *104*(1), 50–56.

Wolff, J. (1870). Ueber die innere architektur der knochen. *Virchow's Arch*, *50*(1), 389–453.

Yoshioka, Y., Siu, D.W., Scudamore, A., Cooke, T. D. V. (1989). Tibial anatomy and functional axes. *Journal of Orthopaedic Research*, *7*, 132–137.

Zhao, D., Banks, S. A., Lima, D. D. D., Jr, C. W. C., & Fregly, B. J. (2007). In Vivo Medial and Lateral Tibial Loads during Dynamic and High Flexion Activities. *J Orthop Res.*, *25(5)*, 593–602.

Chapter 3: Prediction of the Mechanical Properties of Cancellous Bone in the Proximal Tibia by Computed Tomography

OVERVIEW: This chapter examines how accurately current density-modulus relationships for cancellous bone of the proximal tibia can predict its mechanical properties. Computed tomography (CT) scans of each tibia tested in Chapter Two were taken to determine the density of cancellous bone to calculate elastic modulus using density-modulus relationships from the literature specific to the proximal tibia. The CT-derived modulus was compared to the results from mechanical testing. This study was undertaken to determine the most appropriate density-modulus relationship to apply inhomogeneous material properties to cancellous bone in FE analyses of the tibia.

3.1   Introduction

The tibia is the major weight-bearing bone in the lower leg that is commonly injured in traumatic events such as motor vehicle accidents. Dynamic FE models are frequently used to predict the risk of injury where it would be difficult or expensive to experimentally test such loading conditions (Quenneville et al., 2011). Accurate strain predictions are necessary to define fracture risk factors; however, current FE models are limited in their ability to represent bone behavior (Schileo et al., 2007).

Developing accurate FE models requires proper material property assignment. Bone is an inhomogeneous material in terms of the distribution of its mechanical

properties. However, dynamic models typically assign homogeneous properties to bone due to computational limitations, which may affect the accuracy of the model (Quenneville et al., 2011). Static models have achieved great success incorporating inhomogeneous properties by applying density-modulus relationships to predict material properties from CT images (Rho et al., 1995; Keyak et al., 1994).

CT can be used to non-invasively examine the geometry and material properties of bone for the development of subject-specific FE models. Density data can be extracted from CT scans and input into a density-modulus relationship to determine the corresponding modulus for that region of bone. CT numbers have been shown to be highly correlated to both apparent density and ash density (Keyak et al., 1994).

Numerous empirical equations have been developed to correlate bone density to mechanical properties. Carter and Hayes (1977) reported that compressive strength of cancellous bone is proportional to the square of apparent density and that modulus is related to apparent density cubed. This has been disputed by others, such as Rice (1988), who found that both elastic modulus and strength of cancellous bone are more closely related to the square of the apparent density. Additionally, choosing the most appropriate density-modulus relationship increases the accuracy of the FE model since they are specific to the anatomical location and type of bone structure (Morgan et al., 2003). As a result, there is a need for site-specific equations. Austman et al. (2008) determined that relationships are specimen-dependent, so a universal relationship may not suffice in the study of bone behavior across the full range of bone densities. Rather, an optimal density-modulus relationship may be required which would produce consistently low errors

(Austman et al., 2008). Conversely, Schileo et al. (2007) determined that the density-modulus relationship developed by Morgan et al. (2003) was able to account for the whole range of bone density found in the femur. Whole bone, however, is mostly comprised of cortical bone. Therefore, validating the whole bone response is different from the evaluation of individual tissues such as cancellous bone.

Few studies have validated the relationships used in FE models against experimental findings of the same specimens. Moreover, density-modulus relationships have been developed using different experimental techniques, which may affect the applicability of the equation under different conditions. The varying conclusions and equations available mean there is a need to investigate further how these specifically apply to the cancellous bone of the tibia. The purpose of this study was to therefore identify the most appropriate density-modulus relationship for cancellous bone to aid in the assignment of material properties in FE models to achieve the most accurate strain predictions for the proximal tibia.

3.2   Materials and Methods

Four fresh-frozen tibias were individually scanned prior to cutting and testing using a standard clinical CT scanner (GE Medical Systems LightSpeed VCT, Hamilton, Canada) with scan parameters 120 kV and 59.4 mAs and 0.625 mm slice thickness (Figure 3.1). A calibration phantom was included in the field of view consisting of a small microcentrifuge tube of water and a small, 10 mm x 20 mm cylinder of SB3

Figure 3.1   GE Medical Systems LightSpeed VCT scanner.
CT images of each tibia (and slices) were taken with scan parameters: 120 kV and 59.4 mAs and 0.625 mm slice thickness. *(From www.gehealthcare.com).*

compound, an epoxy resin with known ash density of 1.05 g/cm^3 (Gammex-RMI, USA) (Figure 3.2).

The four slices that were cut from each proximal epiphysis were stacked in a plastic container able to hold eight slices separated by plastic dividers (Figure 3.3). The container holding the slices and the calibration phantom was CT scanned under the same standard clinical parameters (Figure 3.4).

Each CT image was converted to a DICOM format and opened using Mimics® (Materialise, Belgium). A mask was created to define each bone slice over the range of Hounsfield units corresponding to bone (0-3000 HU) (Figure 3.5). The mask was then manually edited to fill in any trabecular spaces which fell outside the originally-defined parameters. Each mask was also edited so that any soft tissue or plastic captured were not included. The image was then exported into an STL+ format. Using the whole-bone scans, a mask was also created for each whole tibia and cropped to select for the proximal epiphysis. Bone density data were not extracted from the CT images of the slices due to beam hardening effects, loss of bone marrow during cutting, and advanced age of specimens. Slices were CT scanned in air, which may have contributed to the large, negative HU values observed in the regions. As a result, bone density was recorded from the areas on the CT image of the whole tibia which corresponded with the slices. In order to do this, the STL+ of each slice was imported into the whole bone view. Slices were then positioned into the approximate areas from which they were extracted by aligning the outer contours of the slices with the whole bone (Figure 3.6). The slices were defined as the moveable parts, and the whole bone as the fixed part, to perform a global

(a)   (b)
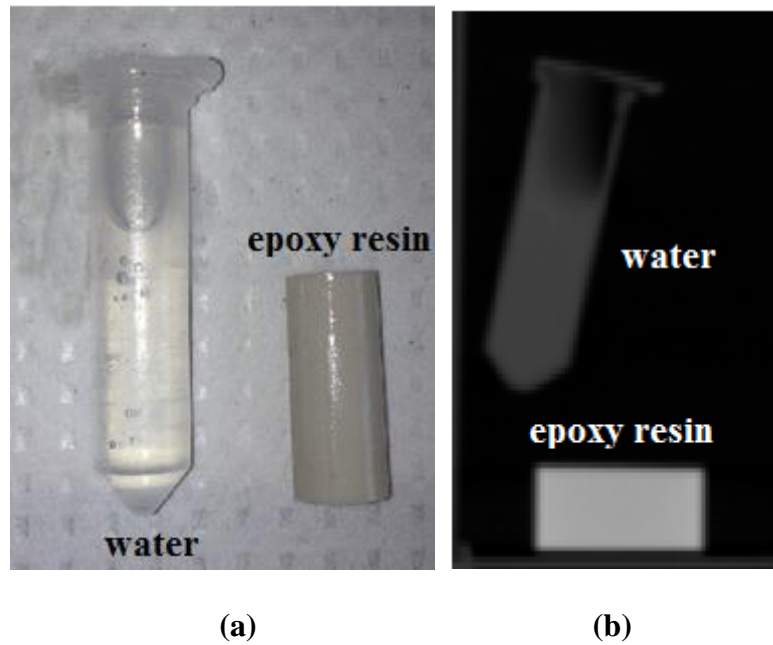
Figure 3.2   **Calibration phantom consisting of (a) water and epoxy resin and (b) corresponding CT image.**
The calibration phantom was used to convert CT numbers (HU) to ash density. The ash density of water is 0 g/cm^3 and 1.05 g/cm^3 for epoxy resin.
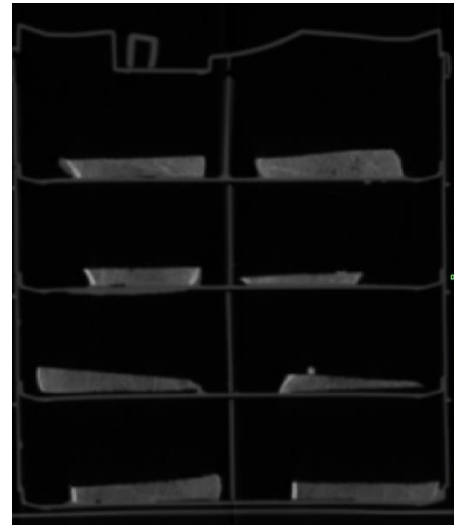
(a)   (b)

Figure 3.3   Slices were (a) stacked in container to take (b) CT scans.
By fitting 8 slices in the plastic container, a reduced number of CT scans needed to be taken.
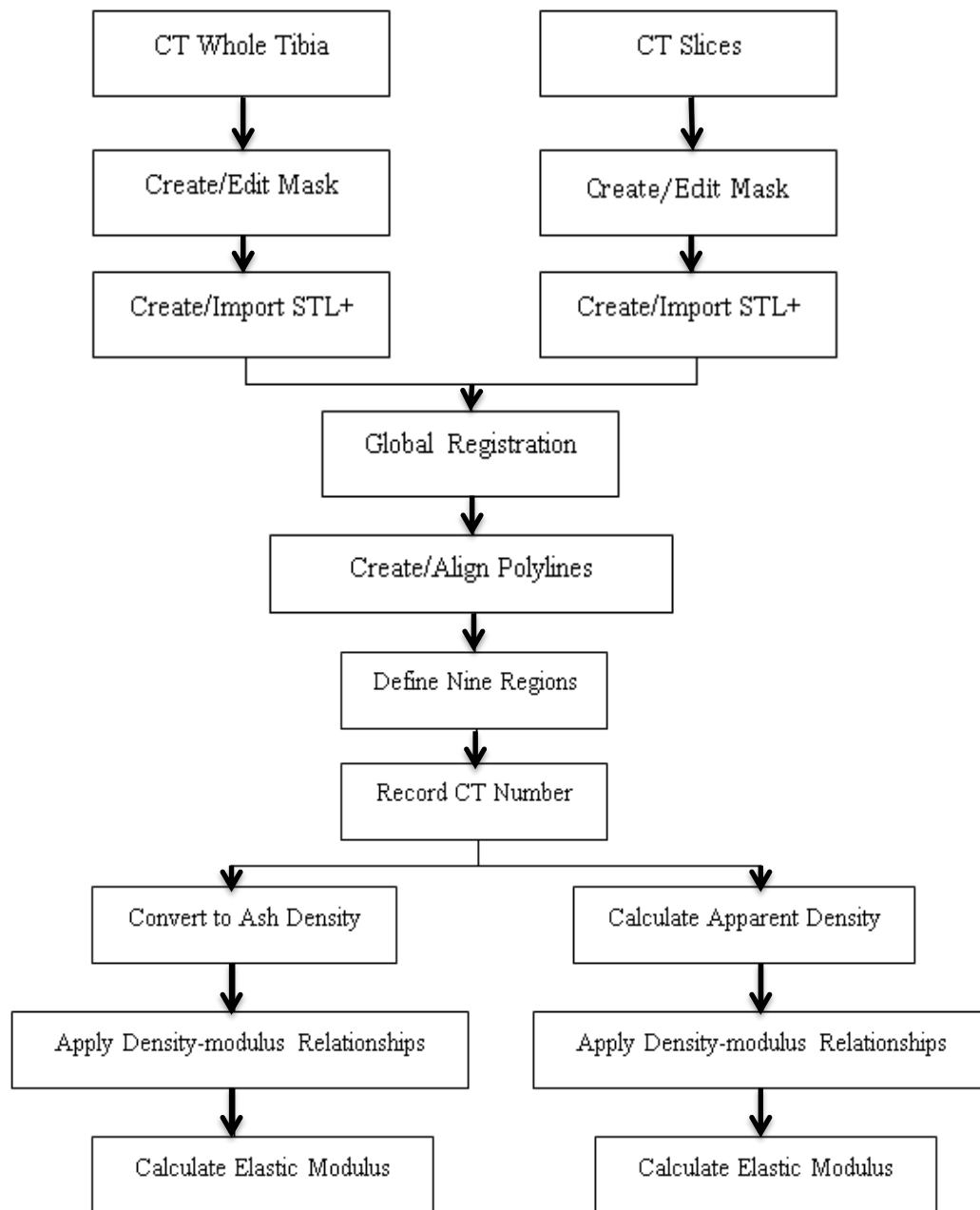
Figure 3.4 **Flowchart of steps taken to get from CT scan to modulus.**
Density data was extracted from CT images (using Mimics®) and input into density-modulus relationships to calculate elastic modulus.
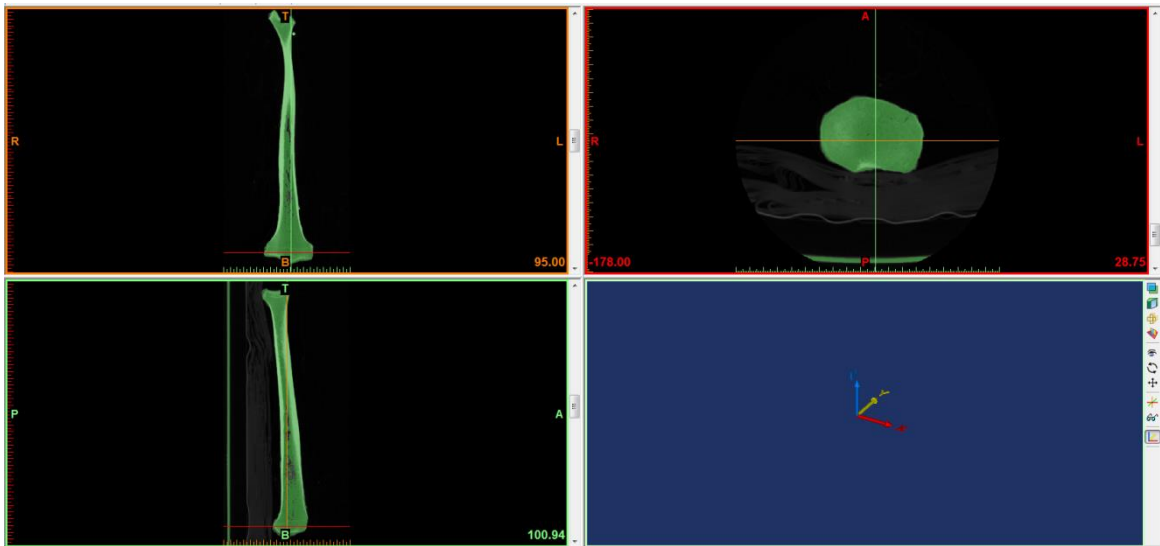
Figure 3.5   **Three views of whole bone mask.**
A mask was created and edited for each tibia and its slices by selecting a bone density range of 0-3000 HU.
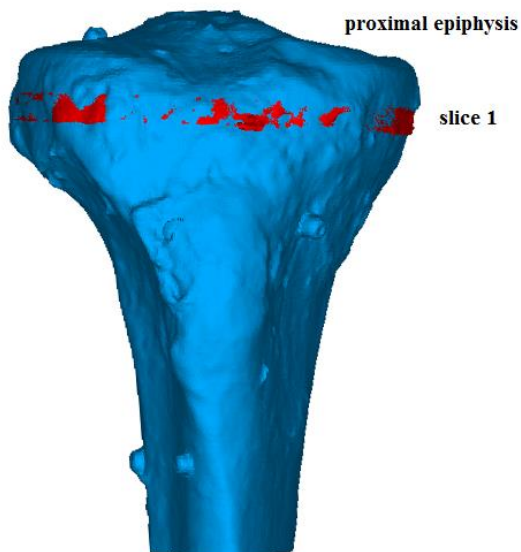
Figure 3.6   **Registering a slice on the whole bone scan.**
Bone density was then extracted from the whole bone, where the images aligned.

registration. Global registration used the following parameters: distance threshold of 1 mm, 100 iterations, and a subsample percentage of 80%. This process was repeated with the remaining three slices so that all the slices were fit onto the whole bone image (Figure 3.7).

In order to determine which images in the whole bone scan corresponded to each slice, polylines were created to match each slice to the whole bone (Figure 3.8). Bone density information was extracted from the CT image of the whole bone where there was significant overlap (>60%) in the polylines of the slice and whole bone. CT numbers were recorded where the polylines from the proximal-most slice aligned with the polylines of the whole bone (Figure 3.8a, b). The number of image slices used corresponded with the thickness of the slice (*e.g.* if the slice was 5 mm thick, five CT image slices of the whole bone were used to calculate bone density). Polylines that failed to match were indicative of cut sites, which occurred over 2 to 3 image slices, and were not included in the calculation of bone density (Figure 3.8c). CT numbers from the subsequent slices were recorded in the same manner.

Each slice was divided into nine regions corresponding to those defined during experimental testing (Figure 3.9). Average HU was calculated over the maximum-sized ellipse that could fit within the borders of each region (Figure 3.9). The ellipse was adjusted so that cortical bone was excluded from measurement, where cortical bone appeared brighter around the edges of the CT images. The average HU of each ellipse was recorded for each region of each image slice. The HU of the calibration phantom was
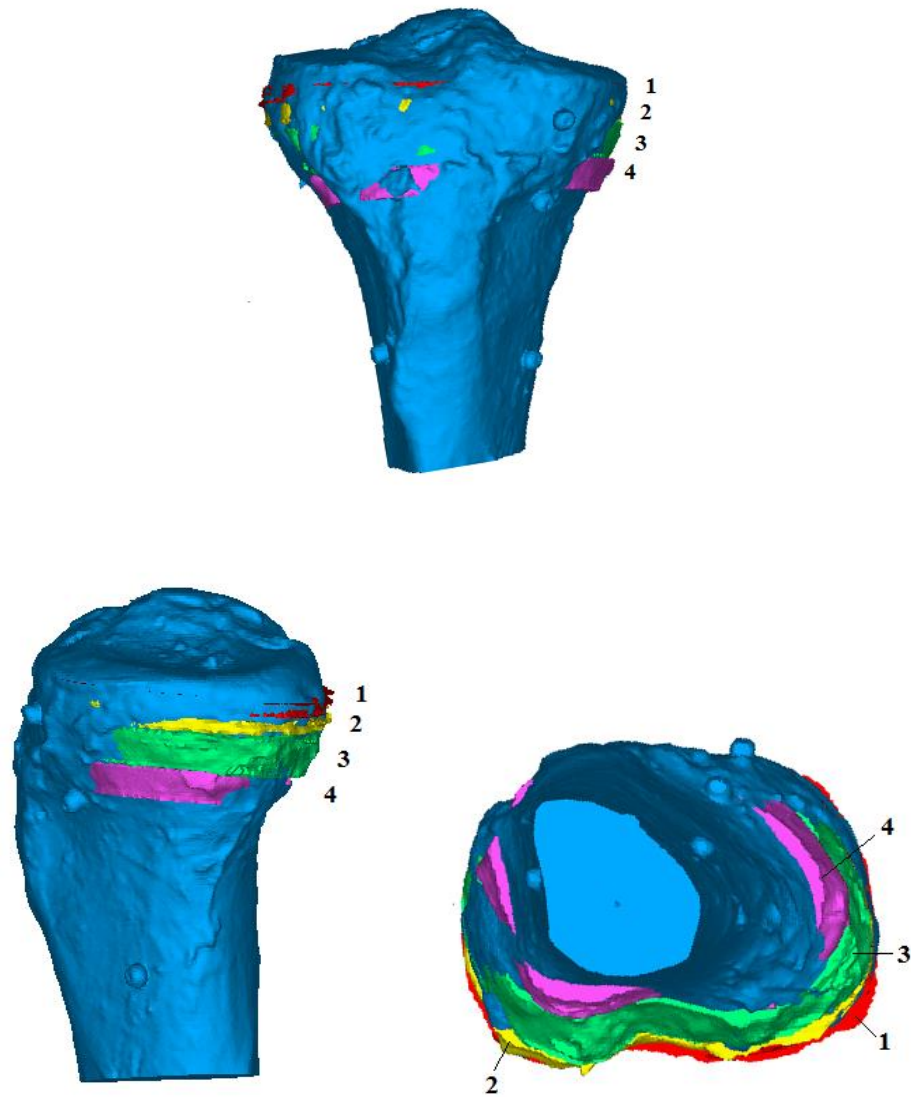
Figure 3.7 **Orthogonal views of the four slices positioned in the proximal tibia.** Global registration was performed to match the slices as closely as possible to the whole bone. Protruding slices (mean offset 0.3 cm) are indicative of misalignment.
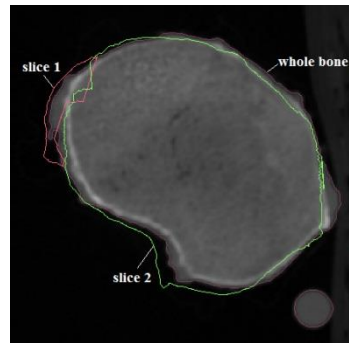
(a)
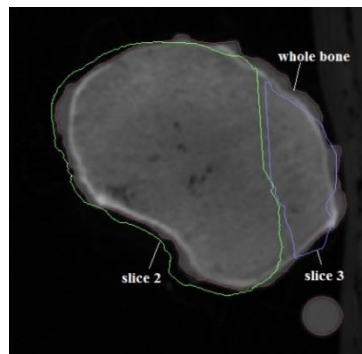
(b)
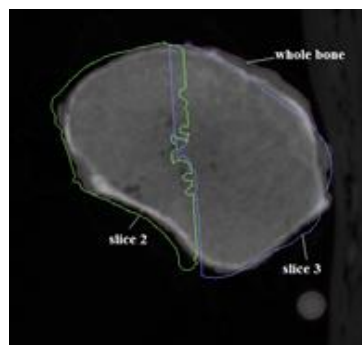
(c)

Figure 3.8   Polylines of the slices and whole bone were aligned where there is a (a) complete match, (b) substantial match, and (c) no match between slice 2 and the whole bone.
Bone density was recorded from areas where there were complete and substantial matches. Images where there was no match were excluded, as they were indicative of cut sites.
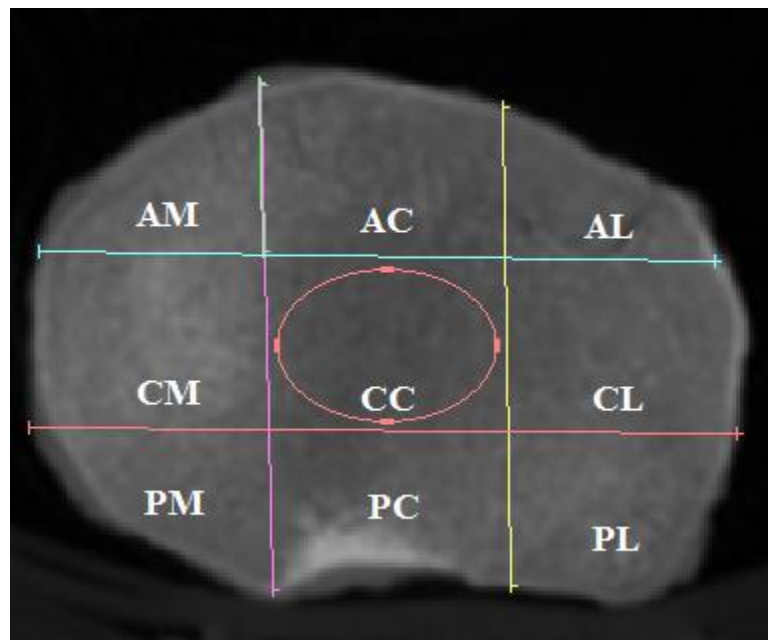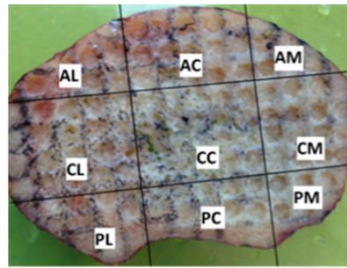
Figure 3.9   **Nine regions on the CT image corresponding to the regions from indentation testing.**
An ellipse of maximum area was fit into each region to determine the average HU.

calculated over ten image slices and averaged. A sensitivity analysis was performed to determine the effect of position and ellipse size on the HU measurement (Appendix H).

The HU of each region of each image slice was converted to ash density by using a linear relationship, which was determined from the calibration phantom (Figure 3.10). The line was defined using known ash densities of water (0 g/cm^3) and epoxy resin (1.05 g/cm^3), and measured HU values. The average HU for each region was converted to ash density using this relationship. Apparent density was also calculated by dividing ash density by 0.6 (Schileo et al., 2007). Ash density or apparent density, as required, was input into three density-modulus relationships specific to the cancellous bone of the proximal tibia to determine the corresponding elastic modulus of each region (Table 3.1). The average elastic modulus was calculated by averaging the values found in each region over all the image slices.

Averaging the elastic modulus values has been reported to be more accurate than averaging density prior to the conversion to modulus (Taddei et al., 2007). This is due to the exponential nature of density-modulus relationships (Figure 3.11). To examine the effect of order on the current results, a voxel mesh of each of the nine regions was created for the first slice of a proximal tibia. A representative equation (Linde et al., 1992) was applied using the calibration phantom measurements and Mimics®. The mesh was exported as an Abaqus® (Dassault Systemes, Waltham, MA, USA) file to include element and material information and opened in Excel. Ten materials were used to simplify the calculation of average modulus. In order to determine if this was a sufficient
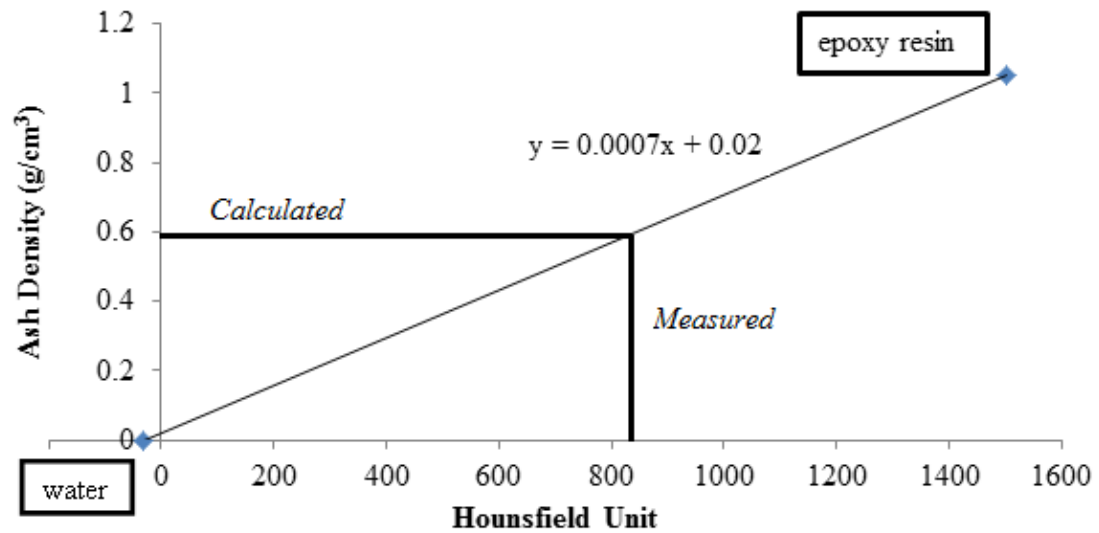
Figure 3.10   **Conversion of HU to ash density with a calibration phantom.**
The calibration phantom, consisting of epoxy resin and water, was CT scanned to linearly relate HU to ash density.

Table 3.1 **Three density-modulus relationships developed for cancellous bone of the proximal tibia.**
This study evaluated the applicability of these equations when indentation testing is used, where apparent density (Linde et al., 1992; Morgan et al., 2003) and ash density (Keyak et al., 1994) were the variables.

Study	Density-Modulus Relationship
Linde et al. (1992)	$E = 4778p_{app}^{1.99}$
Keyak et al. (1994)	$E = 33900p_{ash}^{2.20}$
Morgan et al. (2003)	$E = 15520p_{app}^{1.93}$
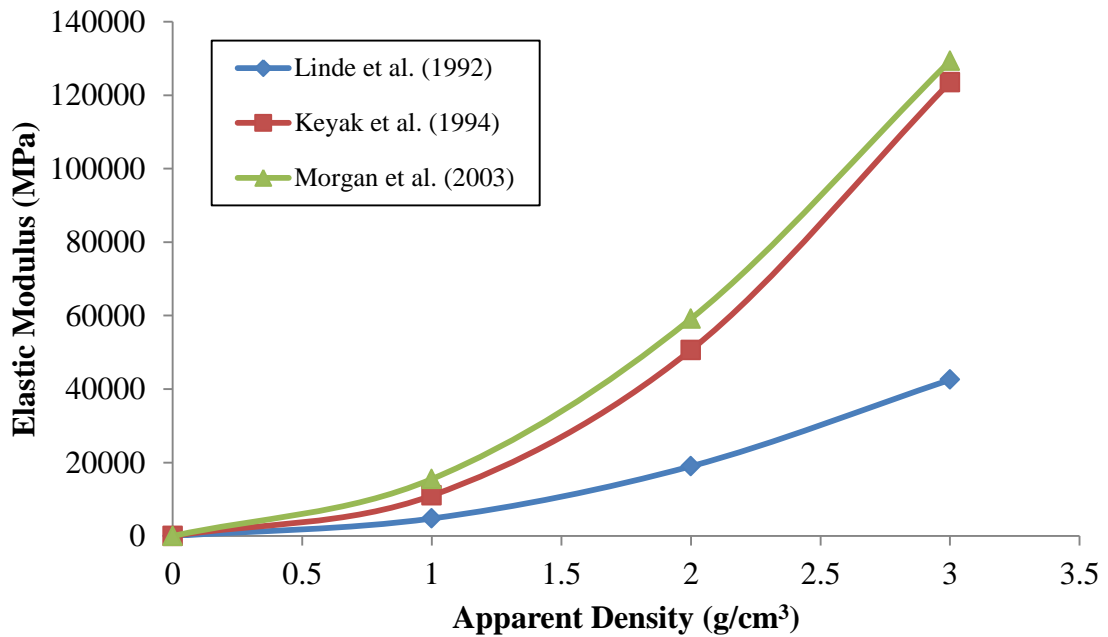
Figure 3.11 **Graphical representation of the density-modulus relationships.** Density-modulus relationship curves are shown for the three different equations that were applied for cancellous bone.

number of materials, average modulus was calculated for by applying the Linde et al. (1992) equation for a representative slice using twenty materials as well. The number of elements for each material was thus obtained, along with the average elastic modulus. The average modulus for the entire region was then calculated and weighted based on the number of elements. This was compared to the modulus from the first method, and the percent error calculated. A paired t-test was conducted to further determine if there were significant differences between the modulus values calculated using the two different averaging methods (Taddei et al., 2007).

The moduli calculated from the CT density data were compared to the experimental data collected in Chapter 2. Although the density-modulus relationships evaluated in this study were formulated using different experimental techniques, they all reported elastic modulus, which was compared to the elastic modulus values found in the current study. The percent error between the CT-predicted and experimental elastic modulus was then calculated for each region to determine which of the three density-modulus relationships was most representative of cancellous bone.

3.3   Results

The SB3 compound had an average HU of 1512.4 with a corresponding ash density of 1.05 g/cm^3. Water had an average HU of -29.3 with an ash density of 0 g/cm^3. The equation of the line was defined for each CT scan to convert bone HU to ash density (Figure 3.10).

Slice scans aligned well with the proximal tibia whole bone scan, with most slices having an average misalignment of 0.3 cm. The size and location of the ellipse within the

region had no effect on CT numbers (Appendix H). The HU readings of cancellous bone from CT scans of the proximal tibia ranged from 5.6 to 880.0 HU. The corresponding ash density values fell between 0.02 and 0.6 g/cm^3, and apparent density ranged from 0.04 to 1.1 g/cm^3. The elastic modulus values calculated using the density-modulus relationship formulated by Linde et al. (1992) ranged from 14.4 to 4696.9 MPa (Figure 3.12). The density-modulus relationship by Keyak et al. (1994) gave modulus values between 18.1 and 10817.9 MPa, and the density-modulus relationship by Morgan et al. (2003) generated modulus values between 55.6 and 15262.4 MPa.

All three density-modulus relationships overestimated the modulus predicted using CT imaging (Table 3.2a, b). The smallest percent error between CT-derived modulus and elastic modulus was observed when using the Linde et al. (1992) density-modulus relationship, where errors ranged from 113-838% in the regions and 480-730% in the slices. The greatest percent error occurred when applying the Morgan et al. (2003) equation, where error ranged from 674-3045% in the regions and 1901-2771% in the slices. Percent error ranged from 231-1847% in the regions and 988-1443% in the slices when the density-modulus relationship by Keyak et al. (1994) was used. Overall, the equation presented by Linde et al. (1992) consistently predicted elastic modulus values closest to the experimental modulus.

Although CT-derived elastic modulus values were greater than those obtained during indentation testing, the trends were the same as those seen in mechanical testing, as outlined in Chapter 2 (Figure 3.12). The highest CT modulus was predicted in the
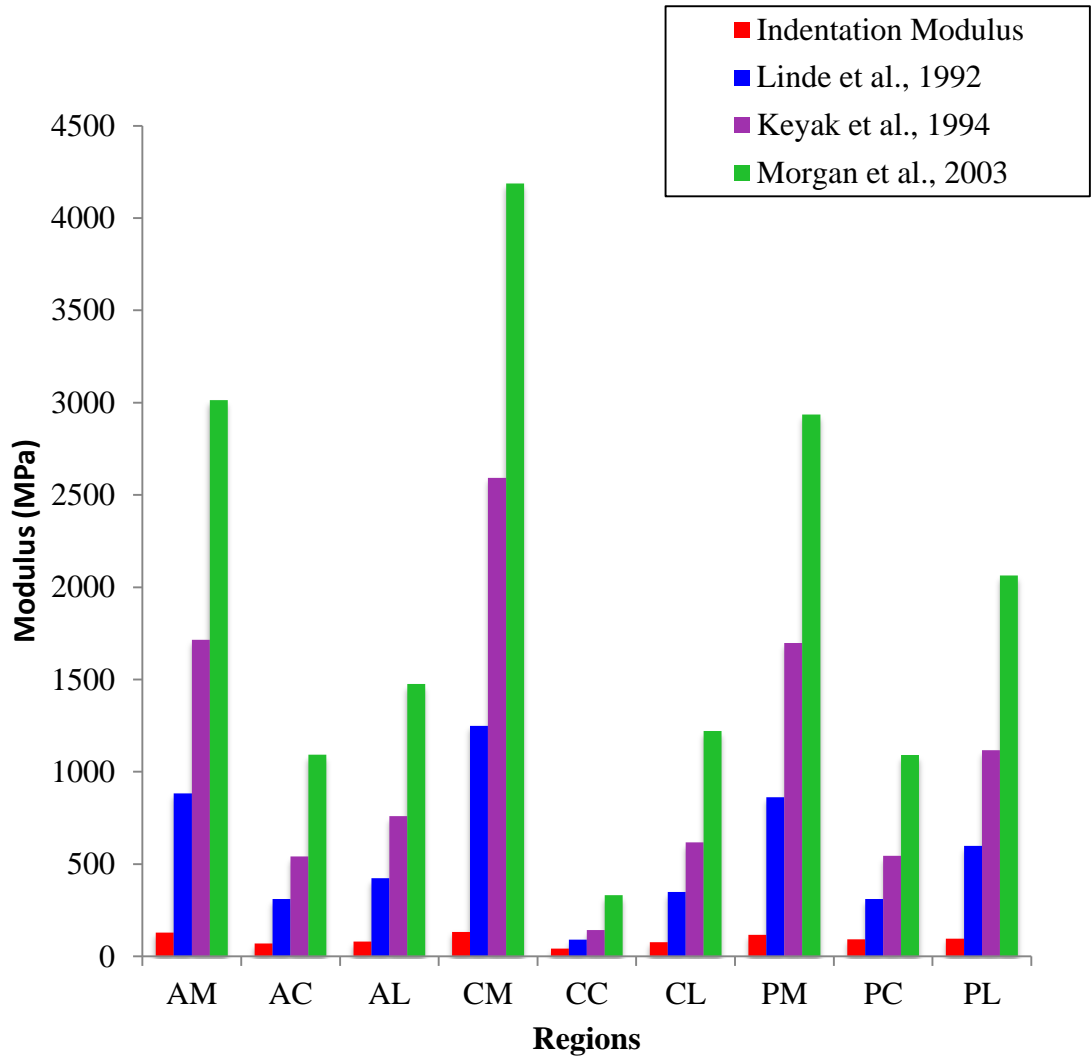
Figure 3.12   **Predicted modulus compared to elastic modulus.**
Elastic modulus was compared to CT-derived modulus predicted by the three density-modulus relationships for each of the nine regions.

Table 3.2   **Percent error of CT-derived elastic modulus in the (a) regions and (b) slices.**
The percent error between CT-derived and elastic modulus was calculated for each of the density-modulus relationships for each of the regions and slices.

	Percent Error (%)		
Region	**Linde et al., 1992**	**Keyak et al., 1994**	**Morgan et al., 2003**
AM	584	1229	2235
AC	348	681	1477
AL	431	853	1752
CM	838	1847	3045
CC	113	231	674
CL	353	703	1488
PM	643	1361	2428
PC	235	487	1078
PL	519	1056	2035

(a)

	Percent Error (%)		
Slice	**Linde et al., 1992**	**Keyak et al., 1994**	**Morgan et al., 2003**
1	536	1177	2053
2	495	1007	1957
3	730	1443	2771
4	480	988	1901

(b)

central medial (CM) region of the medial condyle by all three density-modulus relationships, which ranged from 1249.1 to 4187.0 MPa. All three density-modulus relationships also predicted the lowest modulus, from 91.2 to 331.8 MPa, in the central central (CC) region from the CT images. Using the equation by Linde et al. (1992) as an example, the highest CT-derived modulus was observed in the most proximal slice, which decreased through the distal slices. There were substantial differences among the modulus values calculated by each of the three density-modulus relationships. The least amount of variation in modulus was consistently found in the central central (CC) region, where modulus was overestimated by 113-674% (Table 3.2a). The greatest amount of variation in modulus was always in the central medial (CM) region where percent error ranged from 838 to 3045% depending on the density-modulus relationship used (Table 3.2a,b).

To determine if averaging modulus was more accurate in predicting modulus than averaging densities, the average modulus was calculated for the nine regions of the first slice of a representative tibia using the equation by Linde et al. (1992). This resulted in an average modulus of 196.7 MPa using ten materials and 220.3 MPa using twenty materials for the CC region and an average modulus of 1511.2 MPa using ten materials and 1053.9 MPa using twenty materials for the CM region. In comparison, the modulus calculated by averaging densities over the same slice was 119.4 (CC) and 1477.2 MPa (CM). Using ten materials, the average percent difference between the two methods of calculating elastic modulus was 11.7%. To ensure that there were no significant differences between the two methods, a paired t-test was conducted, and found to have no significant differences (p=0.05). A linear regression for each method showed that using average density to

calculate elastic modulus most closely matched the experimental results, with $R^2 = 0.8$, slope = 1.8, and intercept = 111.6 (Figure 3.13).

3.4   Discussion

The accuracy of a FE analysis is dramatically influenced by the material properties used. CT is a useful tool both for extracting bone geometry and assigning inhomogeneous material properties. In this study, three density-modulus relationships, developed specifically for cancellous bone of the proximal tibia, were evaluated against the previous indentation testing from Chapter Two. This allowed direct comparison of CT-predicted and true modulus values of cancellous bone. Previous studies have demonstrated that CT can be used to predict mechanical properties of cancellous bone (Bentzen et al., 1987; Ciarelli et al., 1991; MacNeil and Boyd, 2007). However, studies have thus far applied bone density from CT images in relationships developed for machined specimens in uniaxial compression. Therefore, it was previously unknown whether the density-modulus relationships can accurately predict mechanical properties observed *in situ*.

The density-modulus relationship presented by Linde et al. (1992) most closely matched the experimental results described in Chapter Two. However, this equation still overestimated the modulus of this bone, and as such it may be of great interest to develop an improved density-modulus relationship. It is interesting to note that the CT-predicted modulus values were closest to the elastic moduli for the softer cancellous bone of the central central (CC) regions. This suggests that these density-modulus relationships may be a better fit for weaker bone, or possibly older specimens. However, when looking at
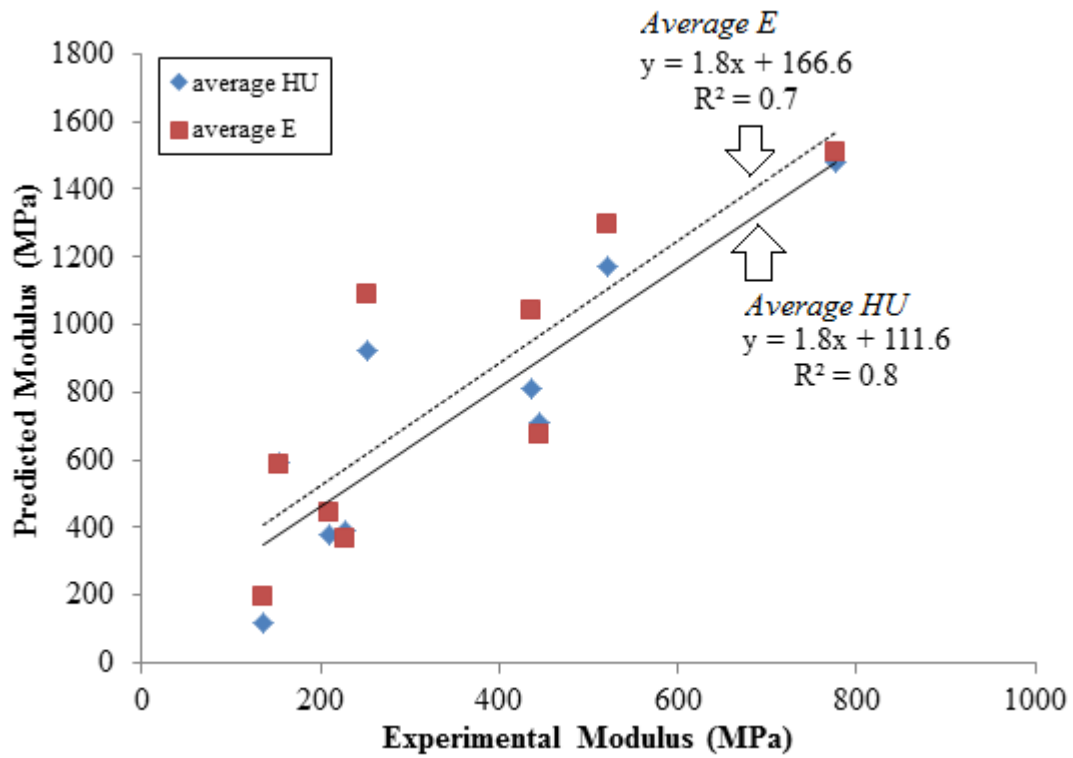
Figure 3.13   Linear regression of average HU versus average modulus.
A line with an $R^2 = 1$, a slope of 1, and an intercept of 0 was indicative of the best method to calculate modulus.

the results from the oldest specimen in the present study (age 63 years), the error was 157%, on the same order as that from all specimens (176%). This may have been on account of having mostly older donor age range (46-63 years). Greater error may be observed when the density-modulus relationships are applied to younger bones, which tend to be stronger, thereby suggesting that these equations are not representative across a range of densities. The modulus values calculated from CT imaging followed the same trends as found in the indentation testing, where the medial region (CM) and most proximal slice had the highest modulus and the central region (CC) had the lowest modulus. Therefore, CT numbers may be a useful tool for predicting the density of cancellous bone, but an improved relationship is necessary to accurately quantify these mechanical properties.

All three density-modulus relationships were developed using uniaxial compression tests on machined specimens. Modulus was calculated as the slope of the stress-strain curve, specimens were ashed to determine ash density, and apparent density was calculated by dividing the bone mass by the specimen volume. However, as trabeculae lose the support of the surrounding trabeculae when specimens are cut out of bone, the stiffness is underestimated, and this may account for some of the differences found in the present study (Linde et al., 1992). The lower values observed in the present study may have been influenced by the advanced age of the donors, the fact that machine compliance was not corrected for, and since damage still occurred at the surface of the specimens when slices were cut out of the proximal tibia. Although the three density-modulus relationships used in this study were developed for the cancellous bone of the

proximal tibia, the coefficient of each relationship was substantially different. Morgan et al. (2003) concluded that density-modulus relationships vary according to the anatomic location due to differences in bone micro-architecture. Therefore, no universal relationship can be applied for the development of FE models.

Linde et al. (1992) compared cylindrical and cubic specimens of varying sizes during the development of their equation. To allow comparisons to be drawn against the relationship developed by Morgan et al. (2003), the present study selected the equation developed for the largest cylindrical specimen, which had a diameter of 7.5 mm. However, a density-modulus relationship developed using smaller diameter cylindrical specimens had a smaller coefficient (1236), which led to a better match between predicted and experimental modulus values in the stronger medial regions in a representative slice where the average percent error was 36% compared to 247% (Figure 3.14). Keyak et al. (1994) developed their density-modulus relationship using ash density as a parameter. In the present study it was found that their relationship overestimated modulus to a greater degree than Linde et al. (1992). Keyak et al. (1994) developed their relationship using the modulus obtained through destructive testing following non-destructive tests, which were lower than values typically found in the literature. Power models using ash density as the independent variable in density-modulus relationships have been shown to be the most accurate (Keller, 1994), which suggests the 0.6 conversion to apparent density might not be sufficient. Morgan et al. (2003) used 8 mm diameter, cylindrical specimens loaded in tension and compression to develop their relationship. They found that elastic modulus was significantly higher using CT images of a subset of specimens in FE analysis. As a
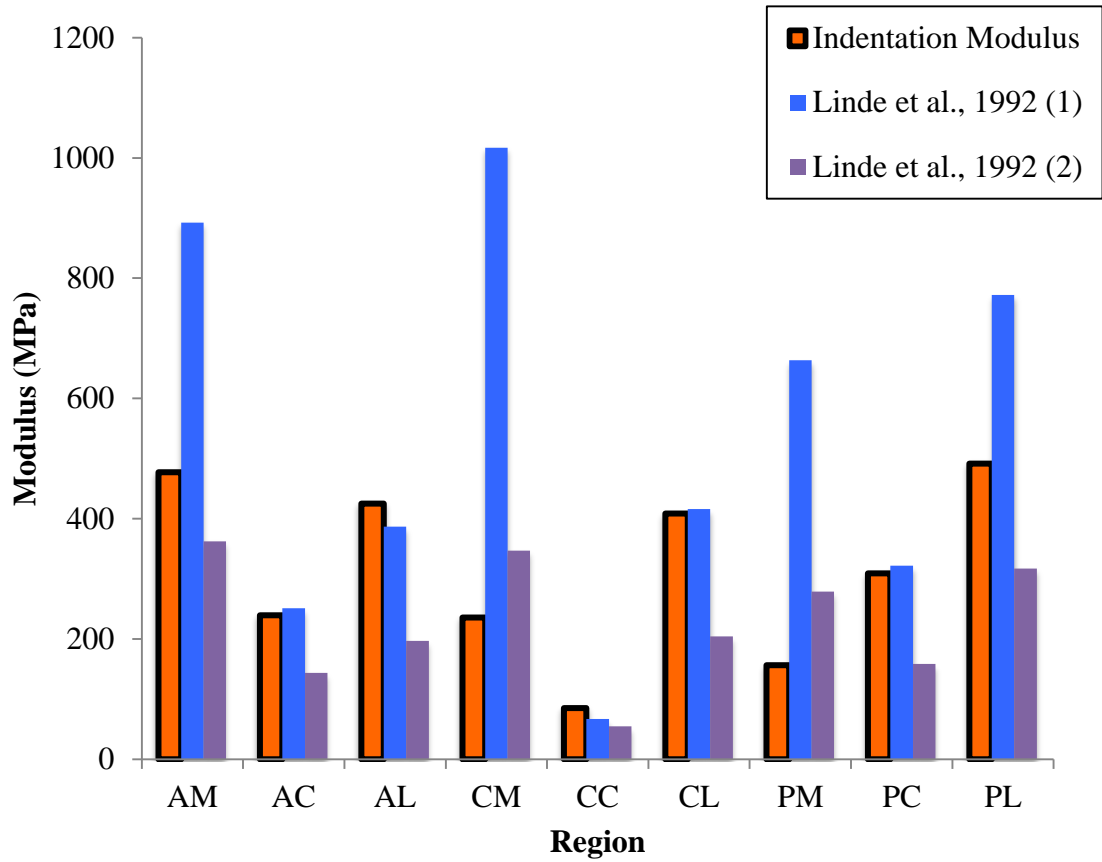
Figure 3.14 **Predicted modulus from two relationships presented by Linde et al. (1992) for a representative slice.**
Equation 1 was developed for a 7.5 mm bone plug ($E = 4778\rho_{app}^{1.99}$).
Equation 2 was developed for a 5.5 mm bone plug ($E = 1236\rho_{app}^{1.45}$).

result, it may be advantageous to use mechanical properties observed through testing *in situ* to develop a representative density-modulus relationship.

Limitations of the present study include the fact that only four bones were used for evaluation. It is possible that with more specimens or different age groups, there would be different conclusions. However, a great strength is that these data were compared to the experimental data from the same four bones. CT numbers have been shown to be affected by image content, positioning, and any damage to the bone (Keyak et al., 1994). Beam hardening effects prevented the use of CT numbers from bone slices which were found to have large, negative HUs. Although a calibration phantom was used to quantify bone mineral content density from the CT scans, it may have been useful to scan the bones submerged in water to simulate soft tissue (Nazarian et al., 2008). Bone density data was therefore extracted from the whole bone by aligning CT images of the slices to the proximal epiphysis. However, computational limitations may have not oriented the slices in the exact location from where they were cut, so density values may not be obtained precisely from the location of testing. Nonetheless, close alignment was achieved as slice offset was typically within 0 to 0.3 cm. Greater misalignment arose in one tibia where slices were CT imaged following indentation testing, which led to matching damaged specimens to the whole bone. Furthermore, there may be discrepancies between the nine regions defined for the CT image and the mechanical tests. Alignment between the CT image and indentation test regions was ensured by using the same boundary conditions. Error was introduced when equating the thickness of the CT image slices of 0.625 mm to 1 mm in the specimen. However, this was deemed necessary in order to get sufficient

overlap between the polylines to record HUs from the CT image slices. Experimentally, the grid was created by first aligning the posterior condyles along a straight line and measuring a parallel line across the widest point of the slice. Regions were then divided into nine equal regions. This approach was repeated using the CT images. CT-predicted elastic modulus was compared to the elastic modulus calculated through mechanical testing as the three relationships were generated using elastic modulus values. Another limitation was that only a single direction (superior-inferior) was studied. Due to anisotropy, the equations may better represent other directions. However, the properties measured in the superior-inferior direction are assumed to be the strongest due to the vertical arrangement of trabeculae resulting from load transmission patterns, so the relationships may be even more inaccurate in the other directions. Density does not account for anisotropy and structure orientation, yet both factors influence the elastic modulus of bone (Linde et al., 1992). Therefore, CT-derived bone density may be useful for determining an isotropic modulus value for FE models.

Although past studies have determined that it is more accurate to use average modulus rather than average HU to evaluate the predictive ability of density-modulus relationships (Taddei et al., 2007), the present study found no difference. Taddei et al. (2007) determined that a line with an $R^2 = 1$, a slope of 1, and an intercept of 0 was indicative of the method with the highest predictive ability of material properties. The present study found a $R^2 = 0.8$ and a $R^2 = 0.7$ by using average HU versus average modulus, respectively. Therefore, there was no difference in the order of calculating modulus. This was most likely the case as the HU of each image slice was converted to

each parameter to be averaged in the final calculation of modulus. Moreover, only ten materials were used in the calculation of average modulus, which may not have been sufficient to characterize the inhomogeneous material properties of the tibia. However, when the number of materials was increased to twenty, modulus changed by only 12-30%, so increasing materials may not have a great effect.

The ability to predict mechanical properties from CT is significantly dependent on the selected density-modulus relationship. This study revealed that the density-modulus relationship presented by Linde et al. (1992) gave the closest results to the experimental values, making it the most accurate relationship to use in FE analysis of cancellous bone of the tibia. The results of this study suggest the development of an improved density-modulus relationship for the tibia is necessary to increase the accuracy of FE models and better predict the risk of injury.

3.5   References

Austman, R. L., Milner, J.S., Holdsworth, D.W., and Dunning, C. E. (2008). The effect of the density-modulus relationship selected to apply material properties in a finite element model of long bone. *Journal of Biomechanics*, *41*, 3171–3176.

Bentzen, S. M., Hvid, I., and Jorgensen, J. (1987). Mechanical Strength of Tibial Trabecular Bone Evaluated by X-Ray Computed Tomography. *J. Biomechanics*, *20*(8), 743–752.

Carter, D.R., Hayes, W. C. (1977). The compressive behavior of bone as a two-phase porous structure. *J Bone Joint Surg Am*, *59*(7), 954–962.

Ciarelli, M.J., Goldstein, S.A., Kuhn, J.L., Cody, D.D., and Brown, M. B. (1991). Evaluation of orthogonal mechanical properties and density of human trabecular bone from the major metaphyseal regions with materials testing and computed tomography. *Journal of Orthopaedic Research*, *9*, 674–682.

Dunham, C.E., Takaki, S.E., Johnson, J.A., Dunning, C. E. . (2005). Mechanical Properties of Cancellous Bone of the Distal Humerus. *Clinical Biomechanics*, *20*, 834–838.

Keller, T. S. (1994). Predicting the compressive mechanical behavior of bone. *J. Biomechanics*, *27*(9), 1159–1168.

Keyak, J. H. (1990). Automated three-dimensional finite element modelling of bone : a new method, *12*, 389–397.

Keyak, J.H., Lee, I.Y., and Skinner, H. B. (1994). Correlations between orthogonal mechanical properties and density of trabeculae bone: use of different densitometric measures. *Journal of Biomedical Materials Research*, *28*, 1329–1336.

Linde, F., Hvid, I., Madsen, F. (1992). The effect of specimen geometry on the mechanical behaviour of trabecular bone specimens. *J Biomechanics*, *25*(4), 359–368.

MacNeil, J.A. and Boyd, S. K. (2007). Load distribution and the predictive power of morphological indices in the distal radius and tibia by high resolution peripheral quantitative computed tomography. *Bone*, *41*, 129–137.

Morgan, E.F., Bayraktar, H.H., and Keaveny, T. M. (2003). Trabecule bone modulus-density relationships depend on anatomic site. *Journal of Biomechanics*, *36*, 897–904.

Nazarian, A., Snyder, B.D., Zurakowski, D., and Muller, R. (2008). Quantitative micro-computed tomography: a non-invasive method to assess equivalent bone mineral density. *Bone*, *43*(2), 302–311.

Quenneville, C.E., McLachlin, S.D., Greeley, G.S., and Dunning, C. (2011). Injury tolerance criteria for short-duration axial impulse loading of the isolated tibia. *Journal of Trauma-Injury Infection and Critical Care*, *70*(1), 12–18.

Rho, J.Y., Hobatho, M.C., Ashman, R. B. (1995). Relations of mechanical properties to density and CT numbers in human bone. *Med Eng Phys*, *17*(5), 347–355.

Rice, J. C. (1988). On the dependence of the elasticity and strength of cancellous bone on apparent density. *J. Biomechanics*, *21*(2), 155–168.

Schileo, E., Taddei, F., Malandrino, A., Cristofolini, L., and Viceconti, M. (2007). Subject-specific finite element models can accurately predict strain levels in long bones. *Journal of Biomechanics*, *40*(13), 2982–2989.

Taddei, F., Schileo, E., Helgason, B., Cristofolini, L., and Viceconti, M. (2007). The material mapping strategy influences the accuracy of CT-based finite element models of bones: an evaluation against experimental measurements. *Medical Engineering & Physics*, *29*, 973–979.

Chapter 4: General Discussion and Conclusions

OVERVIEW: This chapter outlines the purpose and hypotheses detailed in the first chapter, and reviews the findings of the studies completed herein. The strengths and limitations that were encountered are discussed alongside the clinical and scientific significance of the project. To conclude, future applications of the results are examined.

4.1   Summary

Finite element (FE) models are used to study bone response under various conditions. Accurate FE models represent bone with the appropriate material properties to simulate bone behavior in the most realistic manner, ultimately leading to the best results. These models can be used to predict risk of injury to the bone or for the design of orthopaedic devices.

Bone is an inhomogeneous material in terms of the distribution of its mechanical properties (Carter and Hayes, 1977). The definition of material properties is one of the key elements in building accurate FE models. Previous dynamic FE models have simplified bone to be a homogeneous and isotropic material, which may affect the accuracy of the results (Hvid and Hansen, 1985). The purpose of this two-phase study was to quantify regional variations in the mechanical properties of cancellous bone of the proximal tibia, which also served to evaluate the predictive ability of CT-based density-modulus relationships. The overall goal was to aid in the development of improved FE models of the tibia and assist in the long-term success of orthopaedic devices.

The first study (Chapter 2) experimentally determined the extent of regional variations in elastic modulus and yield strength through the proximal tibia. Indentation tests were performed on four sequential transverse slices of cancellous bone cut from the proximal epiphysis of the tibia. The resulting load-displacement data were converted to stress-strain curves to determine the indentation modulus and yield strength at each test site, which were grouped into nine regions according to anatomical landmarks. The most proximal slice had the highest indentation modulus and yield strength. The anterior medial (AM) and central medial (CM) regions had the highest indentation modulus values, along with posterior medial (PM) for greatest yield strength. The central central (CC) region was weakest in both indentation modulus and yield strength by factors of three and four, respectively. As a result, Hypothesis 1 was accepted as modulus and yield strength varied through the depth and over the transverse plane of the proximal tibia with the strongest areas located closest to the joint surface and in the medial condyles. However, only the first slice was significantly higher in elastic modulus and yield strength, which may be due to trabecular organization patterns past the first 5 mm. Furthermore, no differences in regional modulus or yield strength were noticed in the lateral condyles, which may be due to the small sample size. These findings have clinical and scientific applications whereby the areas of highest modulus and yield strength should be used as attachment points for orthopaedic devices and preserved during surgery. Furthermore, this highlighted the importance of including inhomogeneous properties in FE models of the tibia.

The second phase of this research (Chapter 3) evaluated three density-modulus relationships found in the literature that were developed to predict the material properties of cancellous bone of the proximal tibia (Keyak et al., 1994; Linde et al., 1992; Morgan et al., 2003). Computed tomography (CT) images were taken of the slices prior to testing, and registered to the whole bone to identify the corresponding densities of each region tested experimentally. A calibration phantom was used to convert HU to ash density, which was then converted to apparent density using a known scaling value (Schileo et al., 2007). Either ash density or apparent density, as required, was input into each density-modulus relationship to determine the corresponding elastic modulus. CT-derived elastic moduli were compared to the elastic moduli calculated from the mechanical testing from Chapter 2. Although CT was able to capture the regional variations found experimentally, all three density-modulus relationships overestimated modulus. As a result, Hypothesis 2 was accepted, as the investigated density-modulus relationships did not accurately predict elastic modulus of cancellous bone in the proximal tibia. Nonetheless, the equation developed by Linde et al. (1992) predicted modulus values closest to the experimental results. Therefore, this density-modulus relationship is the most appropriate of the three to apply inhomogeneous properties in subject-specific FE models of the tibia. Ultimately, an improved density-modulus relationship specific to cancellous bone of the proximal epiphysis would be the most advantageous in order to enhance accuracy of stress analyses of the tibia.

4.2   Strengths and Limitations

The specific strengths and limitations encountered during each phase of this research are discussed in their respective chapters; however, there were some that are generally applicable to this body of work. Results were collected from the most extensive number of test sites, with an average of 113 per slice, from five tibias, which is dramatically higher than past studies. The large number of slices and regions examined allowed for a thorough investigation of mechanical properties through the proximal epiphysis.

Although the three density-modulus relationships investigated in this study were developed by testing cubic or cylindrical specimens, modulus and yield strength were calculated through indentation testing. This is more representative of *in vivo* loading, as test sites are supported by the surrounding tissue within the slice. While others have suggested equations for various density ranges, this study focused on cancellous bone exclusively. CT imaging was used to predict the elastic modulus for cancellous bone specifically, which allowed for the characterization of a single type of tissue rather than the whole bone response. A significant improvement introduced by this study was that elastic modulus values were directly compared to the elastic modulus values predicted using CT for each of the regions of each tibia.

The small sample size was a limitation; however, regions that were significantly stronger or weaker were identified, despite the natural inter-specimen variation that occurs in the human population. Difficulty arose when making precision cuts to extract transverse slices orthogonal to the long axis of the tibia. As a result, slices were not perfectly perpendicular and varied in thickness and may have potentially been damaged at

the surface. Therefore, comparisons drawn between tibias may have been comparing mechanical properties at varying depths and should be corrected for in the future. It may also be beneficial to use slice thicknesses that are scaled to the total length of the tibia so that comparisons can be made between slices that are proportionally the same distance away from the joint surface. Moreover, the lateral condyle of the tibia is situated higher than the medial condyle. Therefore, it is difficult to directly compare the medial region to the lateral region within the same transverse plane. Cortical bone was excluded from this study by discarding the top layer. However, visual inspection alone may not have been sufficient in detecting residual cortical bone in the subsequent slice, leading to the increased strength noted herein. However, findings were consistent with other studies that showed bone closest to the joint was the strongest and cortical bone was not observed in the CT images of the slices.

Specimens were loaded at a low strain rate in one direction so only the properties in the superior-inferior direction are known. Although the superior-inferior direction may be the primary loading mode *in vivo*, devices (such as plates, screws, and total knee arthroplasties) rely on lateral rigidity as well. Nevertheless, it has been noted that including anisotropic properties may not have a dramatic effect on the accuracy of FE models when loading is held consistent among all specimens (Peng et al., 2006). Testing cancellous bone at a low strain rate ensured that bone marrow had no influence on its properties, which may not give the information needed for dynamic injury-predicting models. The loss of marrow was necessary to conduct mechanical tests; however, bones were kept moist so there were no drying effects. This loss may have influenced CT

images of the slices, which is why the whole bone scans were used to extract density data. CT data was only collected from four bones due to a data transfer error; however, it was clear that the density-modulus relationship developed by Linde et al. (1992) was the most accurate for each tibia, so it is likely that this would be the best in general. There may have been some error introduced when matching the regions of interest from the CT scans to the mechanical tests. However, global registration of the slices to the whole bone ensured that this was most likely not an issue, as the offset was typically in the range of 0-0.3 cm.

4.3   Future Directions

The findings of the present study lay the foundation for future work in analyzing the mechanical properties of cancellous bone in different orientations (such as in the medial-lateral and anterior-posterior directions) and under varying strain rates. It would also be of great interest to experimentally determine the ash density of the specimens used in this study to be correlated to the indentation modulus values found in the same sample. This would allow for the development of a novel density-modulus relationship specific to the cancellous bone of the proximal tibia using a testing method more closely related to *in vivo* loading patterns. Furthermore, a comparison of experimental and imaging density data would be useful in evaluating the ability of CT numbers to predict the ash density of cancellous bone. Ultimately, a FE analysis should be performed to determine whether variations in cancellous properties have a significant effect on the accuracy of these models.

Cortical bone is a distinct structure from cancellous bone, which is characterized by its own set of mechanical properties (Hansen et al., 2008). The material properties of both cancellous and cortical bone need to be accurately assigned in the development of FE models of the tibia. Therefore, the next steps involve quantifying the extent of regional variations in the mechanical properties of cortical bone in the tibia. To this end, the materials techniques have been developed. The diaphysis of each tibia will be cut into longitudinal segments that will be sectioned into four quadrants (anterior, posterior, medial, and lateral). Half of the samples will be quasi-statically tested to failure by a materials testing machine using four-point bending. The remaining samples will be tested to failure at strain rates of 0.1, 1.0, and 10 per second to determine the effects on modulus and yield strength. Cortical specimens will be CT-scanned prior to cutting and testing to extract density data. Density-modulus relationships specific to cortical bone of the tibia will be investigated to determine their accuracy in predicting these important mechanical properties.

4.4 Significance

In conclusion, this work quantified the full variation of modulus and yield strength of cancellous bone in the proximal tibia in order to identify the strongest areas. These regions of strength can serve as attachment sites for orthopaedic devices, such as total knee arthroplasties (TKA). The success of these implants relies on achieving fixation in host bone where attachment in the strongest areas may prevent the device from becoming loose, which would lead to its failure (Bourne and Finlay, 1986). Traditionally, the tibial component consists of a stem that extends through the intramedullary canal (Stern et al.,

1997). However, this study found that the central central (CC) region is the weakest, so alternate fixations methods may be needed. Furthermore, subchondral bone is sometimes removed in these surgical procedures when this area should be preserved to ensure stability of the device and improve long-term outcomes for patients (Dorr and Boiardo, 1986).

The experimental results were compared to CT density data to evaluate the accuracy of density-modulus relationships, which revealed the need for a new equation to better predict mechanical properties of cancellous bone in the proximal tibia. Further investigation is required to determine if the inhomogeneous nature of cancellous bone needs to be accounted for in future dynamic FE models. Accurate FE models can then be used to develop strategies for reducing the risk of injury to the tibia. It is hoped that this knowledge will contribute towards improved surgical outcomes and increased modeling accuracy.

4.5   References

Bourne, R.B. and Finlay, J. B. (1986). The influence of tibial component intramedullary stems and implant-cortex contact on the strain distribution of the proximal tibia following total knee arthroplasty: an in vivo study. *Clinical Orthopaedics and Related Research*, *208*, 95–99.

Carter, D.R., Hayes, W. C. (1977). The compressive behavior of bone as a two-phase porous structure. *J Bone Joint Surg Am*, *59*(7), 954–962.

Dorr, L.D. and Boiardo, R. A. (1986). Technical considerations in total knee arthroplasty. *Clinical Orthopaedics and Related Research*, *205*, 5–11.

Hansen, U., Zioupos, P., Simpson, R., Currey, J. D., & Hynd, D. (2008). The effect of strain rate on the mechanical properties of human cortical bone. *Journal of biomechanical engineering*, *130*(1), 011011.

Hvid, I., Hansen, S. L. (1985). Trabeculae Bone Strength Patterns at the Proximal Tibial Epiphysis. *Journal of Orthopaedic Research*, *3*, 464–472.

Keyak, J.H., Lee, I.Y., and Skinner, H. B. (1994). Correlations between orthogonal mechanical properties and density of trabeculae bone: use of different densitometric measures. *Journal of Biomedical Materials Research*, *28*, 1329–1336.

Linde, F., Hvid, I., Madsen, F. (1992). The effect of specimen geometry on the mechanical behaviour of trabecular bone specimens. *J Biomechanics*, *25*(4), 359–368.

Morgan, E.F., Bayraktar, H.H., and Keaveny, T. M. (2003). Trabecule bone modulus-density relationships depend on anatomic site. *Journal of Biomechanics*, *36*, 897–904.

Peng, L., Bai, J., Zeng, X., and Zhou, Y. (2006). Comparison of isotropic and orthotropic material property assignment on femoral finite element models under two loading conditions. *Medical Engineering & Physics*, *28*, 227–233.

Schileo, E., Taddei, F., Malandrino, A., Cristofolini, L., and Viceconti, M. (2007). Subject-specific finite element models can accurately predict strain levels in long bones. *Journal of Biomechanics*, *40*(13), 2982–2989.

Stern, S., Wills, R.D., and Gilbert, J. L. (1997). The effect of tibial stem design on component micromotion in knee arthroplasty. *Clinical Orthopaedics and Related Research*, *345*(44-52).

APPENDICES

Appendix A

Anatomy Glossary

This glossary contains anatomical terms found throughout the thesis. Definitions are taken from Dorlands online Medical Dictionary, 2013; Oxford Concise Medial Dictionary, 2010; and Merriam-Webster Medical Dictionary, 1995.

Anterior: Toward the front of the body; in humans towards the belly surface.

Anterior crest: Vertical ridge running over the anterior surface of the tibia; attachment for fascia.

Arthroplasty: A surgical procedure where part of the joint is replaced with an implant attached to the bone.

Articulation: The contact junction between two bones.

Cancellous Bone: A spongy, lattice-like structure of bone.

Canaliculi: Connects the Haversian canals.

Cement lines: Boundary of osteon.

Condyle: An articular prominence of a bone.

Cortical Bone: A dense bone structure.

Diaphysis: The shaft of a long bone, a tube made of cortical bone.

Distal: Further from the point of reference; away from the center of the body.

Epicondyle: A projection from the side of the bone, a muscle attachment site.

Epiphyseal Line: Replaces the epiphyseal plate in the metaphysis of long bone.

Epiphyseal Plate: Site of bone growth in the metaphysis of long bone.

Epiphysis: The expanded articular end of a long bone made of cancellous bone.

Femur: The large bone in the upper leg, extending from the pelvis to the knee.

Fibula: Located laterally to the tibia; articulates with the tibia in the lower leg.

Flexion: The movement of a joint that lessens the angle between the two segments.

Fossa: Depression in bone.

Glenoid: The socket on the lateral side of the scapula for articulation with the humerus.

Haversian canal: Channels formed by lamellae for nerve and blood vessels.

Homogeneous: Made of similar elements, having a uniform quality throughout.

Humerus: The bone of the upper arm, extending from the shoulder (scapula) to the elbow (articulating with the ulna and radius).

In situ: In place.

In vitro: In an artificial environment outside a living body.

In vivo: In a living body of a plant or animal.

Intercondylar eminence: Tibial spine between the articular facets of the proximal tibia.

Interstitial regions: Lamellae of osteons that have been destroyed.

Intramedullary canal: The canal down the center of a bone filled with marrow.

Intracondylar: Area between condyles.

Isotropic: Exhibiting properties with the same values in all directions.

Lacunae: Space containing osteocytes.

Lamellae: Concentric circles around Haversian canals in osteons.

Lateral: A position further away from the midline of the body.

Malleolus: Prominence on the bone.

Marrow: The soft tissue filling the cavities of bones.

Medial: A position closer to the midline of the body.

Meniscus: A fibrocartilaginous structure that decreases friction at joint.

Metaphysis: Portion of long bone between epiphysis and diaphysis.

Orthopaedic: Branch of medicine concerning the skeletal system and associated muscles, joints, and ligaments.

Osteocytes: Bone cells.

Osteon: The basic unit of structure in compact bone.

Patella: The bone at the front of the knee; the kneecap.

Posterior: Located towards the back of the body.

Proximal: Closer to the point of reference; towards the center of the body.

Radius: The outer bone of the forearm (thumb side), extending from the humerus at the elbow to the carpal bones at the wrist.

Resorption: The process of breaking down bone and releasing minerals.

Resorption spaces: Areas where bone is resorbed.

Purchase: Achieving stable fixation in bone.

Scapula: The bone in the back of the shoulder; the shoulder blade.

Soft Tissue: Muscle, ligaments, tendons, fat, cartilage, nerves, blood vessels, etc.

Subchondral: Beneath a layer of cartilage.

Talus: One of the bones in the ankle.

Tibia: The larger bone of the lower leg, extending between the knee and the ankle; the shinbone.

Tibial tuberosity: Elevation on the anterior surface of the tibia that acts as a site of attachment for the patellar ligament.

Trabeculae: A supporting or anchoring strand of tissue.

Trabecular Bone: Spindles of cancellous bone, which form a lattice, filled with bone marrow.

Transverse: Placed crosswise, at a right angle to the long axis of a part.

Volkmann's canals: Run perpendicular to Haversian canals carrying small arteries.

Appendix B

Design of the Clamp and Indentor

The clamp and indentor were designed on Autodesk Inventor Professional 2012. The clamp was attached to the low speed diamond wafering saw and secured the tibia in place during cutting. The indentor was attached to a materials testing machine to perform indentation testing on the specimens.

Indentor: A cylindrical indentor was made out of stainless steel and had a diameter of 4 mm.

3/18"-16
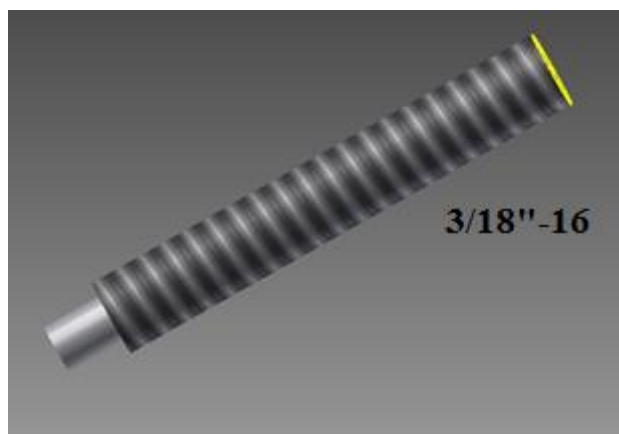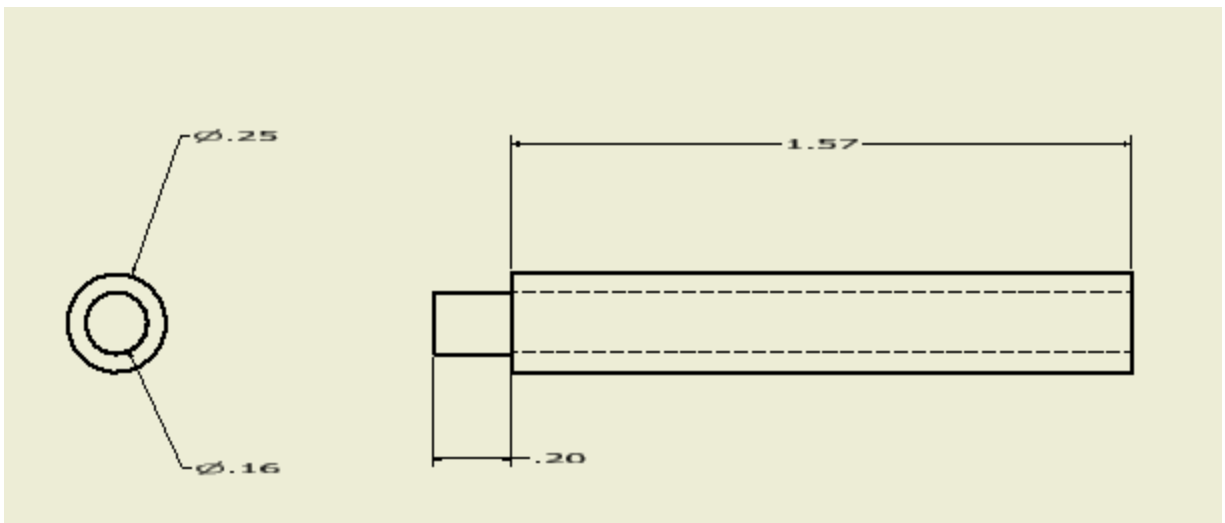
*units = inches

Clamp: The clamp consisted of two parts that (a) attached to the saw and (b) held the tibia at its diaphysis.
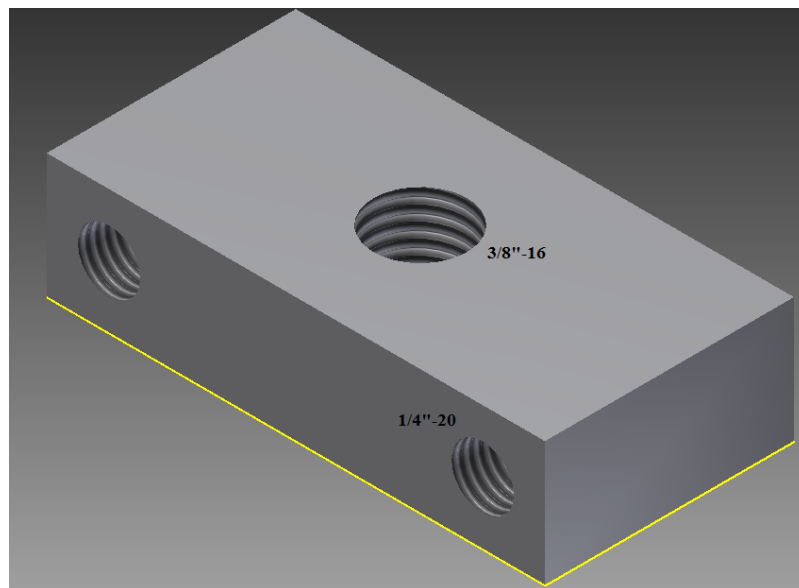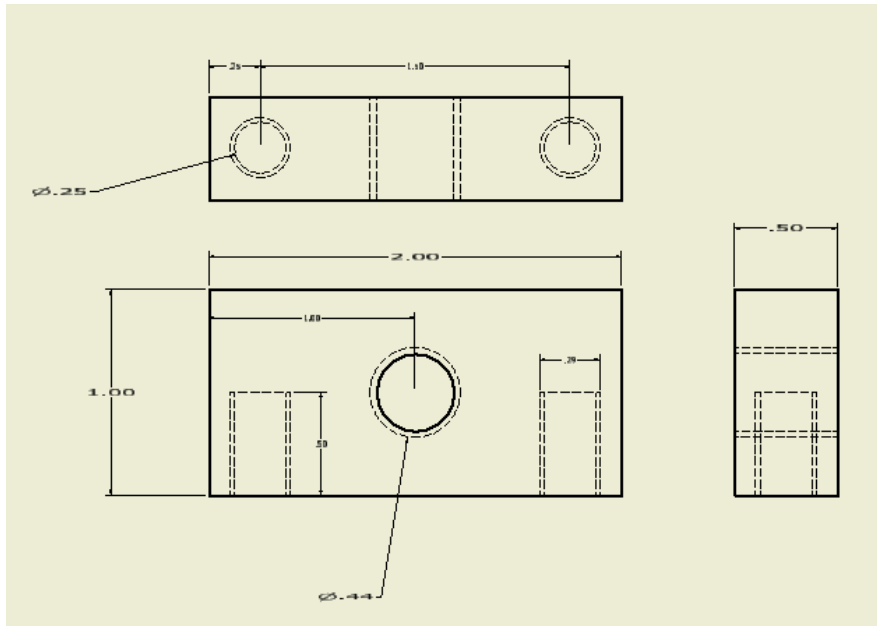
(a)   Upper component of the clamp that is attached to the low speed saw.

*units = inches
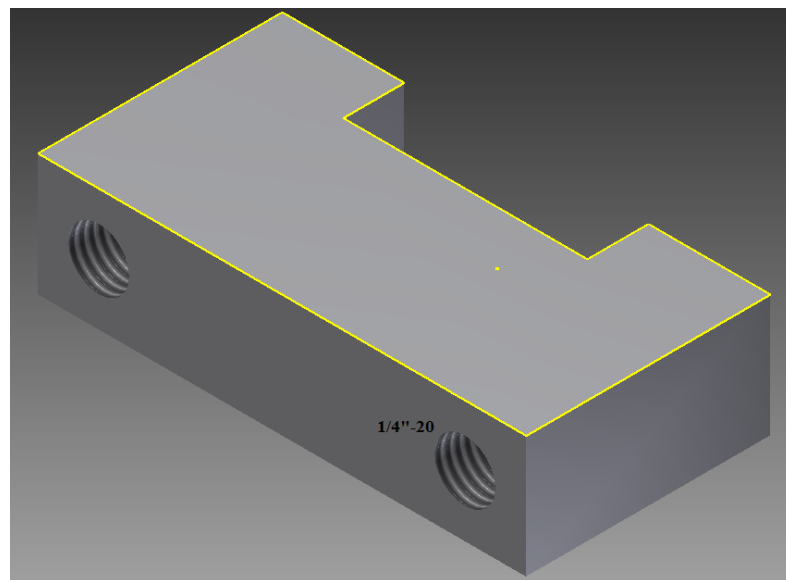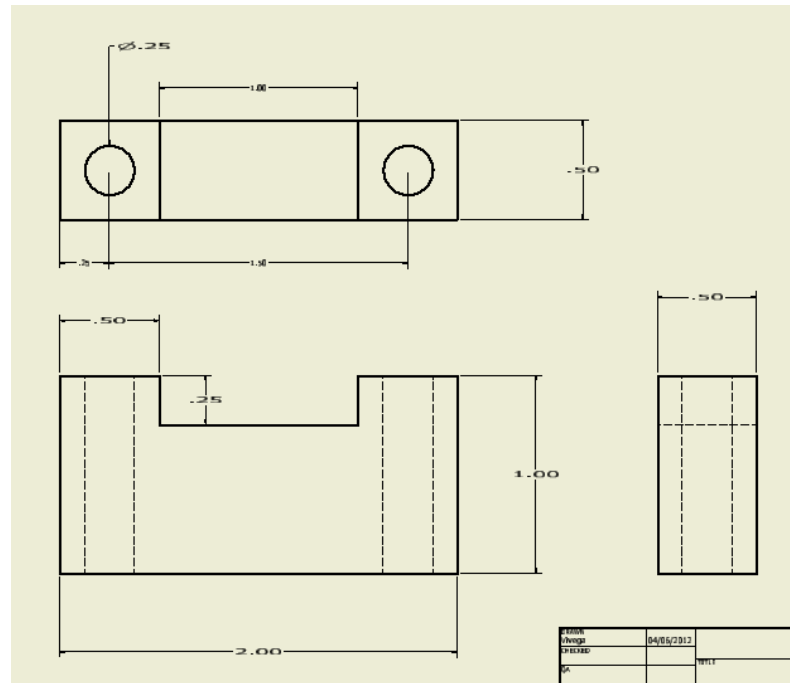
(b)   Lower component joins with the top component to form the complete clamp. The tibia sits in the groove between the upper and lower components.

*units = inches
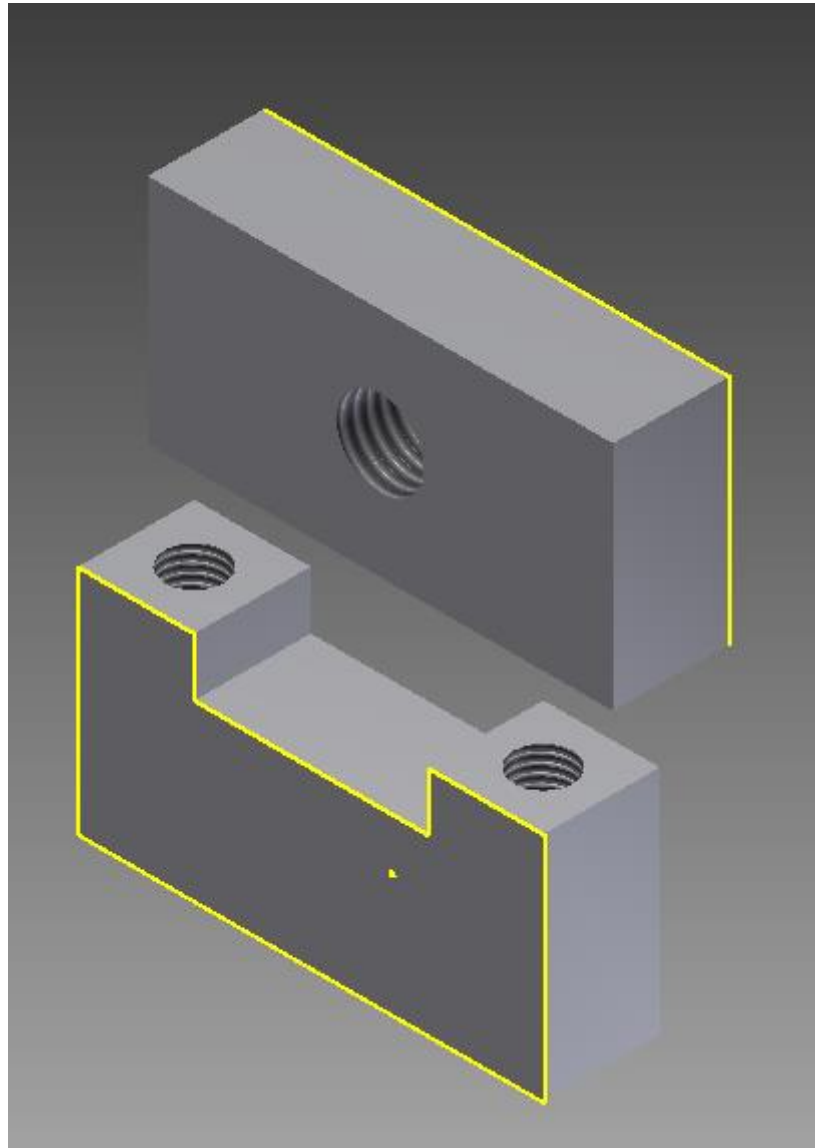
(c)   Assembly of the clamp.

Appendix C

Thickness of Cancellous Slices

Four transverse slices were cut out of the proximal epiphysis of each tibia. It proved to be difficult to cut slices perfectly perpendicular to the long axis, so the variation in thickness between slices is presented here.

Slice	Mean (SD) Thickness (mm)				
	1403	**1393**	**1469**	**1336**	**1325**
1	10.0 (1.1)	2.9 (0.8)	3.4 (0.6)	8.4 (0.5)	5.7 (0.2)
2	6.4 (1.0)	4.6 (0.8)	4.1 (0.6)	6.8 (0.6)	8.7 (0.3)
3	6.3 (0.2)	10.3 (0.5)	6.6 (1.4)	3.7 (0.6)	6.8 (1.0)
4	7.0 (0.1)	7.5 (0.6)	5.2 (1.4)	5.9 (0.2)	6.0 (0.2)

Appendix D

Calculation of a Stress-strain Curve

The load-displacement data at each test site were converted to a stress-strain curve using a custom written program (FreeMat v4.2) to calculate indentation modulus and yield strength.

```
1    %%PROCESSING and SETUP
2    %%open files we are going to work with
3    fr= fopen ('C:\Users\Vivega\Documents\DataIndenter\datafiles\filedir.txt', 'r');
4    fvar= fopen ('C:\Users\Vivega\Documents\DataIndenter\OutputVar.txt', 'w');
5    fdata= fopen('C:\Users\Vivega\Documents\DataIndenter\OutputData.txt', 'w');
6
7    %%General Parameters
8    area=(3.1416*(0.004/2)^2); %mm
9    lorig=7.52; %mm
10   offset=.002;
11   interceptsens=1.02;
12
13   %%Puts some headings in the files
14   fprintf(fvar,'Bone;Slice;Site\n');
15   fprintf(fdata,'Youngs Modulus;Yield Stress;Yield Strain;Area Under Curve;Trial\n');
16
17   %%starts processing the first file, this counts the file number
18   for i=1:29; %put number of files in here
19
20   %%Get the data from the file, and the filename
21   file{i}= fgetline(fr);  %writes first filename to a line
22   dats=real(csvread(eval(file{i})));  %reads all the data from that filename into the matrix 'vals'
23
24   %%puts information about the file into a line, then writes that info into a seperate file
25   name=file{i}(1:end);
26   slash = strstr(file{i},'-');
27   fprintf(fvar,'%i%i%i%i;', name(slash-4),name(slash-3),name(slash-2),name(slash-1));
28   fprintf(fvar,'%i;', name(slash+1));
29
30   isdig=isdigit(name(slash+4));
31   if isdig(1)==1
32   fprintf(fvar,'%i%i;', name(slash+3),name(slash+4));
33   else fprintf(fvar,'%i;', name(slash+3));
34   end
35
36   fprintf(fvar,'\n');
37
38   %%Converts to stress and strain
39   A=[dats(:,2)/area dats(:,3)/lorig];
40
41   %%MEASUREMENT
42   %%Throws up graph and tells you to select the area you want to use
43   hold off
44   plot(A(:,1),'y');
```

```matlab
45      titl=sprintf('%s, %i',file{i},i);
46      topslope=point;
47      bottomslope=point;
48      stop=round(topslope(1,1));
49      start=round(bottomslope(1,1));
50
51      %%Fixes the order of points in case you pick them wrong
52      if stop<start
53          holder=stop;
54          stop=start;
55          start=holder;
56      end
57
58      %%Finds Younge's Modulus
59      fit= polyfit(A(start:stop,2),A(start:stop,1),1);
60
61      %%finds ystress using offset
62      j=1;
63      for f=stop:length(A(:,2))
64          if (((fit(1,1)*A(f,2))+(fit(1,2)-(fit(1,1)*offset)))/A(f,1))>interceptsens
65              ystressind(j)=f;
66              j=j+1;
67          end
68      end
69      if j==1
70          ystressind=length(A(:,2));
71      end
72
73      %%Returns yield stress and strain
74      ystressind=ystressind(1);
75      ystress=A(ystressind,1);
76      ystrain=A(ystressind,2);
77
78      %%Calculates Toughness
79      toughness=0;
80      sub=0;
81      for k=1:ystressind-1;
82          ypos=(A(k,1)+A(k+1,1))/2;
83      sub=abs(ypos*(A(k+1,2)-A(k,2)));
84      toughness=toughness+sub;
85      end
```

```matlab
86
87      %%OUTPUT
88      %Checks Measruments with a plot
89      hold off
90      plot(A(:,2), A(:,1),'y');
91      titl=sprintf('%s, %i',file{i},i);
92      title(titl);
93      hold on
94      plot(ystrain,ystress, '*r');
95      ymx=linspace(A(start,2),A(stop,2),5);
96      ymx2=linspace(A(start,2),A(ystressind,2),5);
97      ymbf=(fit(1,1)*ymx)+fit(1,2);
98      offstrain=(fit(1,1)*ymx2)+(fit(1,2)-(fit(1,1)*offset));
99      plot(ymx,ymbf, 'b');
100     plot(ymx2,offstrain, '--g')
101     %xlim([0,.6]);
102     %ylim([0,4000000])
103
104     %%Prints the plot to a file
105     makefile=sprintf('C:\Users\Vivega\Documents\DataIndenter\plotcheck\Plot%i.jpg', i);
106     constructedfile=fullfile(makefile);
107     print(constructedfile);
108
109     %%Writes relevant information into a file and goes to the next file
110     fprintf(fdata,'%f;',fit(1,1));
111     fprintf(fdata,'%f;',ystress);
112     fprintf(fdata,'%f;',ystrain);
113     fprintf(fdata,'%f;',toughness);
114     fprintf(fdata,'%s',file{i});
115
116     end
117
118     clear;
119     fclose('all');
120
```

Appendix E

Sensitivity Analysis

The influence of boundaries on indentation modulus was investigated by adjusting how the test sites were grouped into nine regions over a transverse slice. Average sensitivity was calculated and compared to the coefficient of variation to determine the extent of variability in the population.

Original Boundaries:

Average Sensitivities with Shifted Boundaries:

$$Percent\ Error = \frac{x_1 - x_2}{\frac{x_1 + x_2}{2}} \times 100\%$$

-4.6	12.9	6.3
11.3	26.6	2.2
12.2	10.5	-6.2

-6.0	-2.1	-2.3
-12.4	-29.6	-7.7
-10.9	5.2	-3.5

	↑	
	↓	

-6.1	7.9	-15.7
-5.4	27.0	12.0
-7.3	14.2	-5.1

	↓	
	↑	

6.1	-16.2	2.9
14.3	-6.7	0.7
10.9	-6.3	-4.8

Coefficient of Variation:

Tibia	Mean Indentation Modulus (MPa)
1325	202.9
1336	231.9
1393	143.5
1469	148.7
1403	134.6

Mean Indentation Modulus (SD)
= 172.3 (42.7) MPa

$C_v = \sigma/\mu = 42.7/172.3 = 0.25$

Appendix F

Indentation Modulus to Elastic Modulus

Indentation modulus was converted to elastic modulus for comparison purposes. The calculation was performed by applying the Timoshenko-Goodier (1970) formula.

$$\text{Indentation Modulus} = \frac{F/A}{\Delta L/L}$$

$$\text{Stiffness} = \frac{F}{\Delta L}$$

$$\therefore \text{Stiffness} = IM\frac{A}{L}$$

$$\text{Elastic Modulus} = S(1 - v^2)/d$$

$$\therefore \text{Elastic Modulus} = (IM)\left(\frac{A}{L}\right)(1 - v^2)\left(\frac{1}{d}\right)$$

Where A = 12.6 mm^2, v = 0.3, and d = 4 mm are constants and the values of IM and L changed with each slice.

Appendix G

Thickness of Discarded Layers

The first layer of each tibia was discarded due to the presence of cortical bone. The thickness of these slices varied as the lateral side is positioned slightly higher than the medial side.

Bone	Medial Thickness (mm)	Lateral Thickness (mm)	Difference
1403	5.73	7.44	1.7
1469	3.75	6.22	2.5
1336	3.34	8.13	4.8
1393	4.94	9.17	4.2
1325	2.80	4.50	1.7

Appendix H

Sensitivity Analysis of Ellipse Size and Location on Modulus

Mimics® was used to calculate average HU in an ellipse placed on the CT image. The effect of the size and location of the ellipse within representative regions are shown here.
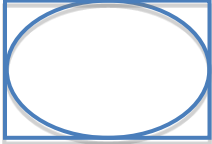
	1336-1-CC[*]	**1336-2-CC**	**1469-2-CC**
	Area = 313.11 mm^2 Mean = 124.34 HU SD = 60.31	Area = 273.28 mm^2 Mean = 145.7 HU SD = 69.02	Area = 322.81 mm^2 Mean = 143.16 HU SD = 52.28
	Area = 216.56 mm^2 Mean = 102.56 HU SD = 48.60	Area = 175.25 mm^2 Mean = 127.18 HU SD = 66.88	Area = 222.70 mm^2 Mean = 136.17 HU SD = 54.14
	Area = 117.78 mm^2 Mean = 92.98 HU SD = 47.66	Area = 79.58 mm^2 Mean = 105.87 HU SD = 62.01	Area = 122.73 mm^2 Mean = 118.27 HU SD = 54.48
	Area = 117.78 mm^2 Mean = 147.41 HU	Area = 79.58 mm^2 Mean = 103.05 HU	Area = 122.73 mm^2 Mean = 131.54 HU
	Area = 117.78 mm^2 Mean = 121.17 HU	Area = 79.58 mm^2 Mean = 171.73 HU	Area = 122.73 mm^2 Mean = 139.66 HU
	Area = 117.78 mm^2 Mean = 142.7 HU	Area = 79.58 mm^2 Mean = 168.54 HU	Area = 122.73 mm^2 Mean = 152.60 HU
	Area = 117.78 mm^2 Mean = 148.45 HU	Area = 79.58 mm^2 Mean = 170.26 HU	Area = 122.73 mm^2 Mean = 137.59 HU ***bone-slice-region**
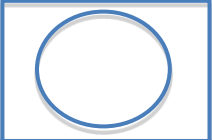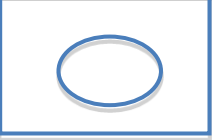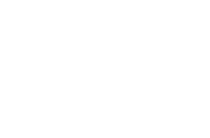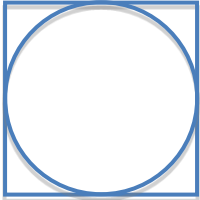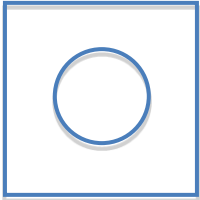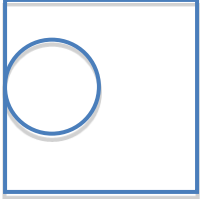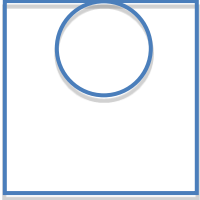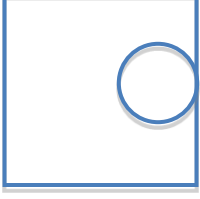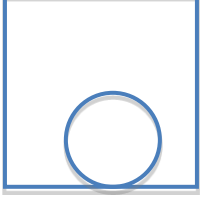
	1336-1-CM	1336-2-CM	1469-2-CM
	Mean = 578.59 HU	Mean = 380.18 HU	Mean = 333.58 HU
	Mean = 643.07 HU	Mean = 391.37 HU	Mean = 356.45 HU
	Mean = 550.85 HU	Mean = 407.26 HU	Mean = 322.75 HU
	Mean = 627.51 HU	Mean = 373.14 HU	Mean = 352.95 HU
	Mean = 619.65 HU	Mean = 322.44 HU	Mean = 312.90 HU
	Mean = 622.87 HU	Mean = 426.20 HU	Mean = 367.33 HU